

UCLA

UCLA Electronic Theses and Dissertations

Title

Multiplexers and Antennas Based on Metamaterial Transmission Line

Permalink

<https://escholarship.org/uc/item/2780h5c9>

Author

Lee, Hanseung

Publication Date

2015

Peer reviewed|Thesis/dissertation

UNIVERSITY OF CALIFORNIA

Los Angeles

Multiplexers and Antennas Based on Metamaterial Transmission Line.

A dissertation submitted in partial satisfaction of the
requirements for the degree Doctor of Philosophy
in Electrical Engineering

by

Hanseung Lee

2015

© Copyright by

Hanseung Lee

2015

ABSTRACT OF THE DISSERTATION

Multiplexers and Antennas Based on Metamaterial Transmission Line.

by

Hanseung Lee.

Doctor of Philosophy in Electrical Engineering

University of California, Los Angeles, 2015

Professor Tatsuo Itoh, Chair

Metamaterial transmission lines are able to control the phase response in the circuit, thereby making it possible to achieve multi-band characteristic in guided structures and full beam scanning ability in leaky-wave antenna applications. Isolation circuits use multi-band trait of a metamaterial transmission line for having infinite impedance at multiple frequencies. With isolation circuits, it is possible to connect microwave filters for having unique property, so called multiplexing functionality. This new approach provides unique advantageous features beneficial to system designer. For instance, there is no need to modify the components (filters and multiplexers) used in the system. Also, the design process is straightforward.

Substrate integrated waveguide (SIW) is a novel guided-wave structure developed in recent years in microwave and millimeter wave areas. It can be synthesized on a planar substrate with linear periodic arrays of metallic vias by planar circuit processes. SIW has significant advantages

such as low insertion loss, low cost and strong integration ability with other planar circuits. Based on the SIW technique and the metamaterial transmission line concept, circular polarized SIW leaky-wave antennas are designed and presented. The proposed frequency scanning antennas provide circular polarized fields using a single radiating transmission line, which can avoid the complexity of conventional approach.

The dissertation of Hanseung Lee is approved.

Oscar M. Stafsudd

Yuanxun E. Wang

Christoph Niemann

Tatsuo Itoh, Committee Chair

University of California, Los Angeles

2015

I would like to dedicate this thesis to my family, especially to my wife, best-friend Jiyeon Kim for all her loving support.

TABLE OF CONTENTS

LIST OF FIGURES	viii
LIST OF TABLES.....	xii
Introduction	1
Chapter 1 Isolation Circuits Based on Metamaterial Transmission Lines for Multiplexers	4
1.1 Introduction	4
1.2 Concept of Proposed Multiplexer	5
1.3 Metamaterial TLs for Mutiband Applications.....	8
1.4 Isolation Circuit Concept	10
1.5 Multiplexers with Conventional Junction Types.....	14
1.5.1 Star Junction Type Multiplexers.....	15
1.5.2 Manifold Junction Type Multiplexers.....	18
1.6 Conclusion	20
1.7 References	22
Chapter 2 Combining Method of Two Filtering Circuits Based on Isolation Circuits	25
2.1 Introduction	25
2.2 Concept of Proposed Method.....	26
2.3 Design Process of Multiplexers Based on CMTC.....	28
2.4 Multiplexers Based on CMTC.....	31
2.4.1 Triplexer	33
2.4.2 Quadruplexer	34
2.4.3 Five-Channel Multiplexer.....	36
2.5 Conclusion.....	37
2.6 References	38
Chapter 3 Contiguous Channel Triplexer Based on CMTC.....	39
3.1 Introduction	39
3.2 Theory	39
3.3 Design Process	45
3.4 Contiguous Triplexer	48
3.5 Conclusion.....	50

3.6 References	51
Chapter 4 Circularly Polarized Single Radiator CRLH SIW Leaky-Wave Antenna.....	52
4.1 Introduction	52
4.2 Antenna Structure and Operation Concept	53
4.3 Proposed CP Antenna	56
4.4 Conclusion	58
4.5 References	59
Chapter 5 Single Radiator Circularly Polarized CRLH SIW Leaky-Wave Antenna Equipped Compact Unit-Cell	60
5.1 Introduction	60
5.2 Unit-Cell Structure and Operating Concept.....	61
5.3 Antenna Design	66
5.3.1 Single CRLH Cell.....	67
5.3.2 Conventional Line	67
5.4 Proposed Circular Polarized Antennas.....	71
5.5 Conclusion.....	74
5.6 References	77
Appendix 1	80
Appendix 2	81
Conclusion.....	84

LIST OF FIGURES

Figure 1. Diagrams and operation concepts of multiplexers based on isolation circuit. (a) Diplexer. (b) Star-junction multiplexer. (c) Manifold-junction multiplexer.	6
Figure 2. (a) Circuit diagram of a CRLH TL unit cell. (b) Phase response of a CRLH TL in the balanced case.....	7
Figure 3. (a) Circuit model of a DL TL unit cell. (b) Phase response of a DL TL in the balanced case. ...	10
Figure 4. (a) An isolation circuit diagram. (b) An example of the input impedance Z_L shown on the Smith chart (case 1: $X > 0$ and $\alpha = 0$). (c) An example of the input impedance Z_L shown on the Smith chart (Case 2: $X < 0$ and $\alpha = 0$).	11
Figure 6. Reflection coefficient of a multiplexer using the adjusting constant, ψ_1 and ψ_2 , on Fig. 4(b). ...	13
Figure 5. (a) An isolation circuit diagram. (b) An example of the input impedance Z_L shown on the Smith chart (case 1: $X > 0$ and $\alpha = 0$). (c) An example of the input impedance Z_L shown on the Smith chart (Case 2: $X < 0$ and $\alpha = 0$).	13
Figure 7. Fabricated star-junction multiplexers based on isolation circuits. (a) Triplexer. (b) Quadruplexer.	14
Figure 8. The star-junction triplexer results: (a) Insertion loss. (b) Matching at port 1. (c) Isolation.	16
Figure 9. The star-junction quadruplexer results: (a) Insertion loss. (b) Matching at port 1. (c) Isolation.	18
Figure 10. Fabricated manifold-junction multiplexers based on isolation circuits. (a) Triplexer. (b) Quadruplexer.....	19
Figure 11. The manifold-junction triplexer results: (a) Insertion loss. (b) Matching at port 1. (c) Isolation.	20
Figure 12. The manifold-junction triplexer results: (a) Insertion loss. (b) Matching at port 1. (c) Isolation.	21
Figure 13. Diagram and operation concept of a multiplexer based on CMTC.	25
Figure 14. Triplexer based on CMTC.....	27

Figure 15. Performances of the diplexer and the filter for the triplexer. (a) Magnitude response of the diplexer. (b) Input impedance of the diplexer shown on the Smith chart. (c) Magnitude response of the filter. (d) Input impedance of the filter shown on the Smith chart.....	28
Figure 16. Frequency response of the triplexer. (a) Insertion loss. (b) Matching at port 1. (c) Isolation. ..	29
Figure 17. Quadruplexer based on CMTC.....	30
Figure 18. Performances of the diplexers for the quadruplexer. (a) Magnitude response of the diplexer 1. (b) Input impedance of the diplexer 1 shown on the Smith chart. (c) Magnitude response of the diplexer 2. (d) Input impedance of the diplexer 2 shown on the Smith chart.	31
Figure 19. Frequency response of the quadruplexer. (a) Insertion loss. (b) Matching at port 1. (c) Isolation.	32
Figure 20. Five-channel multiplexer based on CMTC.....	33
Figure 21. Performances of the triplexer and the diplexer for the five-channel multiplexer. (a) Magnitude response of the triplexer. (b) Input impedance of the triplexer shown on the Smith chart. (c) Magnitude response of the diplexer. (d) Input impedance of the diplexer shown on the Smith chart.	34
Figure 22. Frequency response of the five-channel multiplexer. (a) Insertion loss. (b) Matching at port 1. (c) Isolation.	35
Figure 23. Diagram and operation concept of proposed triplexer based on CMTC.	40
Figure 24. Locus of input impedance of a BPF shown in the Smith chart. (a) Open rejection case. (b) Short rejection case.	40
Figure 25. Dispersion diagram of a CRLH TL (β : the propagation constant of a CRLH TL).	41
Figure 26. Design of CRLH TL connected with f_2 filter. (a) Open rejection case. (b) Short rejection case.	42
Figure 27. Design of CRLH TL connected with f_1 filter. (a) Open rejection case. (b) Short rejection case.	42
Figure 28. Design of CRLH TL connected with f_3 filter. (a) Open rejection case. (b) Short rejection case.	43

Figure 29. Ideal frequency response of proposed triplexer on output ports.....	44
Figure 30. The layout of filtering circuits used for proposed triplexer. (a) Diplexer. (b) 1.125 GHz filter. (Parameters: $l_{11} = 5.9$, $l_{12} = 28.55$, $l_{13} = 14.25$, $l_{14} = 37.45$, $l_{15} = 14.45$, $l_{21} = 6.8$, $l_{22} = 31.7$, $l_{23} = 16.2$, $l_{24} = 41.6$, $l_{25} = 17.4$, $l_{31} = 8.1$, $l_{32} = 35.1$, $l_{33} = 20$, $l_{34} = 46.9$, $l_{35} = 19.8$, $w_0 = 2.3$, $w_1 = 1$, $w_2 = 1.8$, $w_3 = 2$.)	45
Figure 31. Performances of the diplexer and the filter used on proposed triplexer. (a) Magnitude response of the diplexer. (b) Input impedance of the diplexer shown on the Smith chart. (c) Magnitude response of the filter. (d) Input impedance of the filter shown on the Smith chart.	47
Figure 32. Fabricated contiguous channel triplexer based on CMTC.	48
Figure 33. Simulated and measured results of proposed triplexer. (a) Insertion loss. (b) Matching at port 1. (c) Isolation.	49
Figure 34. Proposed antenna configuration. (a) Unit-cell of the proposed CP LWA. (b) Whole structure of the proposed CP LWA. (Unit-cell parameters: $p_1 = 10$ mm, $p_2 = 11$ mm, $l = 4.1$ mm, $w_1 = 0.63$ mm, $w_2 = 0.4$ mm, $w_3 = 12.24$ mm.).....	53
Figure 35. Equivalent circuit model of the unit-cell shown in Fig. 34(a).....	54
Figure 36. Dispersion diagram of the proposed circular polarized antenna unit-cell ($p = 2 \times p_1 + 2 \times p_2$). ...	54
Figure 37. Fabricated novel CP CRLH SIW leaky-wave antenna.....	56
Figure 38. Measured and simulated S-parameters of the proposed CP LWA antenna.....	56
Figure 39. Measured and simulated far field patterns of the proposed circularly polarized antenna in x-z plane. (a) From LH to broadside region. (b) RH region.	57
Figure 40. Measured and simulated axial ratio of the proposed circularly polarized antenna in x-z plane. (a) From LH to broadside region. (b) RH region.	58
Figure 41. (a) Unit-cell of the proposed single radiator CP LWA. (b) Whole structure of the proposed CP LWA. (Unit-cells parameters: $l_m = 5.1$ mm, $l_c = 11$ mm, $l = 4.1$ mm, $w_l = 0.63$ mm, $w_2 = 0.4$ mm, $w_3 = 12.54$ mm, $w_m = 2.5$ mm, $s = 1.57$ mm.)	62

Figure 42. Characteristics of the proposed CP antenna unit-cell. (a) Dispersion diagram ($p = 2 \times l_m + 2 \times l_c$). (b) Space harmonics reconstructed from the dispersion diagram of the proposed unit-cell (n is mode number). (c) Bloch Impedance.....	63
Figure 43. Characteristics of the previous CP antenna unit-cell [19]. (a) Dispersion diagram ($p = 2 \times l_s + 2 \times l_c$). (b) Space harmonics reconstructed from the dispersion diagram of the previous unit-cell (n is mode number). (c) Bloch Impedance.....	64
Figure 44. (a) CRLH SIW cell and its transmission line model. (b) Phase response of the CRLH cell. (c) Characteristic impedance of the CRLH cell.	66
Figure 45. (a) Transmission line model of the proposed CP LWA unit-cell. (b) Scattering parameters of the TL model (with all ideal TLs) changing the characteristic impedance of the microstrip line, Z_m , with fixed Z_c . (c) Zoom view of Fig. 4(b) around the center frequency. (d) S-parameters of the TL model using the ABCD matrix of the CRLH cell (ideal TLs are used for microstrip lines).....	68
Figure 46. Fabricated novel CP CRLH-inspired SIW leaky-wave antenna.....	71
Figure 47. Comparison between the proposed CP antenna and the previous CP antenna having single radiator.....	71
Figure 48. Measured and simulated S-parameters of the proposed CP LWA antenna.....	72
Figure 49. Simulated realized gain patterns of the proposed circularly polarized antenna in x-z plane. (a) LH region. (b) Broadside. (c) RH region.....	73
Figure 50. Measured radiation patterns of the proposed circularly polarized antenna in x-z plane. (a) LH region. (b) Broadside. (c) RH region.....	75
Figure 51. Measured and simulated axial ratio of the proposed circularly polarized antenna in x-z plane. (a) LH region. (b) Broadside. (b) RH region.....	76
Figure 52. Pole-zero plots of the transfer function of reflection coefficient at (a) $\omega = 0$, (b) $\omega = \omega_1$, (c) $\omega = \omega_0$, and (d) $\omega = \omega_2$	81
Figure 53. (a) Amplitude and (b) phase response of the reflection coefficient of a BPF.....	82

LIST OF TABLES

Table 1. Design Summary of The Star Junction Triplexer	17
Table 2. Design Summary of The Star Junction Quadruplexer	17
Table 3. Design Summary of The Manifold Junction Triplexer	22
Table 4. Design Summary of The Manifold Junction Quadruplexer	22
Table 5. Summary of Triplexer Based on CMTC.....	37
Table 6. Summary of Quadruplexer Based on CMTC.....	37
Table 7. Summary of Five-Channel Multiplexer Based on CMTC	38
Table 8. Summary of Contiguous Channel Triplexer	50
Table 9. Simulated Axial Ratio Comparison	76

ACKNOWLEDGMENTS

I would like to thank Professor Tatsuo Itoh for his sincere guidance and to all my colleagues in Microwave Electronics Lab for their indispensable advices and discussion. I am also indebted to the members of my committee, Professor Oscar M. Stafsudd, Professor Yuanxun E. Wang, and Professor Christoph Niemann, for their valuable comments.

VITA

- 2006 B.S. Electrical Engineering, Korea University, Korea.
- 2008 M.S. Electrical Engineering, Seoul National University, Korea.
- 2010 – 2015 Graduate Student Researcher, Department of Electrical Engineering,
University of California, Los Angeles, USA.
- 2014 Teaching Assistant, Department of Electrical Engineering, University of
California, Los Angeles, USA.
- 2010 Best Paper
Asia Pacific Microwave Conference 2011, Australia.
- 2012 Finalist for Best Student Paper
Asia Pacific Microwave Conference 2012, Taiwan.
- 2014 Finalist for Student Paper Competition
International Microwave Symposium 2014, USA.

PUBLICATIONS

Publications-Journal

Hanseung Lee, Jun Choi, Chung-Tse Michael Wu, and Tatsuo Itoh, "Size Reduced Single Radiator Circularly Polarized Leaky-Wave Antenna based on CRLH-Inspired Substrate Integrated Waveguide", *IEEE Trans. on Antennas and Propagation*, under revision.

Hanseung Lee, Youngje Sung, Chung-Tse Michael Wu, and Tatsuo Itoh, "Dual-band and polarization-flexible cavity antenna based on substrate integrated waveguide" *IEEE Antenna and Wireless Propagation Letters*, under revision.

Chung-Tse Michael Wu, Jun. H. Choi, **Hanseung Lee**, and Tatsuo Itoh, "Magnetic-current-loop induced electric dipole antenna based on substrate integrated waveguide cavity" *IEEE Antenna and Wireless Propagation Letters*, vol. 13, pp. 519-522, March 2014.

Hanseung Lee, Chung-Tse Michael Wu, and Tatsuo Itoh, "Study and analysis of contiguous channel triplexer based on combining method of two filtering circuits using CRLH and RH isolation circuit", *International Journal of Microwave and Wireless Technologies*, vol. 6, pp.287-295, June 2014. **(Invited paper)**

Hanseung Lee and Tatsuo Itoh, "Isolation circuits based on metamaterial transmission lines for multiplexers", *Journal of Electromagnetic Engineering and Science*, vol. 13, no. 3, pp.141-150, Sep. 2013. **(Invited paper)**

Hanseung Lee and Sangwook Nam, "Triband branch line coupler using double-Lorentz transmission lines", *Microwave and Optical Technology Letters*, Volume 50, No. 5, May 2008.

Hanseung Lee, Heeduck Chae, Jonghoon Chun, and Sangwook Nam, "High-gain 94 GHz monopulse antenna using folded reflectarray", *Journal of the Korea Electromagnetic Engineering Society*, Volume 17, Issue 7, Jan. 2008.

Publications-Conference

Hanseung Lee, Jun H. Choi, and Tatsuo Itoh, "Active diplexer based on isolation circuits imbedded low noise amplifiers," *2015 European Microwave Conference*,, accepted for publication.

Zhi Shen, Kirti Dhvaj, **Hanseung Lee**, Lijun Jiang, and Tatsuo Itoh, "Broadband high gain SIW ring slot antenna," *2015 European Microwave Conference*,, accepted for publication.

Kirti Dhvaj, **Hanseung Lee**, Lijun Jiang, and Tatsuo Itoh, "Transmission-line equivalent and microstrip structure for planar Mobius loop resonator," *2015 IEEE MTT-S Int. Microwave Symp.*, accepted for publication.

Hanseung Lee and Tatsuo Itoh, "Evolution of Circularly Polarized Composite Right/Left-Handed Leaky-Wave Antenna," *2014 Asia-Pacific Microwave Conference*, Nov. 2014. **(Invited paper)**

Hanseung Lee, Yoshiaki Kasahara, and Tatsuo Itoh, "Study of high efficiency and low sidelobe level CRLH leaky-wave antenna based on short-termination and tapered cells," *2014 European Microwave Conference*, Oct. 2014.

Jun. H Choi, Chung-Tse Michael Wu, **Hanseung Lee**, and Tatsuo Itoh, "Vialess composite right/left-handed stripline and its applications for broadband 3-dB and tunable couplers," *2014 European Microwave Conference*, Oct. 2014.

Hanseung Lee, Jun H. Choi, Yoshiaki Kasahara, and Tatsuo Itoh, "A circularly polarized single radiator leaky-wave antenna based on CRLH-inspired substrate integrated waveguide," *2014 IEEE MTT-S Int. Microwave Symp.*, pp. 1-3, June 2014. **(Student Paper Competition Finalist)**

Hanseung Lee and Tatsuo Itoh, "Combining method of two filtering circuits based on isolation circuits for five-channel multiplexers," *2013 Asia-Pacific Microwave Conference*, pp.339-341, Nov. 2013.

Hanseung Lee, Jim S. Sun, and Tatsuo Itoh, "Contiguous triplexer based on combining method of two filtering circuits using CRLH and RH isolation circuits," *2013 European Microwave Conference*, pp.924-927, Oct. 2013.

Hanseung Lee and Tatsuo Itoh, "Tri-band isolation circuits using both stop-band and pass-band of double-Lorentz transmission lines for quadruplexers," *2013 IEEE MTT-S Int. Microwave Symp.*, pp.1-3, June 2013.

Hanseung Lee and Tatsuo Itoh, "Hybrid combination of tri-band isolation circuits based on conventional and double-Lorentz transmission lines for quadruplexers," *2013 International Symposium on Electromagnetic Theory*, pp.393-396, May 2013. **(Invited paper)**

Hanseung Lee and Tatsuo Itoh, "Size reduced dual-band isolation circuits using hybrid right-handed transmission lines for triplexers," *2012 Asia-Pacific Microwave Conference*, pp.76-78, Dec. 2012. **(Best Student Paper Award Finalist)**

Hanseung Lee and Tatsuo Itoh, "Tri-band isolation circuits based on double-Lorentz transmission lines for quadruplexers," *2012 European Microwave Conference*, pp.585-588, Oct. 2012.

Hanseung Lee and Tatsuo Itoh, "Hybrid combination of dual band isolation circuits based on conventional and CRLH transmission lines for triplexers," *2013 IEEE MTT-S Int. Microwave Symp.*, pp.1-3, June 2012.

Hanseung Lee and Tatsuo Itoh, "Dual band isolation circuits based on CRLH transmission lines for triplexer application," *2011 Asia-Pacific Microwave Conference*, pp. 542-545, Dec. 2011. **(Best Paper Awarded)**

Hanseung Lee, Heeduck Chae, Jonghoon Chun, Sangwook Nam, "94GHz monopulse folded reflectarray antenna," *AP International Symposium 2007*, Aug. 2007.

Hanseung Lee, Jonghoon Chun, Sangwook Nam, "94GHz waveguide monopulse comparator using circular cavity hybrid," *MINT-MIS2007/TSMW2007/MilliLab Workshop*, Feb. 2007.

Heeduck Chae, **Hanseung Lee**, Younghoon Kim and Sangwook Nam, "Efficient Computation of Impedance Matrix 1-Dimensional Periodic Planar Structures Using Rooftop Functions," *IEEE AP-S International Symposium 2007*, pp. 1517-1520, June 2007.

Jungsuek Oh, Jongmin Park, **Hanseung Lee** and Sangwook Nam, "The Electrode structure to reduce channel loss for Human Body Communication Using Human Body as Transmission Medium," *IEEE AP-S International Symposium 2007*, pp. 1517-1520, June 2007.

Introduction

A metamaterial transmission line has been used in various microwave applications. One of major traits of a metamaterial transmission line is that its phase response is non-linear and can be engineered. On the contrary, a conventional transmission line has linear phase response and it does not have phase flexibility. Therefore metamaterial transmission lines are proper for multi-band applications because they can provide freedom to choose arbitrary phase responses at multiple frequencies. Various multi-band components, such as dual-band, tri-band couplers, and dual-band matching circuits have been realized by metamaterial transmission lines. In antenna applications, metamaterial transmission line concept has accelerated the study of leaky-wave antennas. Metamaterial transmission line can be systematically designed to have both positive and negative phase velocity that allows leaky-wave antennas to steer the beam not only toward forward direction but also toward backward direction. Moreover, it even supports broadside radiation under the balanced condition. Conventional transmission line structures are inherently difficult to design a leaky-wave antenna equipped full-beam scanning capability including broadside radiation.

In this dissertation, metamaterial transmission lines are adopted for more advanced multiplexers. Conventional multiplexer methodologies require modification of filters used in multiplexers. Moreover, because of design complexity, conventional methods do not provide analytical design process. Rather they require complex optimization for design parameters. In chapter 1, multiplexers based on metamaterial transmission lines are proposed. The design process is straightforward and it does not demand optimization process. In addition, filters used in the multiplexers have not been modified thereby making possible to use commercial filters.

The basic design block is an isolation circuit which consists of a metamaterial transmission line and a filter. Its operation concept and design process are introduced. Based on connection methods of isolation circuits, multiplexers based on metamaterial transmission lines can be categorized by star-junction type and manifold junction type. Triplexers and quadruplexers based on both junction types are designed and verified.

In chapter 2, an isolation circuit concept is further expanded to a metamaterial transmission line connected with a multiplexer instead of a filter. This approach opens the possibility to combine two multiplexers thereby increasing channel numbers efficiently. Based on the combining method of two filtering circuits (CMTC), the triplexer, the quadruplexer, and the five-channel multiplexer are designed and fabricated. The detailed explanation of the methodology and the design procedure are provided.

Combining method of two filtering circuits (CMTC) presented in chapter 3 is efficient method of designing a contiguous channel triplexer. As explained in chapter 1, a triplexer can be realized by an isolation circuit with either star-junction or manifold-junction. However, both ways are not proper for a contiguous channel triplexer because it is difficult that all isolation circuits used in a triplexer satisfy conditions for a contiguous channel multiplexing. In a conventional triplexer design, the contiguous channel configuration is also difficult because of a strong coupling between channels. In this chapter, the reason of why the CMTC is effective way of realizing a contiguous channel triplexer is presented. The design procedure is also explained.

After advent of metamaterial transmission lines, many leaky-wave antennas based on these new structures have been investigated. There were several approaches for a circular polarized substrate integrated waveguide metamaterial based leaky-wave antenna, but all they have used dual radiators and a broadband quadrature coupler. In chapter 4, the novel method for a single

radiator circular polarized substrate integrated waveguide leaky-wave antenna based on a metamaterial transmission line is proposed. The working principle and the investigation of the unit-cell structure are also provided.

In chapter 5, the single radiator circular polarized leaky-wave antenna is further improved by using a microstrip line instead of a substrate integrated waveguide for a phase delay. The modified unit-cell structure has more compact size than the unit-cell introduced in chapter 4. Therefore, in a same size, the antenna introduced in this chapter has more radiating elements and it brings increased radiation efficiency.

Chapter 1 Isolation Circuits Based on Metamaterial Transmission Lines for Multiplexers

1.1 Introduction

Many modern communication systems are required to handle multiple frequency bands. If a base station for a mobile phone can deal with two or three communication standards, the price of its construction will be lowered with concomitant benefits for customers. Multiband is already intrinsic to cell phone designs for handling cellular, GPS, and WiFi bands. In order to support such multiband systems, a multiplexer is necessary if one antenna covers all the designated spectra and thus becomes an essential component. For multiplexers, many design concepts have been investigated and categorized by star junction type and manifold junction type [1]-[3]. The first star junction type multiplexer is based on synthesizing singly terminated channel filters [4]. After one decade, another method to synthesize doubly terminated filters for star junction type multiplexers was proposed [5]. In the recent approach [6], a general polynomial model is used for filters, and filters are connected with a complex load. The rapid development of manifold junction type multiplexers was caused by the advent of satellite communication systems [7]. In the initial stage, the analytic approach to design the filters, having proper interaction with other filters on the same manifold, was investigated [8]. However, recent manifold junction type multiplexers are mostly designed with optimization methods with the increased computer power [9]. In both star junction and manifold junction type multiplexers, modification of filters and a complex optimization process are generally required. However, the use of a commercial filter without modification, and a simple multiplexer design method are occasionally necessary for a system designer. The simplest multiplexer satisfying such demand is shown in Figure 1(a). The diplexer is made of two isolation circuits, and each isolation circuit consists of a conventional

right-handed (RH) transmission line (TL) connected to a filter. An isolation circuit isolates itself from the input port at the center frequency of the other channel. Hence the signal passes through one isolation circuit while it is rejected by the other. This procedure cannot be extended simply to a multiplexer containing three or more channels. Since a conventional TL can provide one phase response at a target frequency, an isolation circuit can be designed to have the isolation characteristic at only one frequency.

If a TL can have a multiple phase property, it can realize a multiband isolation circuit and result in a channel extension of the multiplexer based on isolation circuits. This characteristic has been found in a metamaterial TL. A composite right/left-handed (CRLH) metamaterial TL has a dual-band characteristic [10]. A double-Lorentz (DL) TL has six parameters, and it satisfies six conditions for a tri-band characteristic [11].

In this chapter, two types of multiplexers based on isolation circuits are presented. One consists of isolation circuits using same type of TLs, and it can be categorized as the star junction type. On the other hand, the other type uses both RH TLs and multiband TLs for making isolation circuits, and its junction shape is similar to a manifold junction. First, the concepts of multiplexers are explained, and the theory for designing an isolation circuit is investigated. The simulated and measured results of the proposed multiplexers are also provided.

1.2 Concept of Proposed Multiplexer

The diplexer shown in Fig. 1 (a) is the starting point for a multiplexer based on isolation circuits. If it is necessary to increase one more channel, an additional isolation circuit can be connected to the junction point like shown in Fig. 1 (b), and each circuit should have open-circuit input impedance at the passing frequencies of other circuits [12]. For satisfying this condition, a CRLH TL having dual band characteristic is necessary. In a similar manner, a four-channel

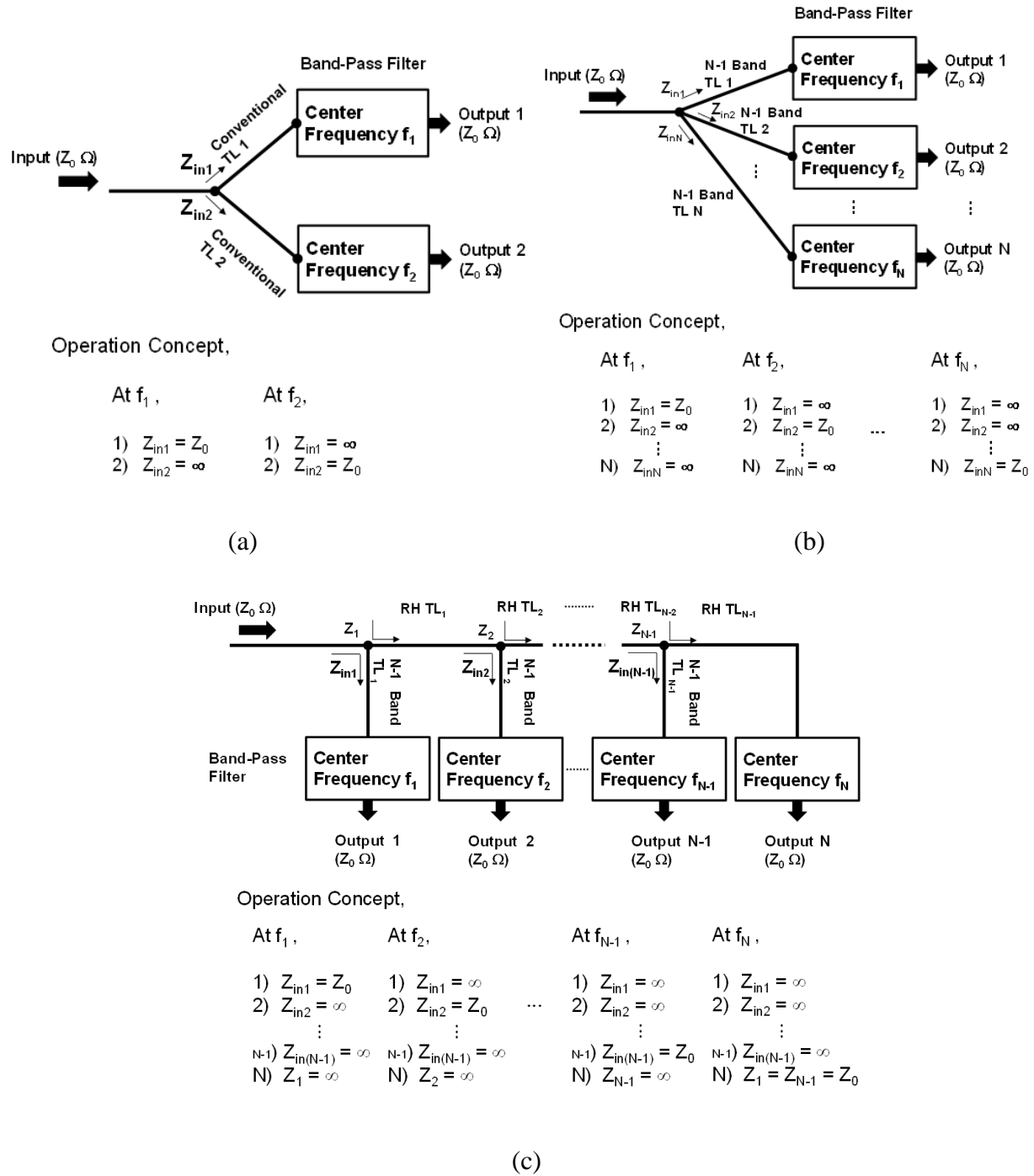


Figure 1. Diagrams and operation concepts of multiplexers based on isolation circuit. (a) Diplexer. (b) Star-junction multiplexer. (c) Manifold-junction multiplexer.

multiplexer or a quadruplexer can be realized by connecting four tri-band isolation circuits composed of DL TLs having tri-band characteristic [13].

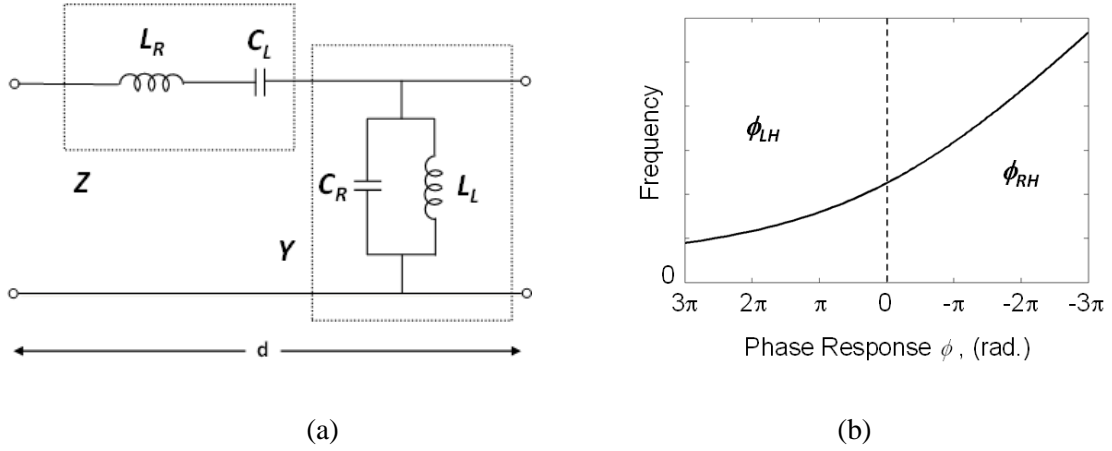


Figure 2. (a) Circuit diagram of a CRLH TL unit cell. (b) Phase response of a CRLH TL in the balanced case.

In the concept of a star junction multiplexer, all isolation circuits are composed with same type of TL. For example, a star junction triplexer is composed with three CRLH TLs followed by three filters. The multiplexer shown in Fig. 1 (c) also consists of multiband TLs and filters for multiband isolation circuits. However, one special isolation circuit composed with RH TLs connecting with a filter exists in this type of multiplexers [14], [15]. This special isolation circuit also has multiband characteristic. The mechanism is as follows: 1) at frequency f_1 , the first isolation circuit consisting of the f_1 filter allows signal path. Meanwhile, other isolation circuits composed with multiband TLs are disconnected from junctions, and the combined phase response of RH TLs (from TL_1 to TL_{N-1}) is already determined for the isolation circuits consisting of RH TLs (from TL_1 to TL_N) and the f_N filter having infinite input impedance. 2) At frequency f_{N-1} , except the isolation circuit having the f_{N-1} filter, all isolation circuits consisting of multiband TLs have infinite input impedance. Also the isolation circuit consisting of the RH TL_{N-1} and the f_N filter is isolated from the junction. 3) At frequency f_N , all isolation circuits composed with multiband TLs are isolated from junctions, and the f_N filter is directly connected

with the input through RH TLs allowing signal path. In the diagrams of Fig. 1, the frequencies from f_1 to f_N do not need to be in ascending order.

1.3 Metamaterial TLs for Mutiband Applications

The circuit parameters of a conventional RH TL are series inductance and shunt capacitance. This structure has a linear phase response, and only a RH phase shift or phase delay exists. However, the dual structure of a RH TL or LH TL, of which the circuit parameters are series capacitance and shunt inductance, has a nonlinear phase response, and only a left-handed phase response or phase advance is supported. Because of a parasitic RH TL, a pure LH TL does not exist in the real world, and a combination of a RH TL and a LH TL, a CRLH TL, has been actively investigated [16]. Figure 2 shows the circuit model and phase response of a CRLH TL. A CRLH TL shows interesting characteristics in the balanced condition, where the series resonant and shunt resonant frequencies are equal. In the balanced condition of a CRLH TL, the phase response and characteristic impedance are simply represented as

$$\phi(\omega) = -N_C \left[\omega \sqrt{L_R C_R} - \frac{1}{\omega \sqrt{L_L C_L}} \right]. \quad (1)$$

$$Z_C = \sqrt{\frac{L_R}{C_R}} = \sqrt{\frac{L_L}{C_L}}. \quad (2)$$

where N_C is the number of CRLH TL unit cells and ω is the angular frequency. A CRLH TL has a dual-band characteristic: two desired phase responses, ϕ_1 and ϕ_2 , can be obtained at two frequencies, ω_1 and ω_2 , using a CRLH TL. Phase shift ϕ_1 at frequency ω_1 and phase shift ϕ_2 at frequency ω_2 bring two equations using (1). Because of the matching-to-termination impedance Z_0 , (2) makes two other equations. So, there are four equations with four unknowns: L_R , C_R , L_L , and C_L . These four circuit parameters are presented with closed forms in Appendix 1 [16].

A dual-CRLH (D-CRLH) TL has not only the dual characteristics of a CRLH TL but also has the dual structure of a CRLH TL, which has the parallel LC in series branch and series LC in shunt branch [17]. A double-Lorentz (DL) TL is a combination of a D-CRLH TL and a parasitic RH TL, of which circuit parameters are series inductance (L_p) and shunt capacitance (C_p). Figure 3(a) shows a circuit diagram of a DL TL. The phase response of a DL TL, shown in Fig. 3(b), is similar to that of a D-CRLH TL, but the existence of a RH phase shift region at a higher frequency band is a significant difference. A DL TL appears as a RH TL at low frequencies because components L_R , L_p , C_R , and C_p are dominant. On the contrary, if both impedance Z and admittance Y could have negative values at a certain frequency band, the DL TL would show CRLH-like behavior, because the effect of L_R and C_R in the structure is reduced at higher frequency. However, if both Z and Y do not support negative values in the frequency band, then the DL TL does not have a LH characteristic.

The phase response and characteristic impedance of a balanced DL transmission line are presented as (3) and (4), respectively [18].

$$\phi(\omega) = -N_D \left[\omega \sqrt{L_p C_p} + \sqrt{\frac{C_p}{L_p}} \frac{\omega L_R}{1 - \omega^2 L_R C_L} \right]. \quad (3)$$

$$Z_C = \sqrt{\frac{L_p}{C_p}} = \sqrt{\frac{L_L}{C_L}} = \sqrt{\frac{L_R}{C_R}}. \quad (4)$$

where N_D is the number of DL TL unit cells. Because a DL TL has a tri-band characteristic, three desired phase responses, ϕ_1 , ϕ_2 , and ϕ_3 , can be obtained at three frequencies, ω_1 , ω_2 , and ω_3 . This results in three equations using (3). Because of the matching-to-termination impedance Z_0 , (4) makes three other equations. Hence there are six equations with six unknowns, L_p , C_p , L_R , C_R , L_L ,

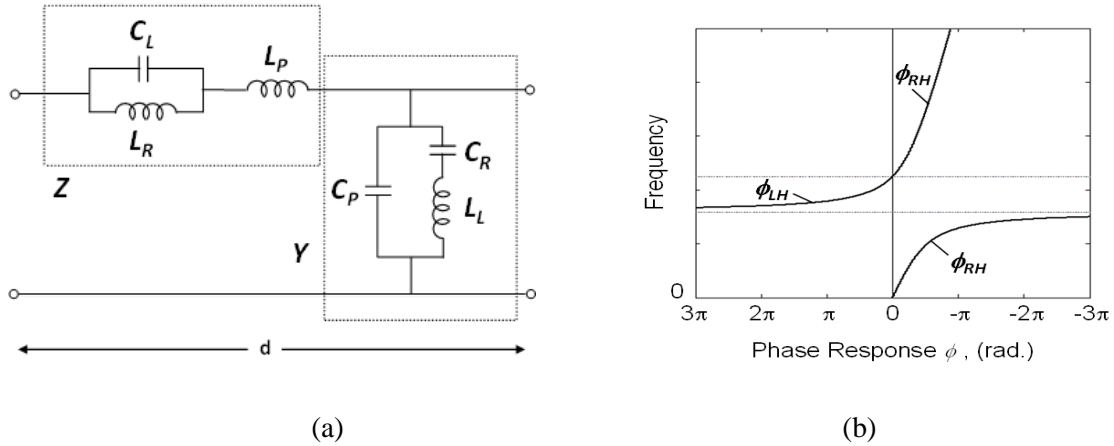
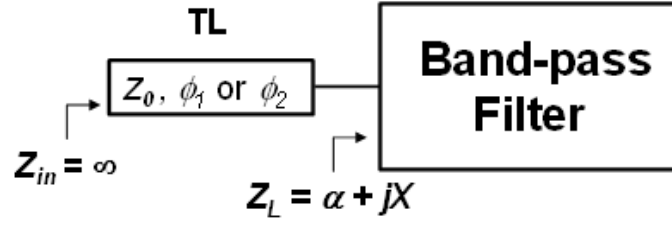


Figure 3. (a) Circuit model of a DL TL unit cell. (b) Phase response of a DL TL in the balanced case.

and C_L . Solving these simultaneous equations gives circuit parameters of a DL TL satisfying tri-band characteristic.

1.4 Isolation Circuit Concept

The method to determine a proper phase response of a TL for an isolation circuit is discussed in this section. Figure 4(a) represents an isolation circuit comprising a TL connected to a filter or a multiplexer. For simplicity, a case dealing with only one phase is considered. In Fig. 4(b) and (c), each triangle on the Smith chart shows an input impedance of a filter or a multiplexer at target frequency. In both cases, the real part of the impedance (α) is assumed zero. Figure 4(b) represents a positive imaginary impedance and Fig. 4(c) shows a negative imaginary impedance. Since the input impedance is not infinite, a TL is required to rotate the triangle to the open position, represented by a hollow circle on the Smith chart, for an isolation characteristic. Two rotations are possible in both cases. Clockwise rotation represents a RH phase response or a delay, ϕ_1 , having a negative value. A left-handed (LH) phase response or a phase advance, ϕ_2 , having a positive value, is represented as a counter-clockwise rotation on the Smith chart. If the



(a)

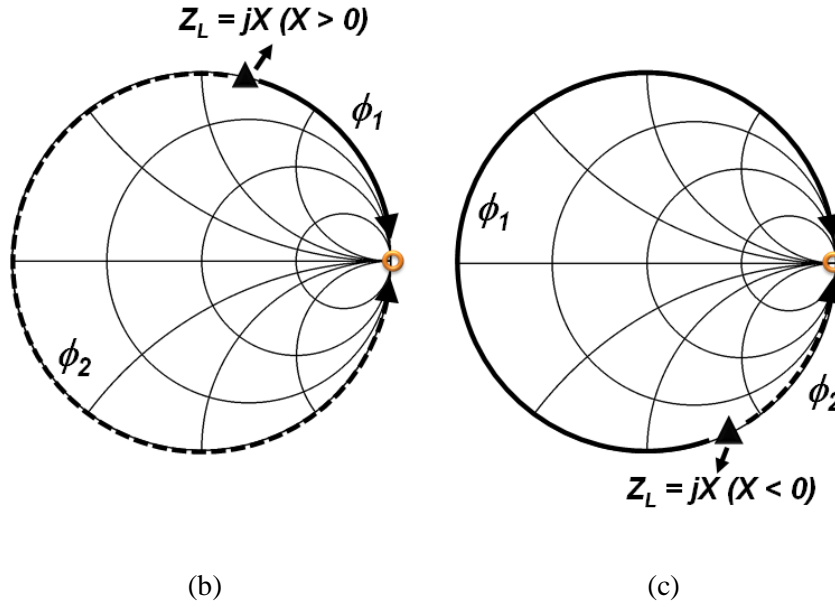


Figure 4. (a) An isolation circuit diagram. (b) An example of the input impedance Z_L shown on the Smith chart (case 1: $X > 0$ and $\alpha = 0$). (c) An example of the input impedance Z_L shown on the Smith chart (Case 2: $X < 0$ and $\alpha = 0$).

real part of the input impedance of a filter or a multiplexer (α) is zero, the transmission line impedance equation can be used to solve the required phase response [19].

$$Z_{in} = Z_0 \frac{Z_L + jZ_0 \tan(-\phi_{1,2})}{Z_0 + jZ_L \tan(-\phi_{1,2})}. \quad (5)$$

Since the input impedance of the circuit Z_{in} should be infinite, the denominator of (2) is zero, and the required phase response, $\phi_{1,2}$, is

$$\phi_1 = \begin{cases} -\arctan(Z_0/X), & X > 0 \\ -\pi - \arctan(Z_0/X), & X < 0 \end{cases} \quad (6a)$$

$$\phi_2 = \begin{cases} \pi - \arctan(Z_0/X), & X > 0 \\ -\arctan(Z_0/X), & X < 0 \end{cases} \quad (6b)$$

These equations can be simplified to a more general form:

$$\phi = n\pi - \arctan(Z_0/X) + \psi. \quad (6c)$$

where n is the integer and Z_0 is the characteristic impedance of the transmission line. Here, ψ is the adjusting constant as will be explained below. A more rigorous equation considering the term α is also represented as

$$\phi = n\pi - \frac{\arg\{(\alpha^2 + X^2 - Z_0^2) + j2Z_0X\}}{2} + \psi. \quad (6d)$$

Adjusting the constant ψ obtains reasonable circuit parameters. In the phase responses of a balanced CRLH TL and a DL TL, the absolute value of a phase shift at a higher frequency should be larger than that at a lower frequency on the right-handed (RH) region. However, it might be necessary that the absolute phase shift at the higher frequency is smaller than that at the lower frequency in certain conditions, like Fig. 5(a). A designer would want the two target points a' (at frequency f_1 , lower than f_2) and b' (at frequency f_2 , higher than f_1) on the Smith chart moving to an open position after combining the TL. Phase shifts ϕ'_1 (for a') and ϕ'_2 (for b') of the TL are necessary, and a CLRH TL and a DL TL cannot support this because the phase shift $|\phi'_1|$ at the lower frequency is larger than $|\phi'_2|$. It is therefore necessary to use the adjusting constant ψ to satisfy the natural phase response of the TL [18]. Constants ψ_1 and ψ_2 in Fig. 5(b) are used for such a purpose. The final phase response $|\phi_1|$ is smaller than $|\phi_2|$. Even the two final points, a and b, are not located in an exact open position. If a and b are not far from an open

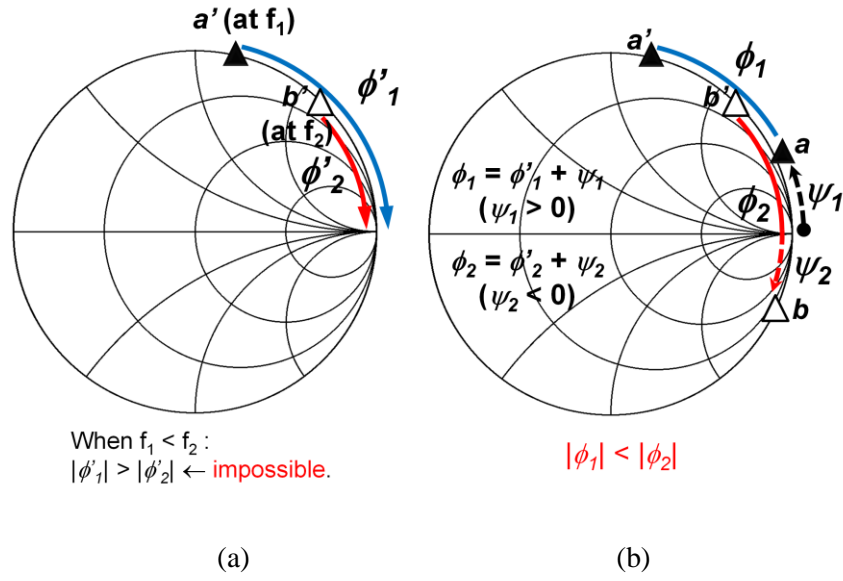


Figure 6. (a) An isolation circuit diagram. (b) An example of the input impedance Z_L shown on the Smith chart (case 1: $X > 0$ and $\alpha = 0$). (c) An example of the input impedance Z_L shown on the Smith chart (Case 2: $X < 0$ and $\alpha = 0$).

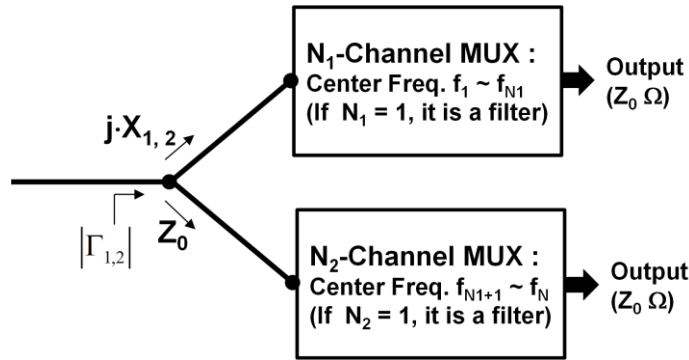


Figure 5. Reflection coefficient of a multiplexer using the adjusting constant, ψ_1 and ψ_2 , on Fig. 4(b).

condition, this isolation circuit could be isolated enough albeit with some return loss cost. Figure 6 shows the simple diagram of this case, and the reflection coefficient is

$$|\Gamma_{1,2}| = \frac{Z_0^2}{Z_0^2 + 4X_{1,2}^2} \quad (7)$$

where X_1 and X_2 are the reactance values of a and b on Fig. 5(b), respectively, and the exact matching of the other circuit is assumed. For reference, if the value of X equals $\pm 1.5 \times Z_0$, 10 dB return loss is guaranteed, and if 20 dB return loss is required with that, then X is $\pm 5.0 \times Z_0$. Adjusting constant ψ is also able to help determine the appropriate circuit parameters of a TL. Because a multiband TL is realized by lumped elements (inductors and capacitors) and a microstrip line, it operates in a restricted frequency range which is mainly affected by the values of the lumped elements. To adjust the operating frequency band, a designer might need to compromise between a design circuit parameter and the real value of a lumped element, and a constant ψ might help to choose the appropriate circuit parameters.

1.5 Multiplexers with Conventional Junction Types

In order to verify the design concepts, star junction type multiplexers and manifold junction

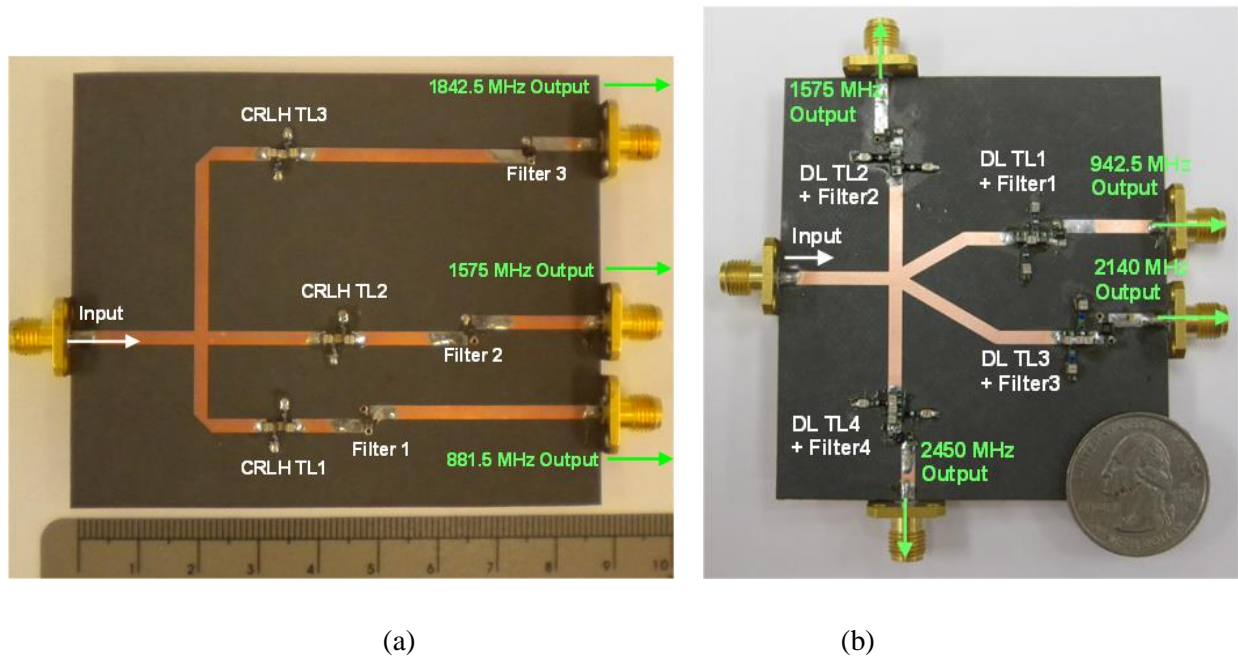


Figure 7. Fabricated star-junction multiplexers based on isolation circuits. (a) Triplexer. (b) Quadruplexer.

type multiplexers are designed and fabricated. A RT/Duroid 5870 substrate ($\epsilon_r = 2.33$, height = 0.787 mm) and commercial SAW filters are used for multiplexers. Four filters (having 881.5 MHz, 942.5 MHz, 1575 MHz, and 1842.5 MHz center frequencies) are made by Panasonic while the manufacturers of other filters, with 2140 MHz and 2450 MHz center frequencies, are EPCOS and Murata, respectively.

1.5.1 Star Junction Type Multiplexers

The triplexer based on dual-band isolation circuits is shown in Fig. 7(a). Because of using commercial filters, this triplexer has smaller size than the previous work [12]. The center frequencies of commercial filters are 881.5 MHz, 1575 MHz, and 1842.5 MHz, and each isolation circuit allows signal path at the center frequency of its filter. However, it rejects signal at two operating frequencies of other isolation circuits. For designing CRLH TLs used on dual-band isolation circuits, two target input impedances of each filter are necessary and they are represented in Table 1. After calculating required two phases from two input impedances with (6c) or (6d), the circuit parameters of each CRLH TL can be solved from (16)-(19) in Appendix 1. The results are summarized in Table 1. For a CRLH TL, lumped elements and microstrip lines are used. A LH part of a CRLH TL was realized using lumped elements whereas a microstrip line was used for a RH TL part. Fig. 8 (a), (b), and (c) show the simulated and measured results of the triplexer. Fig. 8(a) shows the insertion losses, which are less than 2.2 dB. Fig. 8(b) shows the return losses better than 15.1 dB, and the isolation is greater than 33.5 dB in Fig. 8(c).

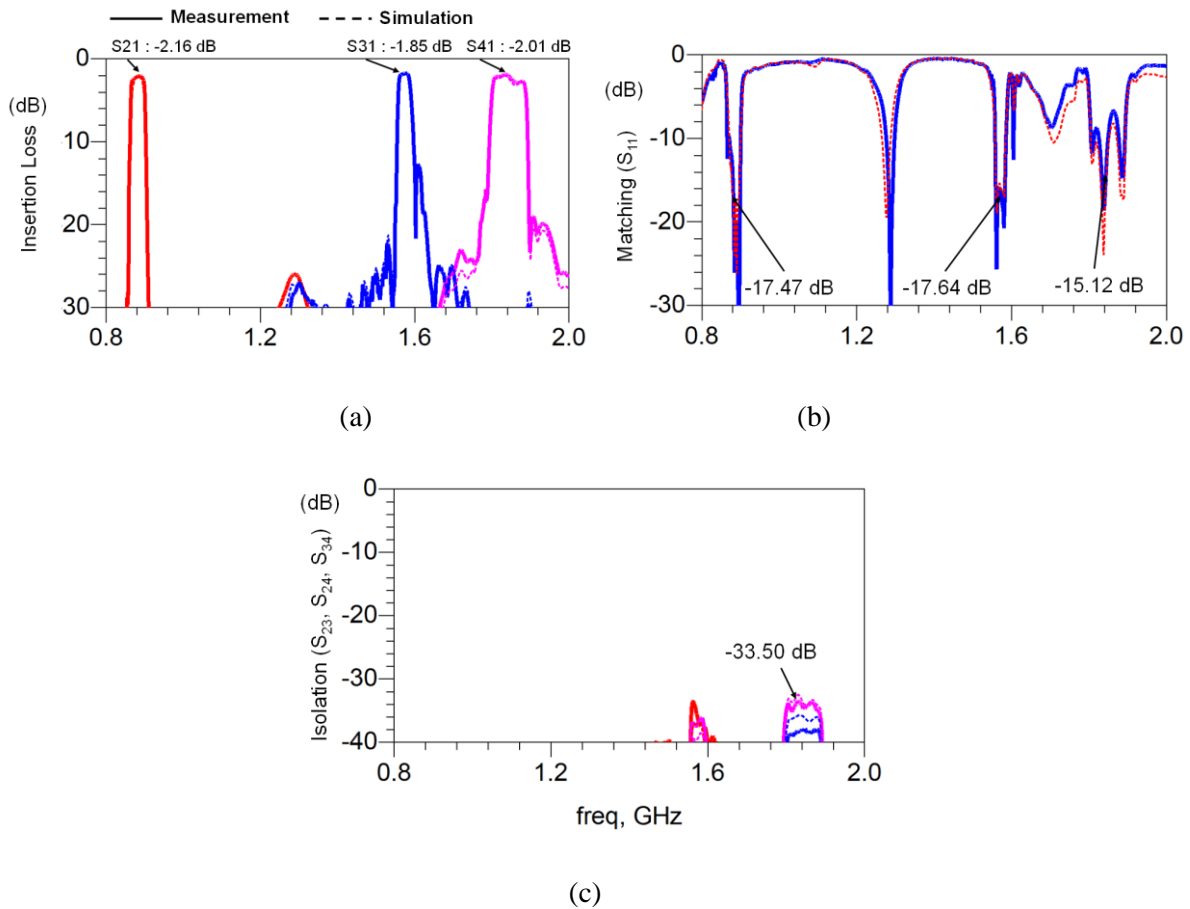


Figure 8. The star-junction triplexer results: (a) Insertion loss. (b) Matching at port 1. (c) Isolation.

Fig. 7(b) shows the fabricated quadruplexer based on tri-band isolation circuits [13]. The center frequencies are 942.5 MHz, 1575 MHz, 2140 MHz, and 2450 MHz. In a manner similar to that of a dual-band isolation circuit, a DL TL for a tri-band isolation circuit can be designed by getting required phases from input impedances of a filter used on the isolation circuit. Then, circuit parameters of the DL TL are solved from (3) to (4) with the required phase responses and corresponding frequencies. Table 2 shows the input impedances of each filter, the required phase responses, and the circuit parameters of the DL TL satisfying isolation characteristic.

Table 1. Design Summary of The Star Junction Triplexer

	Impedance of Filter (Ω)		Required Phase Delay/Advance (deg.)		Circuit Parameter of CRLH TL (L : nH, C : pF)			
					L_R	C_R	L_L	C_L
881.5 MHz Isolation Circuit	1575 MHz -j(25.25)	1842.5 MHz -j(18.20)	ϕ_{11} -101.80	ϕ_{12} -126.30	5.5	2.2	25.3	10.1
1575 MHz Isolation Circuit	881.5 MHz -j(58.65)	1842.5 MHz -j(25.55)	ϕ_{21} 40.45	ϕ_{22} -117.07	6.67	2.67	8.27	3.31
1842.5 MHz Isolation Circuit	881.5 MHz -j(58.70)	1575 MHz -j(23.75)	ϕ_{31} 40.42	ϕ_{32} -115.41	8.86	3.54	6.77	2.71

Table 2. Design Summary of The Star Junction Quadruplexer

	Impedance of Filter (Ω)			Required Phase Delay/Advance (deg.)			Circuit Parameter of DL TL (L : nH, C : pF)					
							L_R	C_R	L_L	C_L	L_p	C_p
942.5 MHz Isolation Circuit	1575 MHz -j(27.75)	2140 MHz -j(13.75)	2450MHz -j(8.10)	ϕ_{11} 60.90	ϕ_{12} -90.41	ϕ_{13} -114.19	1.80	0.72	16.18	6.47	7.50	3.00
1575 MHz Isolation Circuit	942.5 MHz -j(54.25)	2140 MHz -j(16.95)	2450 MHz -j(11.30)	ϕ_{21} -137.33	ϕ_{22} -98.82	ϕ_{23} -117.76	2.75	1.10	20.43	8.17	7.31	2.92
2140 MHz Isolation Circuit	942.5 MHz -j(90.60)	1575 MHz -j(45.15)	2450 MHz -j(27.15)	ϕ_{31} -151.12	ϕ_{32} 47.89	ϕ_{33} -118.66	6.23	2.49	6.01	2.4	9.17	3.67
2450 MHz Isolation Circuit	942.5 MHz j(18.30)	1575 MHz j(44.70)	2140 MHz j(332.65)	ϕ_{41} -69.89	ϕ_{42} 131.84	ϕ_{43} -2.88	3.92	1.57	8.24	3.29	3.12	1.25

A D-CRLH part of a DL TL was realized using lumped elements while a microstrip line was used for a RH TL part. The simulated and measured results of the quadruplexer are shown in Fig. 9(a), (b), and (c). The worst case of insertion losses shown in Fig. 9(a) is 4.07 dB. This result can be improved by further adjusting the reactance of lumped elements. Insertion losses of other output ports are less than 2.9 dB. Fig. 9(b) shows the return losses larger than 11.3 dB, and the isolation is larger than 27.5 dB in Fig. 9(c).

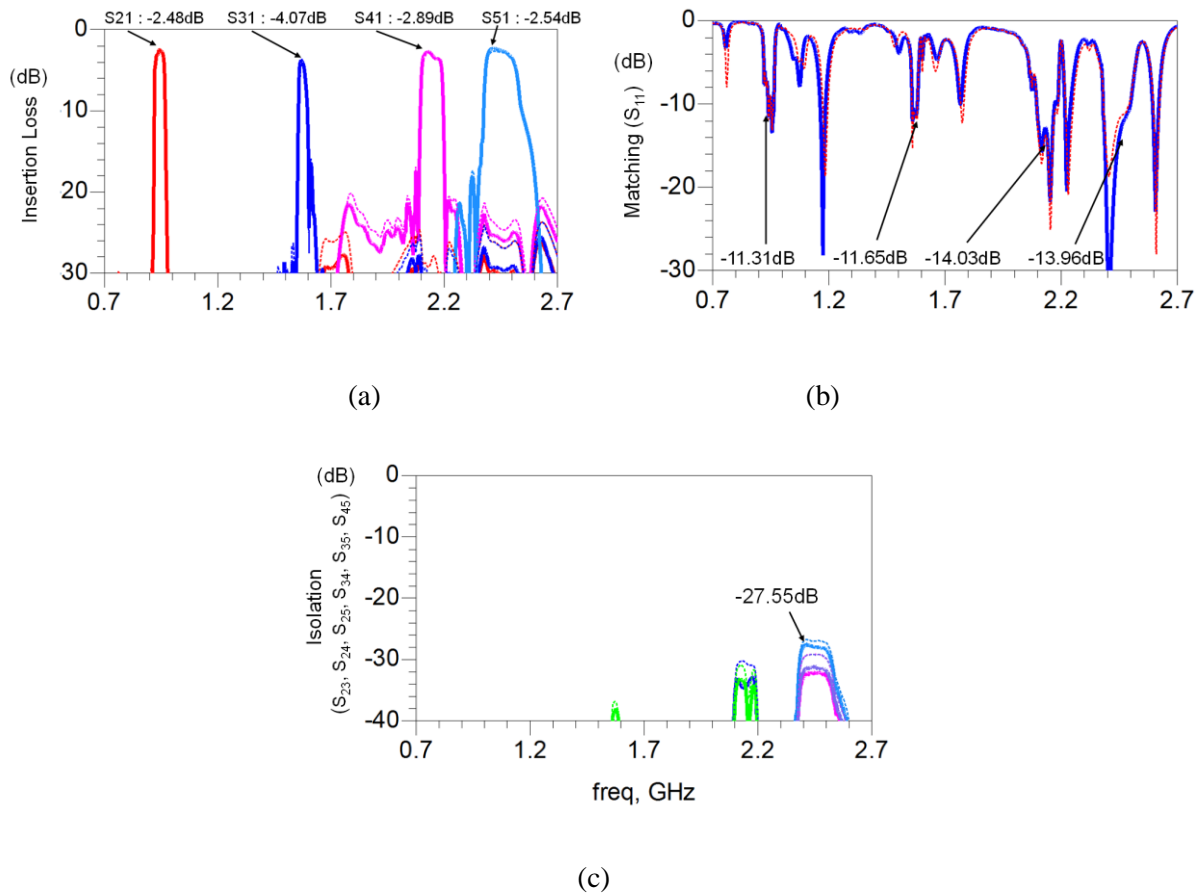
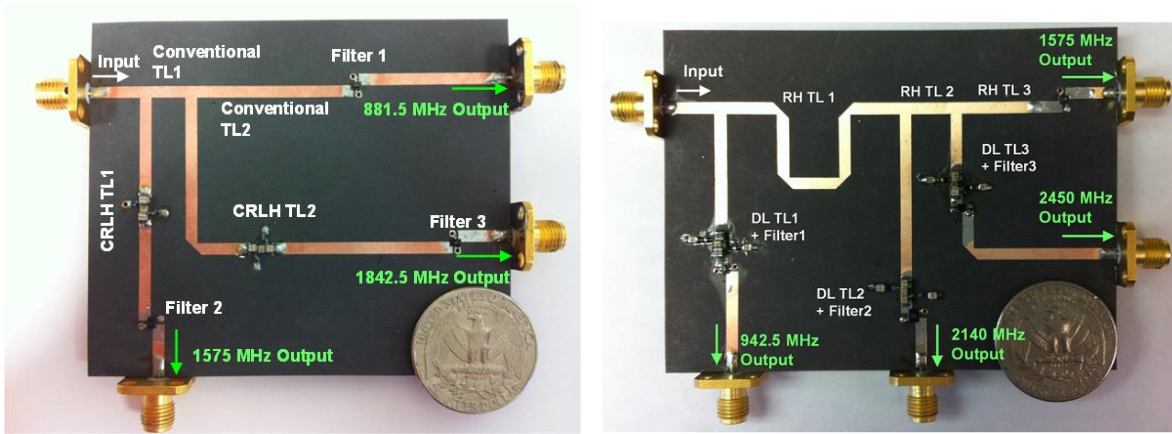


Figure 9. The star-junction quadruplexer results: (a) Insertion loss. (b) Matching at port 1. (c) Isolation.

1.5.2 Manifold Junction Type Multiplexers

Figure 10(a) shows the picture of the manifold junction triplexer based on dual-band isolation circuits [14]. Its center frequencies are 881.5 MHz, 1575 MHz, and 1842.5 MHz. The design process of a dual-band isolation circuit based on a CRLH TL is same with that of the star junction triplexer shown in previous section. However, the special isolation circuit based on RH TLs has different operation concept and design method. At 1575 MHz, the combined phase response of RH TL1 and RH TL2 should satisfy the condition that the input impedance of the special isolation circuit (consisting of two RH TLs and 881.5 MHz filter) is infinite. Similarly,



(a)

(b)

Figure 10. Fabricated manifold-junction multiplexers based on isolation circuits. (a) Triplexer. (b) Quadruplexer.

the phase response of RH TL2 should be determined having open condition with the filter at 1842.5 MHz. Table 3 shows the summary of designed isolation circuits. Fig. 11(a), (b), and (c) show the simulated and measured results of the triplexer. The insertion losses shown in Fig. 11(a) are less than 2.1 dB. Fig. 11(b) shows the return losses better than 14.3 dB, and the isolation is greater than 32.4 dB in Fig. 11(c).

The manifold junction quadruplexer based on tri-band isolation circuits is shown in Fig. 10(b) [15]. The design process is similar with the triplexer case, except that the quadruplexer uses DL TLs and three RH TLs instead of two RH TLs. Table 4 shows the design summary of the quadruplexer. Fig. 12(a), (b), and (c) show the simulated and measured results of the quadruplexer, and simulation results are well matched with measured results. Fig. 12(a) shows the insertion losses, which are less than 4.1 dB. Fig. 12(b) shows that the return losses are better than 13.7 dB, and the isolation is greater than 27.1 dB as shown in Fig. 12(c).

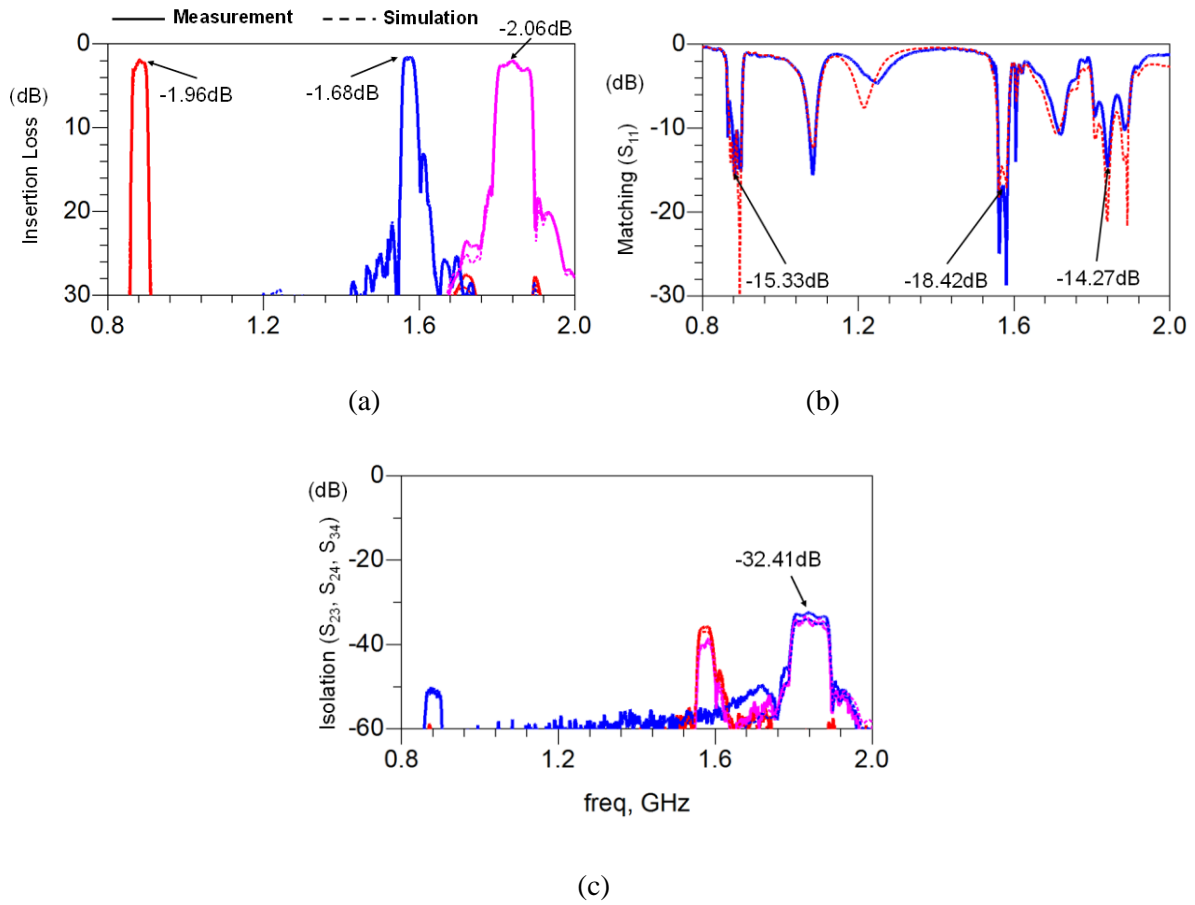


Figure 11. The manifold-junction triplexer results: (a) Insertion loss. (b) Matching at port 1. (c) Isolation.

1.6 Conclusion

Multiplexers based on isolation circuits are presented. The concepts, theories, and design processes have been explained to help the reader design and fabricate proposed multiplexers. These multiplexers have significant advantages. A straightforward and easy design process and the freedom to choose any filters without modification are attractive to a system designer. In this chapter, two conventional junction types of triplexers and quadruplexers are designed and fabricated. Novel junction type, combining method of two filtering circuits (CMTC), will be explained in the following chapter.

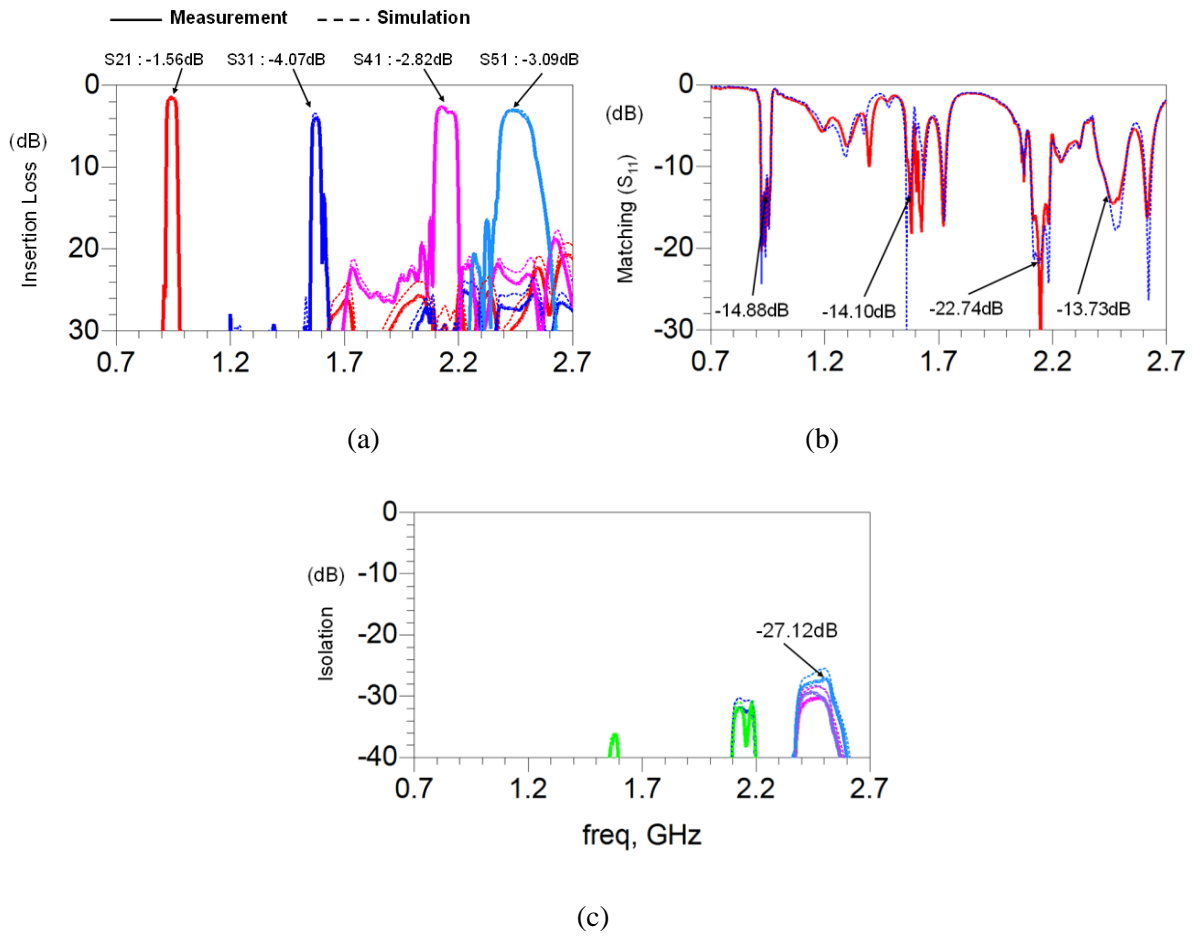


Figure 12. The manifold-junction triplexer results: (a) Insertion loss. (b) Matching at port 1. (c) Isolation.

Table 3. Design Summary of The Manifold Junction Triplexer

	Impedance of Filter (Ω)		Required Phase Delay/Advance (deg.)		Circuit Parameter of CRLH TL (L : nH, C : pF)			
					L_R	C_R	L_L	C_L
1575 MHz Isolation Circuit	881.5 MHz -j(58.65)	1842.5 MHz -j(25.55)	ϕ_{21} 40.45	ϕ_{22} -117.07	6.67	2.67	8.27	3.31
1842.5 MHz Isolation Circuit	881.5 MHz -j(58.70)	1575 MHz -j(23.75)	ϕ_{31} 40.42	ϕ_{32} -115.41	8.86	3.54	6.77	2.71
881.5 MHz Isolation Circuit	1575 MHz -j(25.25)	1842.5 MHz -j(18.20)	ϕ_{11} -116.79	ϕ_{12} -110.00	X	X	X	X

Table 4. Design Summary of The Manifold Junction Quadruplexer

	Impedance of Filter (Ω)			Required Phase Delay/Advance (deg.)			Circuit Parameter of DL TL (L : nH, C : pF)					
							L_R	C_R	L_L	C_L	L_p	C_p
942.5 MHz Isolation Circuit	1575 MHz -j(27.75)	2140 MHz -j(13.75)	2450MHz -j(8.10)	ϕ_{11} 60.90	ϕ_{12} -90.41	ϕ_{13} -114.19	1.80	0.72	16.18	6.47	7.50	3.00
2140 MHz Isolation Circuit	942.5 MHz -j(90.60)	1575 MHz -j(45.15)	2450 MHz -j(27.15)	ϕ_{31} -151.12	ϕ_{32} 47.89	ϕ_{33} -118.66	6.23	2.49	6.01	2.4	9.17	3.67
2450 MHz Isolation Circuit	942.5 MHz j(18.30)	1575 MHz j(44.70)	2140 MHz j(332.65)	ϕ_{41} -69.89	ϕ_{42} 131.84	ϕ_{43} -2.88	3.92	1.57	8.24	3.29	3.12	1.25
1575 MHz Isolation Circuit	942.5 MHz -j(54.25)	2140 MHz -j(16.95)	2450 MHz -j(11.30)	ϕ_{21} -137.30	ϕ_{22} -108.80	ϕ_{23} -102.80	X	X	X	X	X	X

1.7 References

- [1] G. Macchiarella, "Synthesis of Star-Junction Multiplexer," *IEEE Microwave Magazine*, vol. 12, no.6, pp. 101-109, Oct. 2011.
- [2] G. Macchiarella and S. Tamiazzo, "Synthesis of Star-Junction Multiplexers," *IEEE Trans. Microwave Theory Tech.*, vol. 58, no. 12, pp. 3732–3741, Dec. 2010.
- [3] R. J. Cameron and M. Yu, "Design of manifold-coupled multiplexers," *IEEE Microwave Magazine*, vol. 8, no.5, pp. 46-59, Oct. 2007.

- [4] E.G. Cristal and G.L. Matthaei, "A Technique for the Design of Multiplexers Having Contiguous Channels," *IEEE Trans. Microwave Theory Tech.*, vol. 10, pp. 83-93, Jan. 1964.
- [5] J.D. Rhodes and R. Levy, "A generalized multiplexer theory," *IEEE Trans. Microwave Theory Tech.*, vol. 27, no. 2, pp. 99-111, Feb. 1979.
- [6] K. L. Wu and W. Meng, "A direct synthesis approach for microwave filters with a complex load and its application to direct diplexer design," *IEEE Trans. Microwave Theory Tech.*, vol. 55, no. 5, pp. 1010–1017, May 2007.
- [7] J.D. Rhodes and R. Levy, "Design of general manifold multiplexers," *IEEE Trans. Microwave Theory Tech.*, vol. 27, no. 2, pp. 111–123, Feb. 1979.
- [8] A.E. Atia, "Computer aided design of waveguide multiplexers," *IEEE Trans. Microwave Theory Tech.*, vol. MTT-22, pp. 322-336, Mar. 1974.
- [9] M.A. Ismail, D. Smith, A. Panariello, Y. Wang, and M. Yu, "EM-based design of large-scale dielectric resonator filters and multiplexers by space mapping," *IEEE Trans. Microwave Theory Tech.*, vol. 52, no. 1, pp. 386–392, Jan. 2004.
- [10] I. Lin, M. Vincentis, C. Caloz, T. Itoh, "Arbitrary dual-band components using composite right/left-handed transmission lines," *IEEE Trans. Microwave Theory Tech.*, vol. 52, pp. 1142–1149, April 2004.
- [11] A. Rennings, T. Liebig, C. Caloz, et al., "Double-Lorentz transmission line metamaterial and its application to tri-band devices," *2007 IEEE MTT-S Int. Microwave Symp.*, pp. 1427-1430, June 2007.
- [12] H. Lee and T. Itoh, "Dual band isolation circuits based on CRLH transmission lines for triplexer application," *2011 Asia-Pacific Microwave Conference*, pp. 542-545, Dec. 2011.
- [13] H. Lee and T. Itoh, "Tri-band isolation circuits based on double-Lorentz transmission lines for quadruplexers," *2012 European Microwave Conference*, pp. 585-588, Oct. 2012.
- [14] H. Lee and T. Itoh, "Hybrid combination of dual band isolation circuits based on conventional and CRLH transmission lines for triplexers," *2012 IEEE MTT-S Int. Microwave Symp.*, June 2012.
- [15] H. Lee and T. Itoh, "Hybrid combination of tri-band isolation circuits based on conventional and double-Lorentz transmission lines for quadruplexers," *2013 International Symposium on Electromagnetic Theory*, May 2013.

- [16] C. Caloz and T. Itoh, *Electromagnetic Metamaterials, Transmission Line Theory and Microwave Applications*, New York: Wiley, 2005.
- [17] C. Caloz, "Dual composite right/left-handed (D-CRLH) transmission line metamaterial," *IEEE Microwave Wireless Compon. Lett.*, vol. 16, no. 11, pp. 585-587, November 2006.
- [18] H. Lee and S. Nam, "Triband branch line coupler using double-Lorentz transmission lines," *Microwave and Optical Technology Lett.*, vol. 50, no. 5, pp. 1174-1177, May 2008.
- [19] D. M. Pozar, *Microwave Engineering*, J. Willey & Sons, 2005.

Chapter 2 Combining Method of Two Filtering Circuits Based on Isolation Circuits

2.1 Introduction

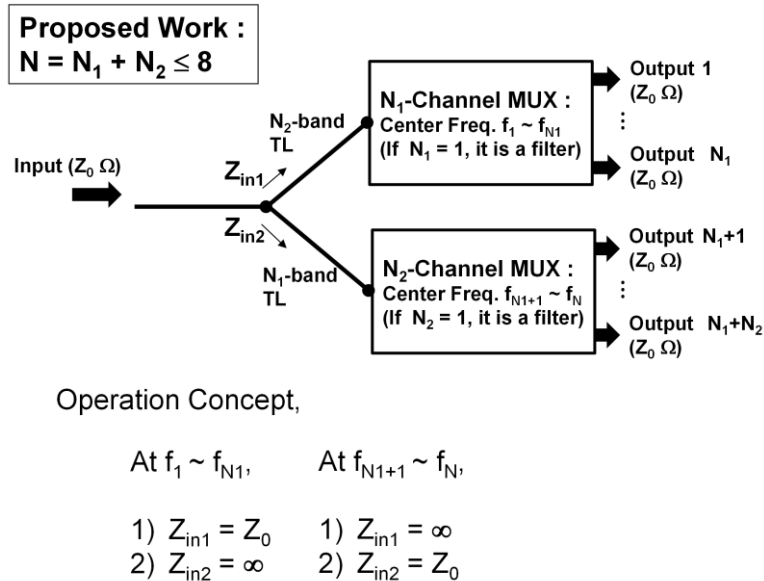


Figure 13. Diagram and operation concept of a multiplexer based on CMTC.

In order to support multiband communication systems, a multiplexer is necessary if one antenna covers all the necessary spectra and has thus become an important component. The function of a multiplexer is: 1) to send a signal having a specific frequency to a target output, and vice versa, and 2) to prevent the signal from entering other channels. For this functionality, many design concepts are investigated and categorized by manifold type and star junction type. A traditional multiplexer design generally requires the modification of filters and a complex optimization process. However, the use of a commercial filter or a multiplexer without modification, and a simple multiplexer design method are occasionally necessary for a system designer. In the previous chapter, multiplexers based on isolation circuits are proposed and they satisfy such demands.

In this chapter, an isolation circuit concept is further expanded by combining two multiplexers thereby increasing the number of channels. An isolation circuit is composed of a transmission line (TL) connected to a filter or a multiplexer, and the combination of two isolation circuits has multiplexer functionality. Figure 13 shows the schematic of the proposed method. On the contrary with the junction type shown in chapter 1, a multiplexer can be a component of an isolation circuit (not a single filter) and only two isolation circuits are necessary. Hence, a channel number for this type of multiplexer can easily be increased, and is simple to design and fabricate. Also, commercial filters or multiplexers can be used, because it is not necessary to modify filters or multiplexers used in this methodology. First, the concept of the multiplexer suggested in this chapter is explained. Then the general design process for the proposed multiplexer is shown. The simulated and measured results of the proposed multiplexers are also provided.

2.2 Concept of Proposed Method

The diplexer shown in Fig. 1 (in chapter 1) is the starting point for a multiplexer based on isolation circuits. In this case, single-band isolation circuits are used and the limitation, namely that it has an isolation characteristic at only one frequency, arises from a conventional TL. However, research of a multiband metamaterial TL makes a multiband isolation circuit possible, and brings increased multiplexer channels. The channel extension method of Fig. 13 uses two isolation circuits, as shown in the diplexer of Fig. 1. The difference between the diplexer and the proposed multiplexer is the use of a multiband TL and a multiplexer, instead of a conventional TL and a filter. The channel number of a this multiplexer can be increased by combining two multiplexers, or a filter and a multiplexer. The total number of channels, N , is

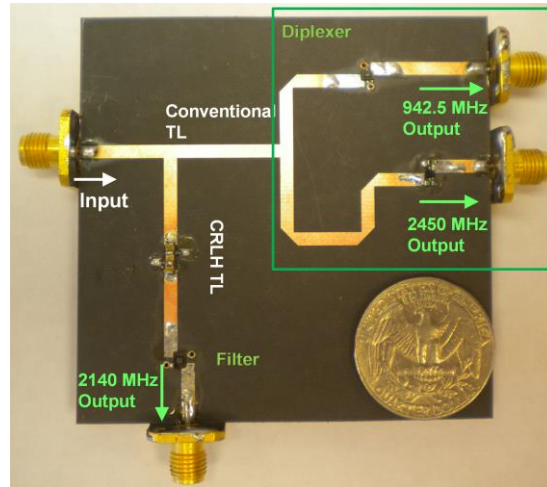


Figure 14. Triplexer based on CMTC.

$$N = N_1 + N_2 \quad (8)$$

where N_1 and N_2 are the channel numbers of each multiplexer (if N_1 or N_2 is one, it is a filter), and four is the maximum value, because a TL having a five-band characteristic does not exist at this time. Hence the maximum value of N is eight.

The operation concept is also represented in Fig. 13. The first isolation circuit, comprising an N_2 -band TL and an N_1 -channel multiplexer, is isolated from the input port at the center frequencies of another isolation circuit (from f_{N_1+1} to $f_{N_1+N_2}$). On the contrary, the second isolation circuit, consisting of an N_1 -band TL and an N_2 -channel multiplexer, has an isolation characteristic at frequencies from f_1 to f_{N_1} . Therefore, one circuit allows a signal path while the other circuit prevents a signal flow. For example, a signal having an f_1 frequency cannot enter the second isolation circuit, but the signal goes through the N_2 -band TL of the first isolation circuit. Thereafter the signal is only detected at output port 1 because of the frequency selective characteristic of the N_1 -channel multiplexer. For verification of the concept, a triplexer ($N_1 = 2$

and $N_2 = 1$), a quadruplexer ($N_1 = 2$ and $N_2 = 2$), and a five-channel multiplexer ($N_1=3$ and $N_2=2$)

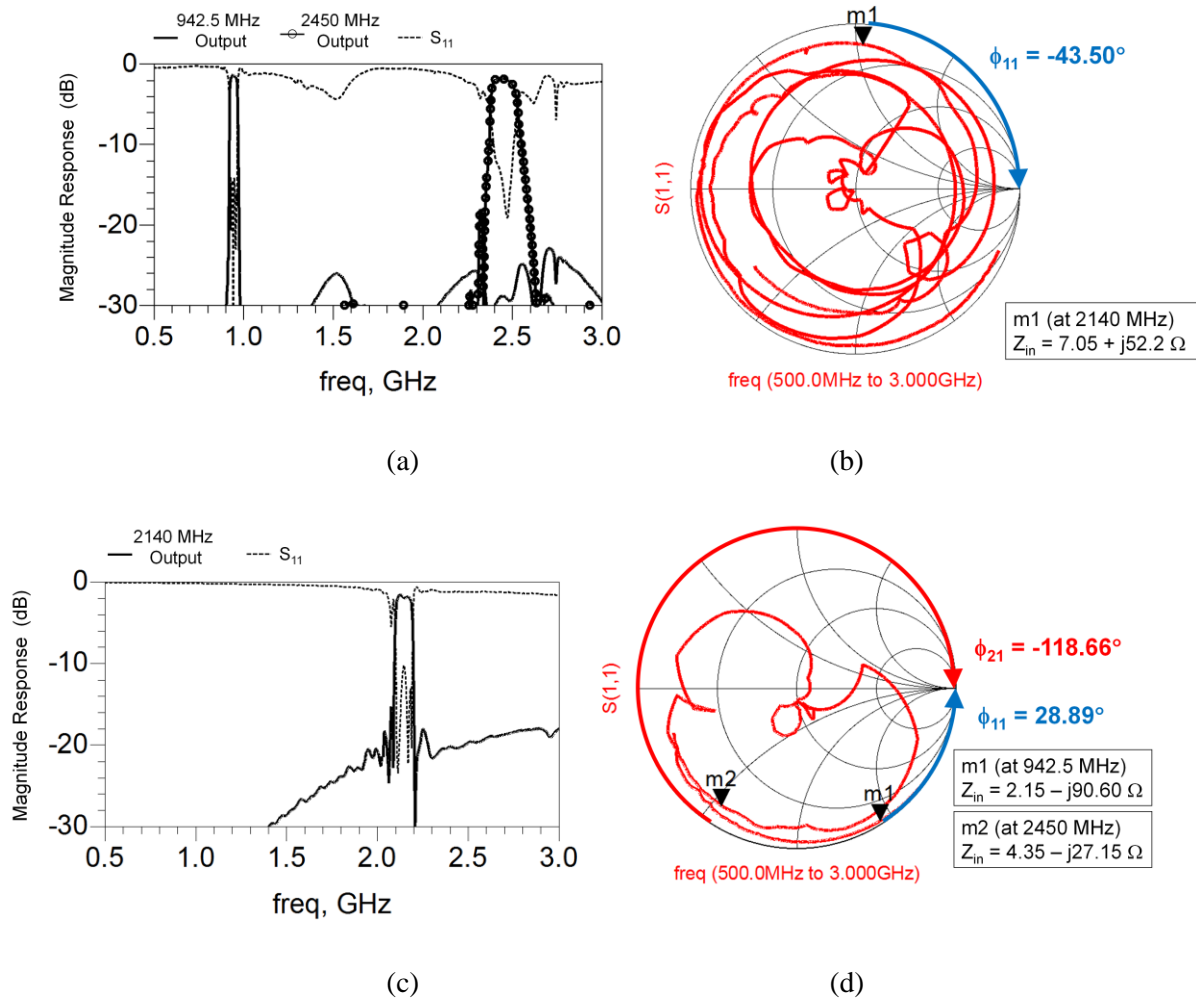


Figure 15. Performances of the diplexer and the filter for the triplexer. (a) Magnitude response of the diplexer. (b) Input impedance of the diplexer shown on the Smith chart. (c) Magnitude response of the filter. (d) Input impedance of the filter shown on the Smith chart.

are investigated.

2.3 Design Process of Multiplexers Based on CMTC

In this section, the design process of the multiplexer is presented. For clear explanation, this process is applied to the triplexer, shown in Fig. 14, using the diplexer, of which the center

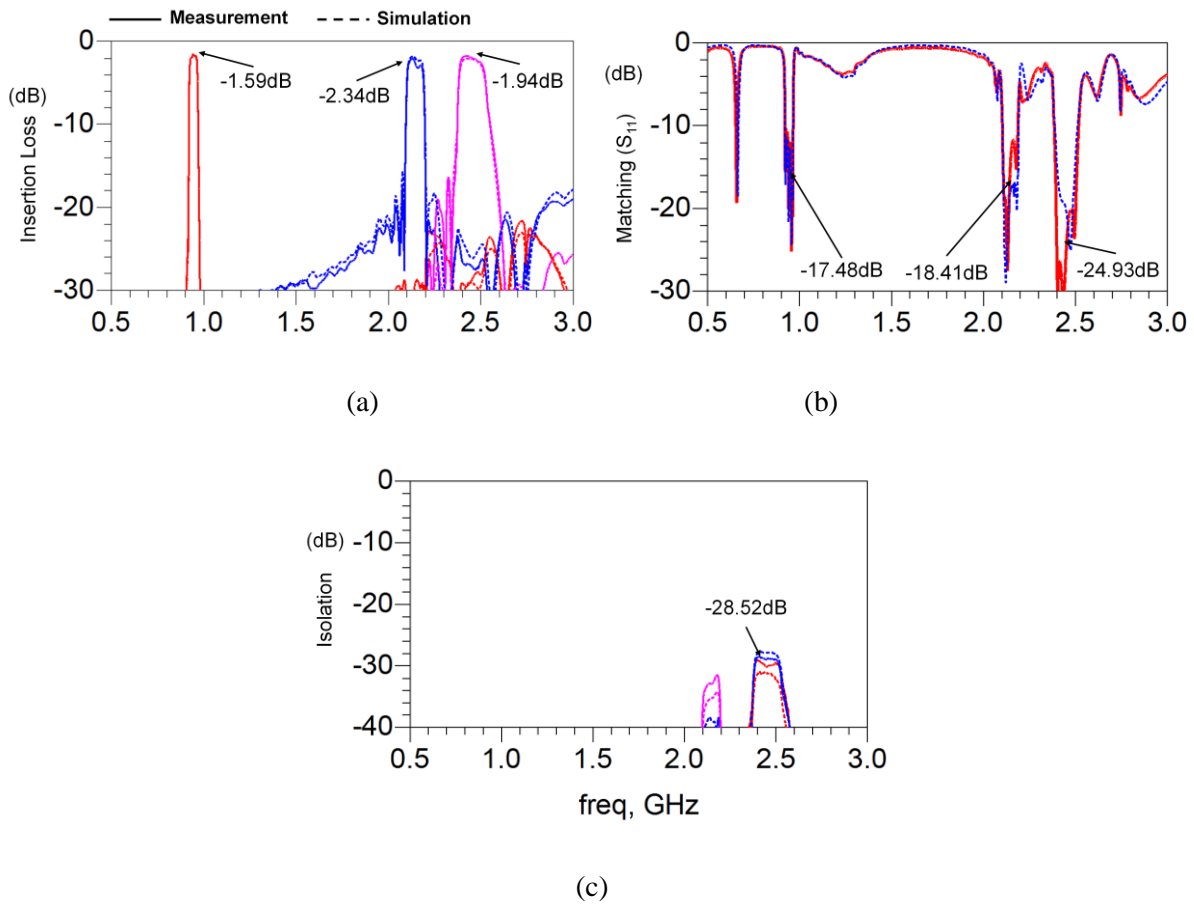


Figure 16. Frequency response of the triplexer. (a) Insertion loss. (b) Matching at port 1. (c) Isolation.

frequencies are 942.5 MHz and 2450 MHz, and the 2140 MHz filter. For reference, the diplexer follows the design concept of Fig. 1. Figure 15 shows the measured magnitude characteristics and input impedances of the diplexer and the 2140 MHz Filter.

1. Find the input impedances of each multiplexer or filter at operating frequencies of the other isolation circuit. In the triplexer case, it is necessary to find the input impedance of the diplexer at 2140 MHz (marker 1 in Fig. 15(b)) and the input impedances of the 2140 MHz filter at 942.5 MHz and 2450 MHz (markers 1 and 2 on Fig. 15(d)).
2. Find the proper phase shifts for each multiplexer or filter using Eq. (6c) or (6d) in order to obtain an open condition at target frequencies. In the triplexer case, the necessary phase

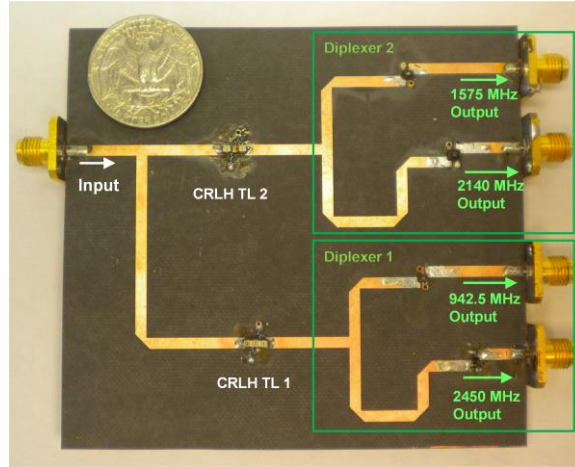


Figure 17. Quadruplexer based on CMTC.

delay ϕ_{11} for the diplexer is -43.50° , and the required phase shifts ϕ_{21} and ϕ_{22} for the filter are 28.89° and -118.66° , respectively.

3. Obtain the circuit parameters of the TL satisfying the required phase shift at the target frequency. If there are two phase shifts at two target frequencies, a CRLH TL, having a dual-band characteristic, is necessary, and Eq. (16)-(19) in Appendix 1 can be used for the circuit parameters of the CRLH TL [1]. Equations (3) and (4) in chapter 1 are necessary for solving the circuit parameters of a DL TL and are used in cases where there are three phase shifts at three target frequencies [2]. In the triplexer case, the circuit parameters of the CRLH TL for the filter are solved by submitting $(\phi_{21}, \phi_{22}) = \{0.50 \text{ rad. } (28.89^\circ), -2.07 \text{ rad. } (-118.66^\circ)\}$ and $(\omega_{21}, \omega_{22}) = (2 \times \pi \times 942.5 \text{ MHz}, 2 \times \pi \times 2450 \text{ MHz})$ pair and $N = 2$ to Eq. (16)-(19) in Appendix 1. The circuit parameters of the CRLH TL are $L_R = 4.37 \text{ nH}$, $C_R = 1.73 \text{ pF}$, $L_L = 11.06 \text{ nH}$, and $C_L = 4.42 \text{ pF}$. For the diplexer case, a conventional RH TL, having an electrical length of -43.5° at 2140 MHz is necessary.
4. Combine the multiplexer or filter with the corresponding TL. In the triplexer case, the CRLH TL, designed in Step 3, and the filter make one dual-band isolation circuit, and the

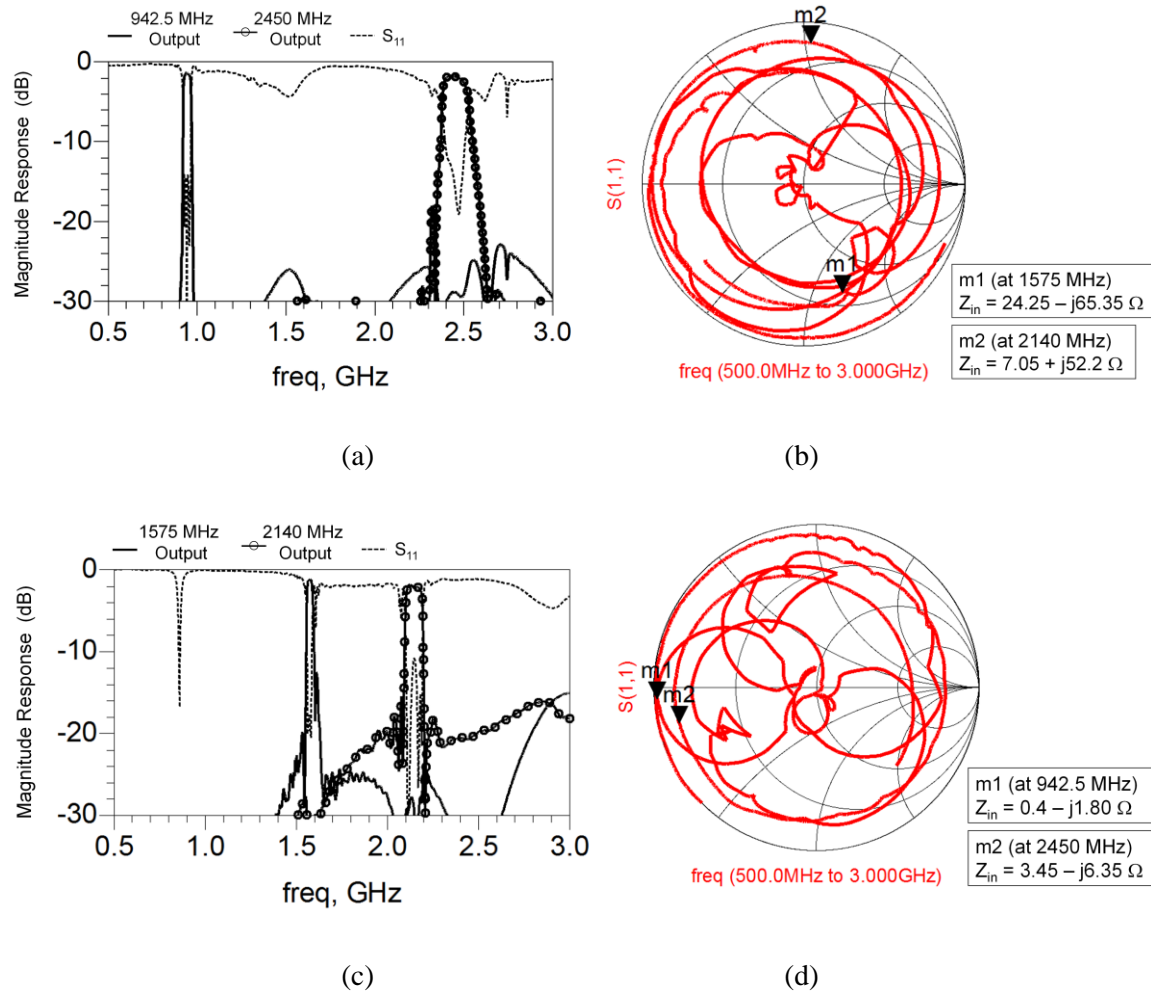


Figure 18. Performances of the diplexers for the quadruplexer. (a) Magnitude response of the diplexer 1. (b) Input impedance of the diplexer 1 shown on the Smith chart. (c) Magnitude response of the diplexer 2. (d) Input impedance of the diplexer 2 shown on the Smith chart.

combination of the diplexer and the conventional TL makes another isolation circuit.

5. Connect two isolation circuits with an input port.

2.4 Multiplexers Based on CMTC

In order to verify the design concept, the triplexer, the quadruplexer, and the five-channel multiplexer are designed and fabricated. Some information regarding the triplexer is given in the previous section, and its operating frequencies are 942.5 MHz, 2140 MHz, and 2450 MHz. The

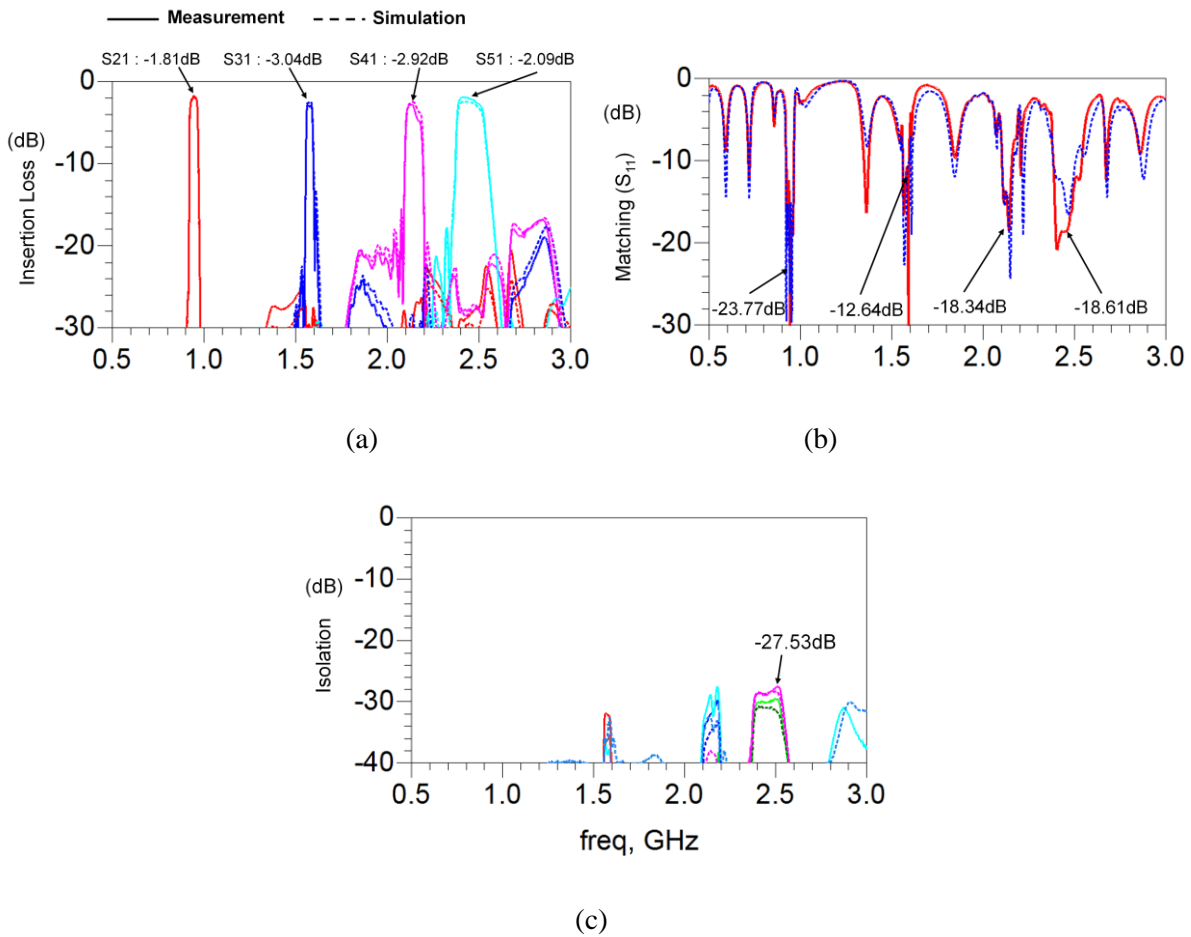


Figure 19. Frequency response of the quadruplexer. (a) Insertion loss. (b) Matching at port 1. (c) Isolation.

quadruplexer is a combination of two dual-band isolation circuits and operates at 942.5 MHz, 1575 MHz, 2140 MHz, and 2450 MHz. The tri-band isolation circuit, comprising the diplexer and the DL TL, and the dual-band isolation circuit, consisting of the triplexer and the CRLH TL, together make the five-channel multiplexer. Its center frequencies are 942.5 MHz, 1575 MHz, 1842.5 MHz, 2140 MHz, and 2450 MHz. A RT/Duroid 5870 substrate ($\epsilon_r = 2.33$, height = 0.787 mm) and commercial SAW filters are used for multiplexers. Three filters (having 942.5 MHz, 1575 MHz, and 1842.5 MHz center frequencies) are made by Panasonic and the manufacturers

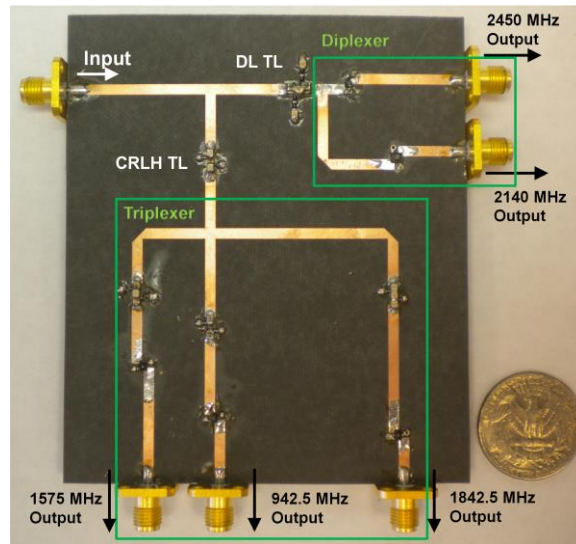


Figure 20. Five-channel multiplexer based on CMTC.

of other filters, with 2140 MHz and 2450 MHz center frequencies, are from EPCOS and Murata, respectively.

2.4.1 Triplexer

In Section 2.3, the design process of the triplexer is investigated, and the derived data are summarized in Table 5. The triplexer is composed of the single band isolation circuit, a combination of the diplexer and the conventional TL, and the dual band isolation circuit, which consists of the filter and the CRLH TL. Figure 14 shows the fabricated triplexer. Lumped elements and microstrip lines comprise the CRLH TL. A LH TL part of the CRLH TL was realized using lumped elements, and a microstrip line was used for the RH TL part. For a single band isolation circuit, the microstrip line, having -43.50° phase delay at 2140 MHz, is used.

Figure 16 shows the simulated and measured results of the triplexer. Figure 16(a) shows the insertion losses, which are less than 2.36 dB. The return losses, shown in Fig. 16(b), are larger than 17.48 dB. Figure 16(c) shows that the isolation is greater than 28.52 dB.

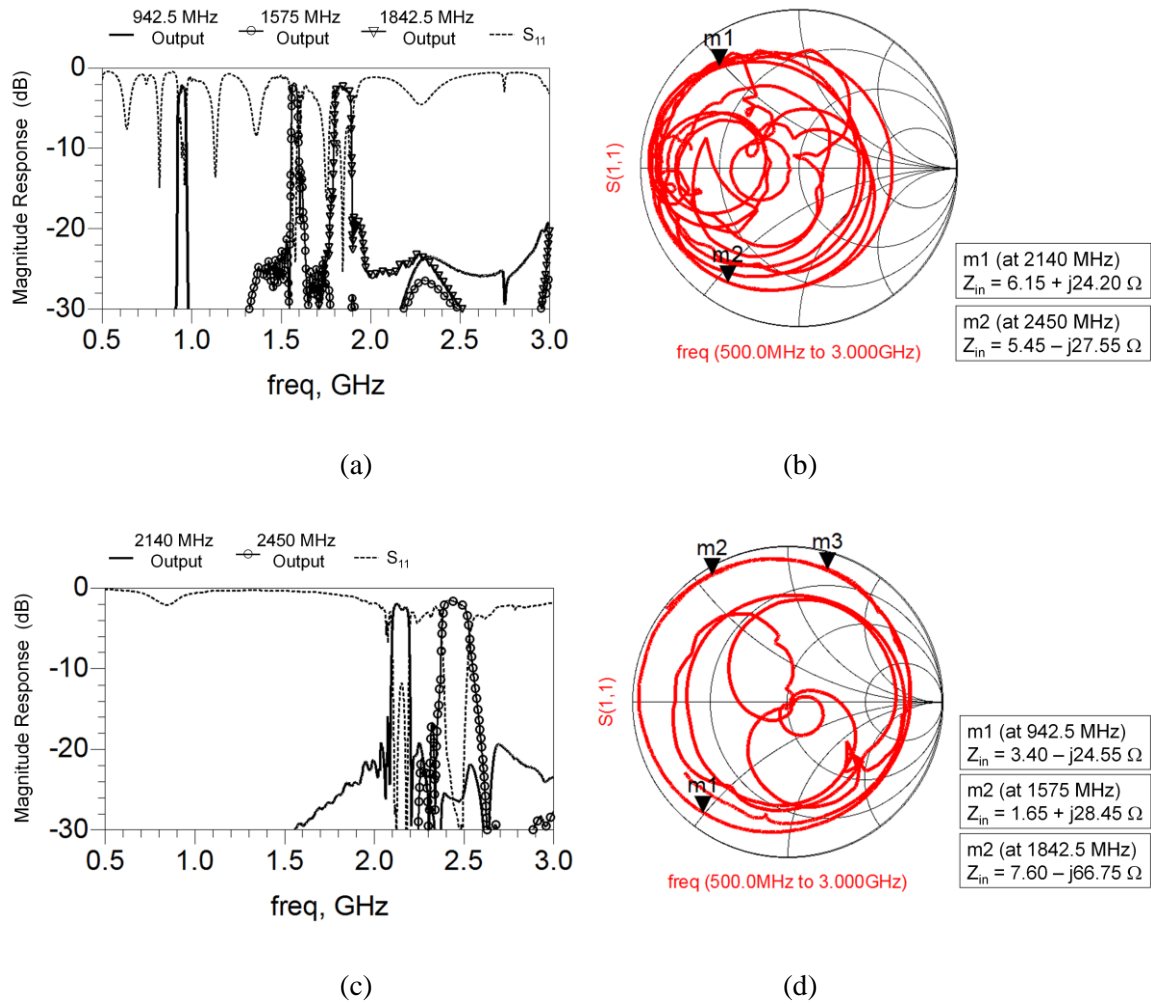


Figure 21. Performances of the triplexer and the diplexer for the five-channel multiplexer. (a) Magnitude response of the triplexer. (b) Input impedance of the triplexer shown on the Smith chart. (c) Magnitude response of the diplexer. (d) Input impedance of the diplexer shown on the Smith chart.

2.4.2 Quadruplexer

Figure 17 shows the fabricated quadruplexer. The quadruplexer is composed of two diplexers, diplexer 1 and diplexer 2, and two CRLH TLs: CRLH TL 1 and CRLH TL 2. Both diplexers follow the concept of Fig. 1. Each diplexer and its corresponding CRLH TL make a dual-band isolation circuit. Figure 18 shows the measured magnitude characteristics and input impedances

of diplexer 1 and diplexer 2. The diplexer 1 is the same diplexer used in the triplexer, but it should be isolated from the input port at two target frequencies, 1575 MHz and 2140 MHz, after combining the CRLH TL 1. The two input impedances, at 942.5 MHz and 2450 MHz, of diplexer 2 are represented in Fig. 18(d). From this information, the circuit parameters of CRLH TLs for the isolation circuits are solved by the process represented in Section IV. Table 6 shows the summary of the quadruplexer design.

Simulated and measured results of the quadruplexer are shown in Fig. 19. The insertion losses are less than 3.04 dB and the return losses are larger than 12.64 dB. In addition, the isolation is

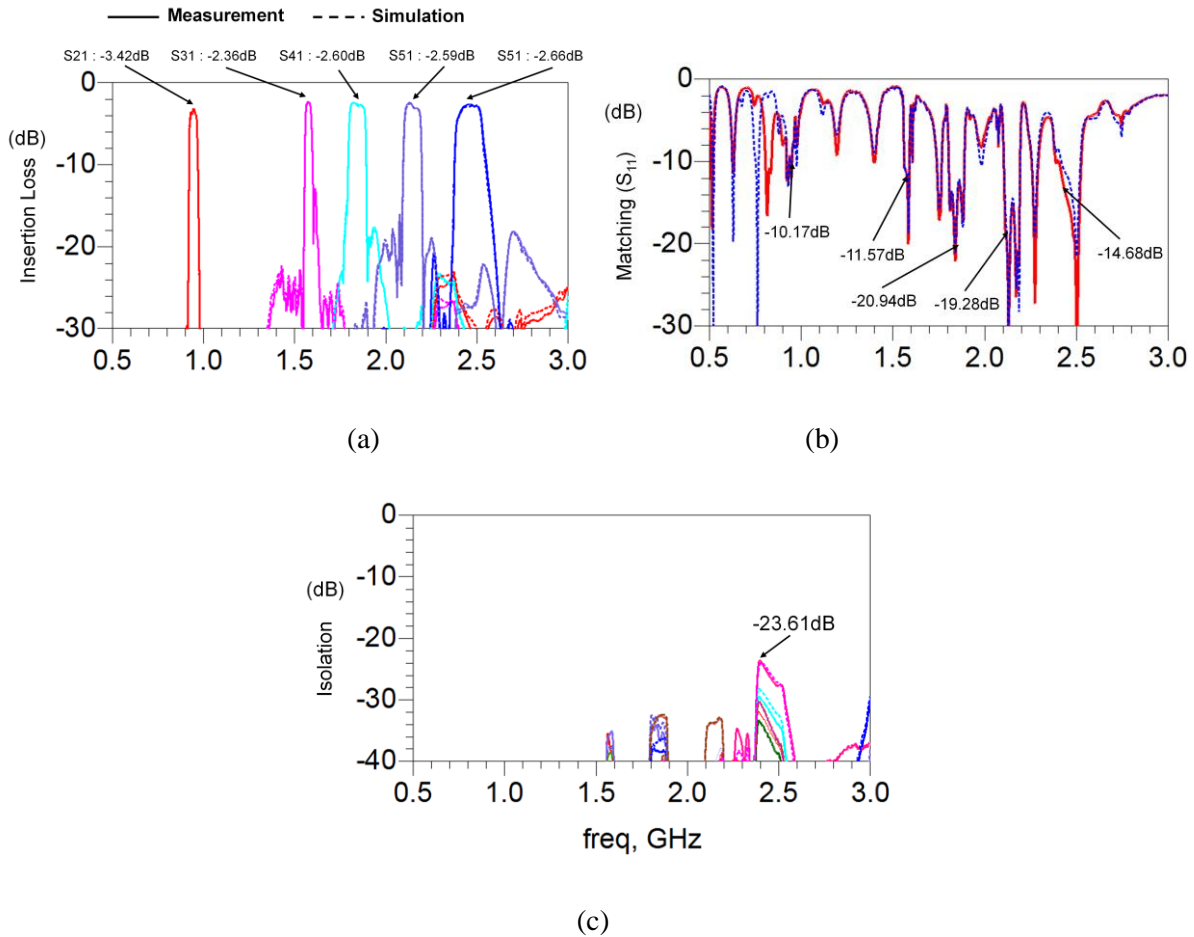


Figure 22. Frequency response of the five-channel multiplexer. (a) Insertion loss. (b) Matching at port 1. (c) Isolation.

larger than 27.53 dB.

2.4.3 Five-Channel Multiplexer

The five-channel multiplexer is composed of a dual-band isolation circuit and a tri-band isolation circuit. A dual-band isolation circuit consists of a CRLH TL and a triplexer. The triplexer is based on dual-band isolation circuits [3]. The center frequencies of the triplexer are 942 MHz, 1575 MHz, and 1842.5 MHz. A tri-band isolation circuit is the combination of a DL TL [4] and a diplexer, which is designed by the concept of Fig. 1, and operates at 2140 MHz and 2450 MHz. Figure 20 shows the fabricated five-channel multiplexer. The measured results of the triplexer and the diplexer are shown on Fig. 21. Markers 1 and 2 on Fig. 21(b) show the input impedances (represented on the Smith chart) of the triplexer at two target frequencies 2140 MHz and 2450 MHz. Figure 21(d) shows the input impedances of the diplexer represented on the Smith chart. Markers 1, 2, and 3 represent three input impedances at center frequencies of the triplexer, 942.5 MHz, 1575 MHz, and 1842.5 MHz. The required circuit parameters of the CRLH TL and the DL TL are solved by the process represented in section 2.3. By the way, the required RH phase delays of markers 2 and 3 in Fig. 21(d) are -60.35° and -36.62° , respectively. But a DL TL does not allow these phase responses because the frequency of marker 2 is smaller than that of marker 3. Hence, the adjusting constants ψ_{22} ($+20^\circ$) and ψ_{23} (-20°) are used for the tri-band isolation circuit. The design summary of the five-channel multiplexer is shown in Table 7. Figure 22 shows the simulated and measured results of the five-channel multiplexer. The worst case for the insertion loss is 3.42 dB at 942.5 MHz. In other pass bands, insertion losses are less than 2.66 dB. Figure 11(b) shows the return losses, and they are larger than 10.17 dB. Isolation is better than 23.61 dB.

2.5 Conclusion

Combining method of two filtering circuits (CMTC) for multiplexers has been presented. The concept, theories, and design process have been explained to help the reader design and fabricate a proposed multiplexer. With this approach, the number of channels can easily be increased by the sum of channels of two multiplexers. The advantages of multiplexers introduced in chapter 1 are still maintained. In this chapter, the triplexer, the quadruplexer, and the five-channel multiplexer are designed and fabricated. The measured results of each multiplexer show good agreement with the simulation results.

Table 5. Summary of Triplexer Based on CMTC

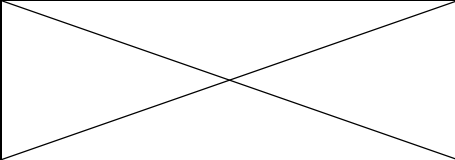
		Circuit 2 (CRLH TL + Filter)		Circuit 1 (RH TL + Diplexer)	
Impedance of Filter or Diplexer (Ω)		At 942.5 MHz	2.15 - j90.60	At 2140 MHz	7.05 + j52.2
		At 2450 MHz	4.35 - j27.15		
Required Phase Response (deg.)		ϕ_{21}	28.89	ϕ_{11}	-43.50
		ϕ_{22}	-118.66		
Circuit Parameters of CRLH TL (L : nH, C : pF)	L_R	4.32			
	C_R	1.73			
	L_L	11.06			
	C_L	4.42			

Table 6. Summary of Quadruplexer Based on CMTC

		Circuit 1 (CRLH TL1 + Diplexer 1)		Circuit 2 (CRLH TL2 + Diplexer 2)	
Impedance of Diplexer (Ω)		At 1575 MHz	24.25 - j65.35	At 942.5 MHz	0.4 - j1.80
		At 2140 MHz	7.05 + j52.20	At 2450 MHz	3.45 - j6.35
Required Phase Response (deg.)		ϕ_{11}	-144.93	ϕ_{21}	87.94
		ϕ_{12}	-223.50	ϕ_{22}	-97.29
Circuit Parameters of CRLH TL (L : nH, C : pF)	L_R	8.27		4.36	
	C_R	3.31		1.74	
	L_L	13.56		6.58	
	C_L	5.42		2.63	

Table 7. Summary of Five-Channel Multiplexer Based on CMTC

	Circuit 1 (CRLH TL + Triplexer)		Circuit 2 (DL TL + Diplexer)	
	Impedance of Triplexer or Diplexer (Ω)	At 2140 MHZ	$6.15 + j24.20$	At 942.5 MHZ
At 2450 MHZ		$5.45 - j27.55$	At 1575 MHZ	$1.65 + j28.45$
			At 1842.5 MHZ	$7.60 - j66.75$
Required Phase Response (deg.)	ϕ_{11}	-77.56	ϕ_{21}	63.78
	ϕ_{12}	-104.19	ϕ_{22}	-40.35 ($\psi_{22} = +20^\circ$)
			ϕ_{23}	-56.62 ($\psi_{23} = -20^\circ$)
Circuit Parameters of CRLH TL (L : nH, C : pF)	L_R	4.36	L_R	6.43
	C_R	1.74	C_R	2.57
	L_L	7.51	L_L	15.80
	C_L	3.01	C_L	6.32
			L_P	5.72
			C_P	2.29

2.6 References

- [1] I. Lin, M. Vincentis, C. Caloz, T. Itoh, "Arbitrary dual-band components using composite right/left-handed transmission lines," *IEEE Trans. Microwave Theory Tech.*, vol. 52, pp. 1142–1149, April 2004.
- [2] A. Rennings, T. Liebig, C. Caloz, et al., "Double-Lorentz transmission line metamaterial and its application to tri-band devices," *2007 IEEE MTT-S Int. Microwave Symp.*, pp. 1427-1430, June 2007.
- [3] H. Lee and T. Itoh, "Dual band isolation circuits based on CRLH transmission lines for triplexer application," *2011 Asia-Pacific Microwave Conference*, pp. 542-545, Dec. 2011.
- [4] H. Lee and T. Itoh, "Tri-band isolation circuits based on double-Lorentz transmission lines for quadruplexers," *2012 European Microwave Conference*, to be published.

Chapter 3 Contiguous Channel Triplexer Based on CMTC

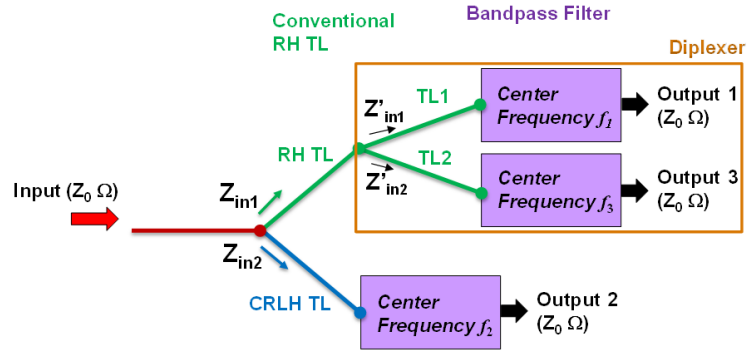
3.1 Introduction

The star-junction or the manifold-junction triplexer based on dual-band isolation circuits is introduced in chapter 1 [1]. Each isolation circuit isolates itself from the input port at two operating frequencies of other circuits. In this concept, a composite right/left handed (CRLH) TL having dual-band characteristic is essential [2][3], because the isolation circuits used for the triplexer should be designed to have the isolation characteristic at two frequencies. By the way, both junction types are less effective for a contiguous or narrow guard band triplexer than the novel junction concept, the combining method of two filtering circuits (CMTC) shown in Fig. 23. The reason for this comes from the intrinsic characteristic of a band-pass filter (BPF) and a phase response of a CRLH TL. In the following section, detailed investigation will be discussed.

In this chapter, the contiguous channel triplexer based on CMTC is presented. The concept of the triplexer and the theory for an isolation circuit are explained. Also, the reason why the proposed method is attractive for a contiguous channel triplexer design is investigated. The design process and the measured results of the proposed triplexer are also provided.

3.2 Theory

The proposed contiguous channel triplexer is based on CMTC, and the diagram is shown in Fig. 23 [4][5]. The triplexer comprises two isolation circuits. One is composed with a CRLH TL and a filter. Another isolation circuit comprises a conventional TL connected with a diplexer. The diplexer shown in this chapter is also made by the use of CMTC, however any kind of a diplexer can be used in this methodology. In Fig. 24, the frequencies, in ascending order, are f_1 , f_2 , and f_3 , and the center frequency of the filter used on CRLH isolation circuit should be f_2 for easier design of the CRLH TL, and this will be explained in the following paragraph.



At f_1 , (1GHz)	At f_2 , (1.125GHz)	At f_3 , (1.25GHz)
1) $Z_{in1} = Z_0$	1) $Z_{in1} = \infty$	1) $Z_{in1} = Z_0$
2) $Z_{in2} = \infty$	2) $Z_{in2} = Z_0$	2) $Z_{in2} = \infty$
3) $Z'_{in1} = Z_0$		3) $Z'_{in1} = \infty$
4) $Z'_{in2} = \infty$		4) $Z'_{in2} = Z_0$

Figure 23. Diagram and operation concept of proposed triplexer based on CMTC.

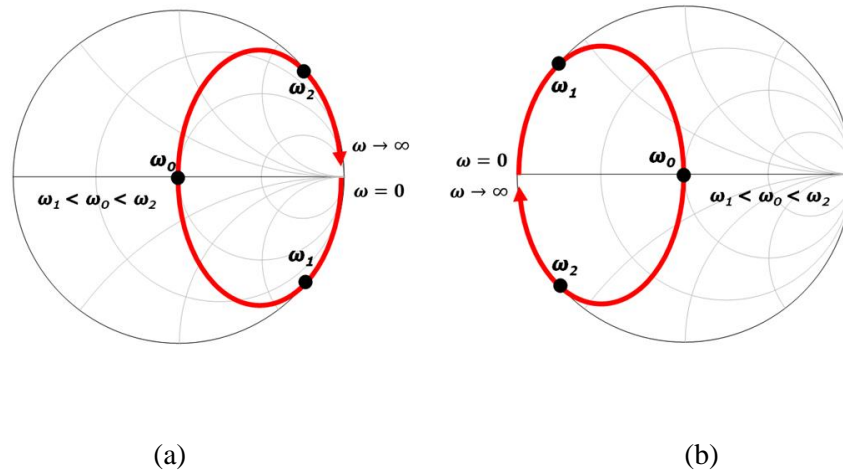


Figure 24. Locus of input impedance of a BPF shown in the Smith chart. (a) Open rejection case. (b) Short rejection case.

The proposed triplexer consists of a RH TL connected with a diplexer and a CRLH TL connected with a band-pass filter (BPF). The appropriate phase response of the RH TL is determined by investigating the input impedance of the diplexer at the center frequency of the filter used in the CRLH isolation circuit. Adding proper phase delay of the RH TL, the isolation

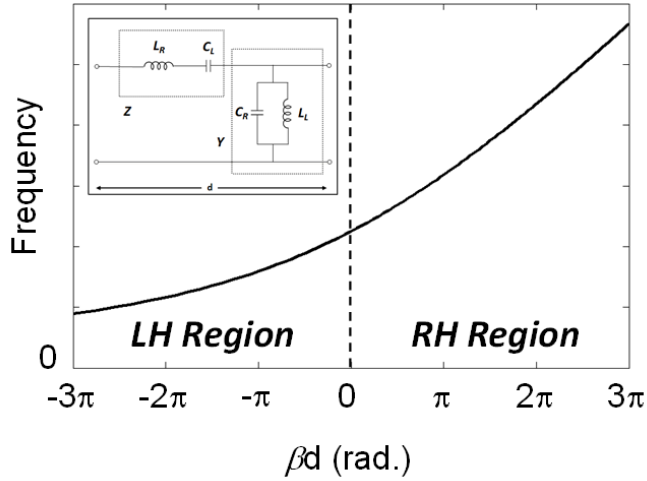


Figure 25. Dispersion diagram of a CRLH TL (β : the propagation constant of a CRLH TL).

circuit consisting of the diplexer can have open circuit input impedance which is not difficult to design with a RH TL. However, designing a CRLH TL for a contiguous channel triplexer is difficult or impractical in the circumstances that the filter connected with the CRLH TL has f_1 or f_3 center frequencies ($f_1 < f_2 < f_3$). The reason for this comes from the intrinsic characteristic of a BPF and a phase response of a CRLH TL. Fig. 24 shows the locus of input impedance of a BPF shown in the Smith chart. An input impedance of a BPF having open rejection characteristics, in which the input impedance of the filter becomes closer to infinite impedance as the frequency moves away from the pass-band, is represented in Fig. 24(a) while Fig. 24(b) shows that of a BPF having short rejection characteristic (closer to zero impedance as far away from pass-band). In both cases, impedance follows locus with clockwise rotation as frequency is increasing because a general BPF always has a positive group delay. Detailed explanation of this is provided in Appendix 2. Fig. 25 shows the phase response of a CRLH TL, and both left-handed (LH) and right-handed (RH) phase responses exist.

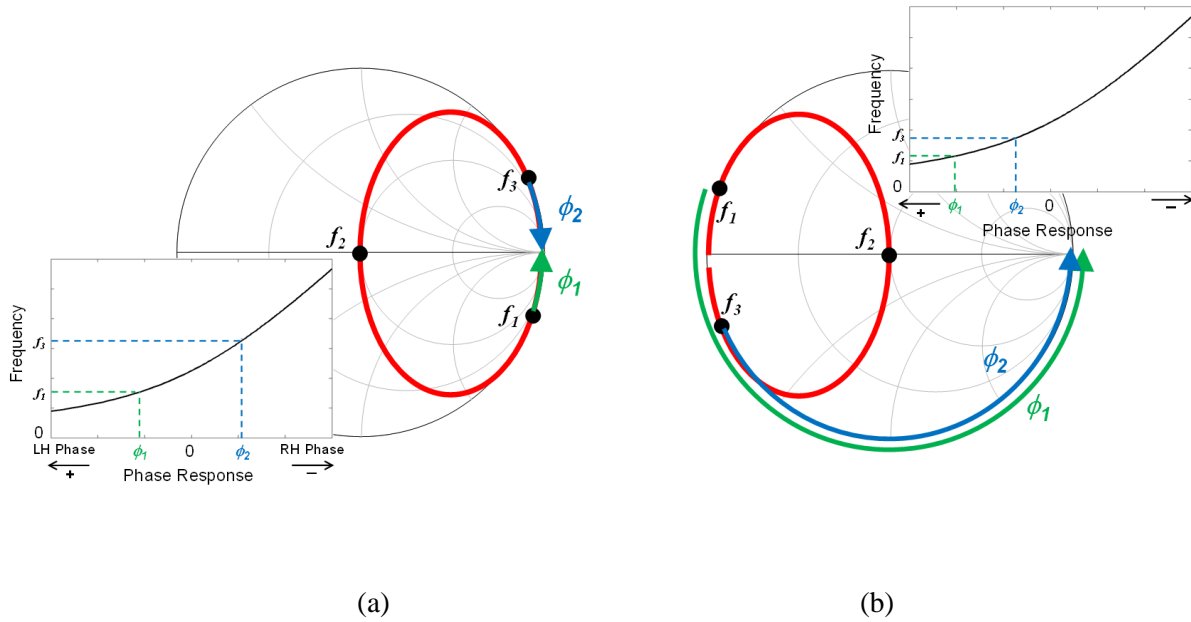


Figure 26. Design of CRLH TL connected with f_2 filter. (a) Open rejection case. (b) Short rejection case.

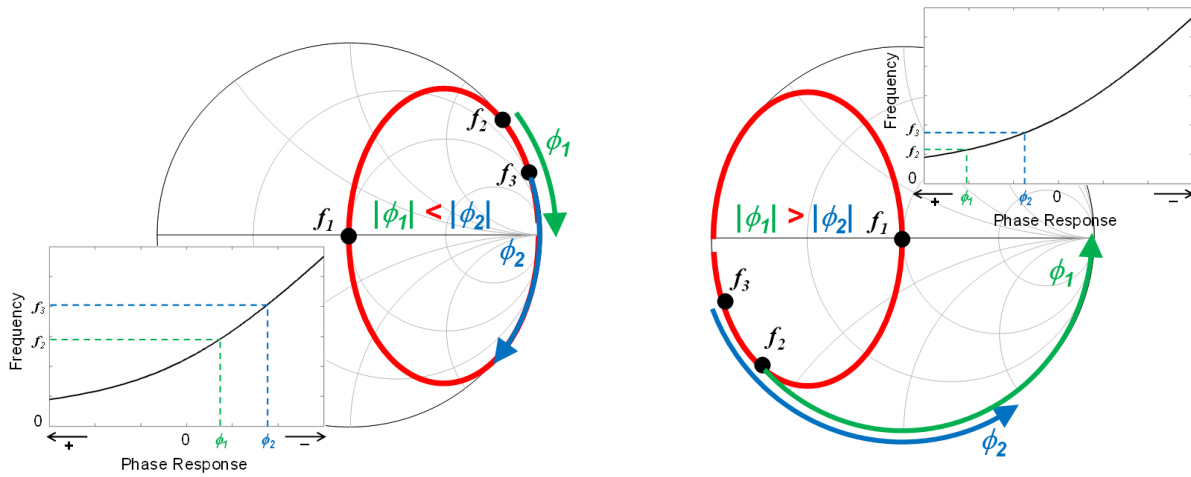


Figure 27. Design of CRLH TL connected with f_1 filter. (a) Open rejection case. (b) Short rejection case.

If a filter connected with a CRLH TL has f_2 center frequency, the input impedances of the filter at f_1 and f_3 are located on the Smith charts as shown in Fig. 26. With proper phase response of the CRLH TL, two impedance points can be moved to open-circuit impedance. Fig. 26(a) shows the open rejection case, and the CRLH TL can be designed by selecting LH and RH phase

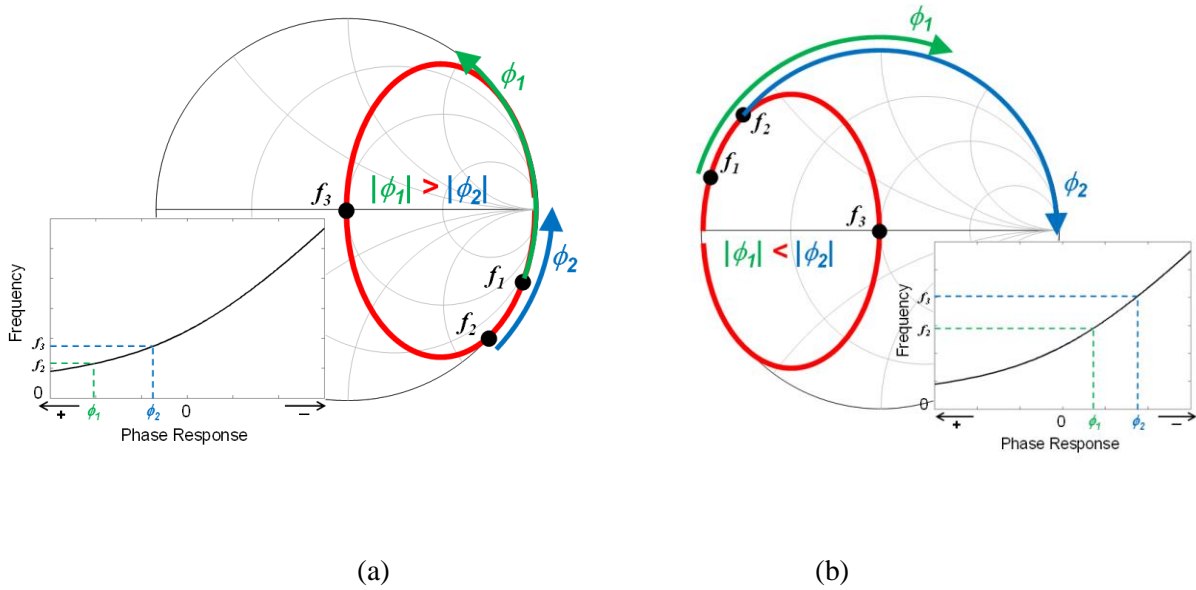


Figure 28. Design of CRLH TL connected with f_3 filter. (a) Open rejection case. (b) Short rejection case.

responses (phase advance and phase delay) at f_1 and f_3 , respectively. In the short rejection case shown in Fig. 26(b), same strategy used in the open rejection case could be difficult for design of the CRLH TL because required absolute phase responses at both f_1 and f_3 are large. Instead, only LH region of the CRLH TL can be used in this case. In the phase response of the CRLH TL shown in Fig. 26(b), both f_1 and f_3 belong to the LH region and the absolute phase response at f_1 has larger value than that at f_3 . With this CRLH TL connected to the filter having the short rejection, open-circuit impedance can be realized at two target frequencies. This procedure cannot be used simply to a BPF (used on CRLH isolation circuit) having f_1 or f_3 center frequency. Fig. 27 shows input impedance of the f_1 filter represented on the Smith chart. In the open rejection case shown in Fig. 27(a), the impedance point at f_3 requires smaller phase delay (RH phase response) than that at f_2 for having open-circuit impedance. However, a phase delay at higher frequency is always larger than that at lower frequency in a CRLH TL. Hence, the CRLH TL cannot satisfy the requirement of the f_1 filter connected with the CRLH TL having open-

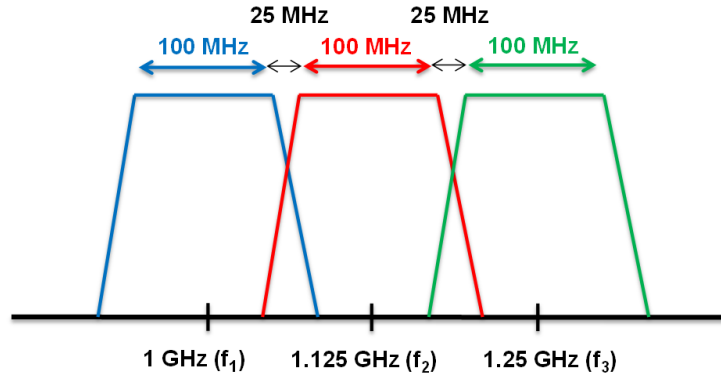


Figure 29. Ideal frequency response of proposed triplexer on output ports.

circuit impedance at both f_2 and f_3 . With similar procedure of the open rejection case, it is difficult to design a CRLH TL for the short rejection f_1 filter. In Fig. 27(b), the impedance point at f_2 needs less phase advance (LH phase response) than that at f_3 . However, a CRLH TL cannot support such phase response in the LH region. In the case of the filter having f_3 center frequency, it is still difficult to design a CRLH TL satisfying the required phase response for a dual-band isolation circuit. Figure 28(a) shows the case of the open rejection f_3 filter. For open-circuit impedance at f_1 and f_2 , less phase advance at f_1 and more phase advance at f_2 are necessary, however, it is difficult to satisfy such condition using a CRLH TL. Figure 28(b) shows the short rejection case, and more phase delay at f_1 and less phase delay at f_2 are necessary. The phase response of a CRLH TL does not support this.

Considering Fig. 26 to 28, it is found that using a filter having f_2 center frequency is easier for a CRLH isolation circuit of a contiguous channel triplexer. In addition, such case studies reveal that a star-junction or a manifold-junction triplexer, shown in chapter 1, is not appropriate for a contiguous channel triplexer because CRLH TLs should be designed for f_1 or f_3 filters. However, the star-junction or the manifold-junction triplexer concept is valid in non-contiguous channel

triplexers because interaction between channels is not strong and the adjusting constant ψ of (6c) can be used.

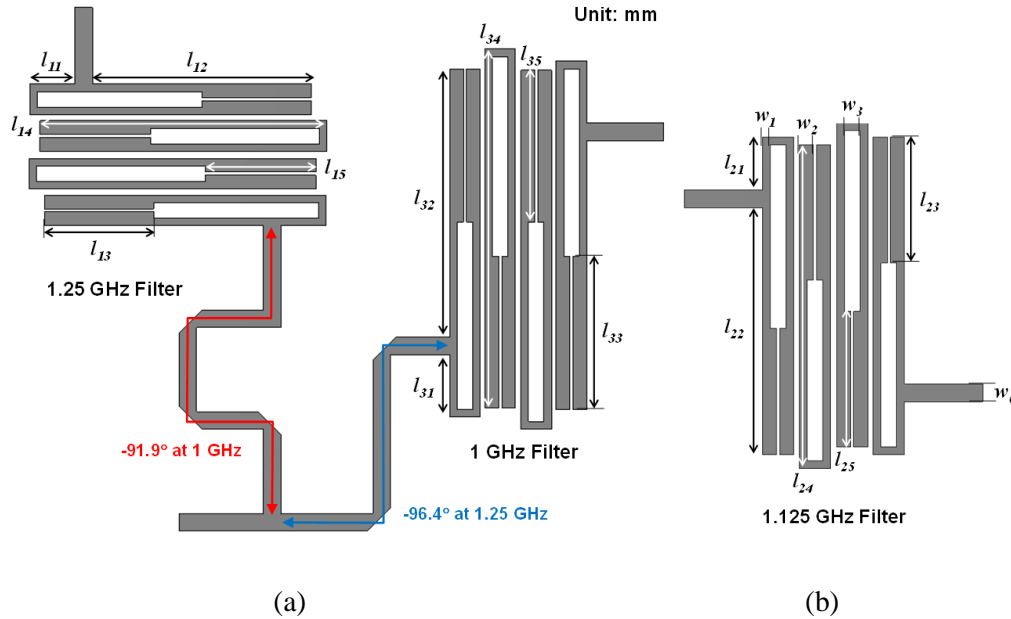


Figure 30. The layout of filtering circuits used for proposed triplexer. (a) Diplexer. (b) 1.125 GHz filter. (Parameters: $l_{11} = 5.9$, $l_{12} = 28.55$, $l_{13} = 14.25$, $l_{14} = 37.45$, $l_{15} = 14.45$, $l_{21} = 6.8$, $l_{22} = 31.7$, $l_{23} = 16.2$, $l_{24} = 41.6$, $l_{25} = 17.4$, $l_{31} = 8.1$, $l_{32} = 35.1$, $l_{33} = 20$, $l_{34} = 46.9$, $l_{35} = 19.8$, $w_0 = 2.3$, $w_1 = 1$, $w_2 = 1.8$, $w_3 = 2$.)

3.3 Design Process

In this section, the design process of the proposed triplexer is presented. Fig. 29 shows the frequency response of the triplexer at output ports with ideal conditions. The combination of a diplexer shown in Fig. 30(a), whose center frequencies are 1 GHz and 1.25 GHz, and a 1.125 GHz filter shown in Fig. 30(b) realizes the proposed triplexer. For compact size, hairpin-line filters are used for filtering circuits in the proposed triplexer [6]. The fractional bandwidths of the filters are around 10 %, and it could be difficult to design the proposed triplexer with use of a filter having wide bandwidth because of band limitation of an isolation circuit. For reference, the diplexer is composed with two filters and it follows the simple design concept of Fig.1. Fig.

31(a) and (b) show the measured magnitude characteristics and input impedance of the diplexer, respectively. The measured results of the 1.125 GHz filter are shown in Fig. 31(c) and (d). The frequency configuration of the triplexer is represented in Fig. 29, and its design procedure is as follows:

1. Find an input impedance of a diplexer at the center frequency of a filter used on a CRLH isolation circuit, and check input impedances of the filter at operating frequencies of the diplexer used on the other isolation circuit. In the proposed triplexer, the input impedance of the diplexer at 1.125 GHz (marker 1 in Fig. 30(b)) and the input impedances of the 1.125 GHz filter at 1 GHz and 1.25 GHz (markers 1 and 2 on Fig. 30(d)) are necessary for our design.
2. Find the proper phase responses for each diplexer or filter using Eq. (6a) or (6b) in order to obtain open-circuit impedance at the target frequencies. In the proposed triplexer, the desired phase delay ϕ_{11} for the diplexer is -33.80° , and the required phase shifts ϕ_{21} and ϕ_{22} for the filter are 93.33° and 61.99° , respectively.
3. Calculate circuit parameters of a CRLH TL and a length of a RH TL with solved phase responses in the procedure 2 above. In the proposed triplexer, the circuit parameters of the CRLH TL are solved by submitting $(\phi_{21}, \phi_{22}) = \{1.63 \text{ rad. } (93.33^\circ), 1.08 \text{ rad. } (61.99^\circ)\}$ and $(\omega_{21}, \omega_{22}) = (2 \times \pi \times 1 \text{ GHz}, 2 \times \pi \times 1.125 \text{ GHz})$ pair and $N = 2$ to Eq. (16)-(19) in Appendix 1. The circuit parameters of the CRLH TL are $L_R = 1.96 \text{ nH}$, $C_R = 0.78 \text{ pF}$, $L_L = 7.50 \text{ nH}$, and $C_L = 3.00 \text{ pF}$. For the diplexer, a conventional RH TL, having an electrical length of -33.80° at 1.125 GHz is necessary.

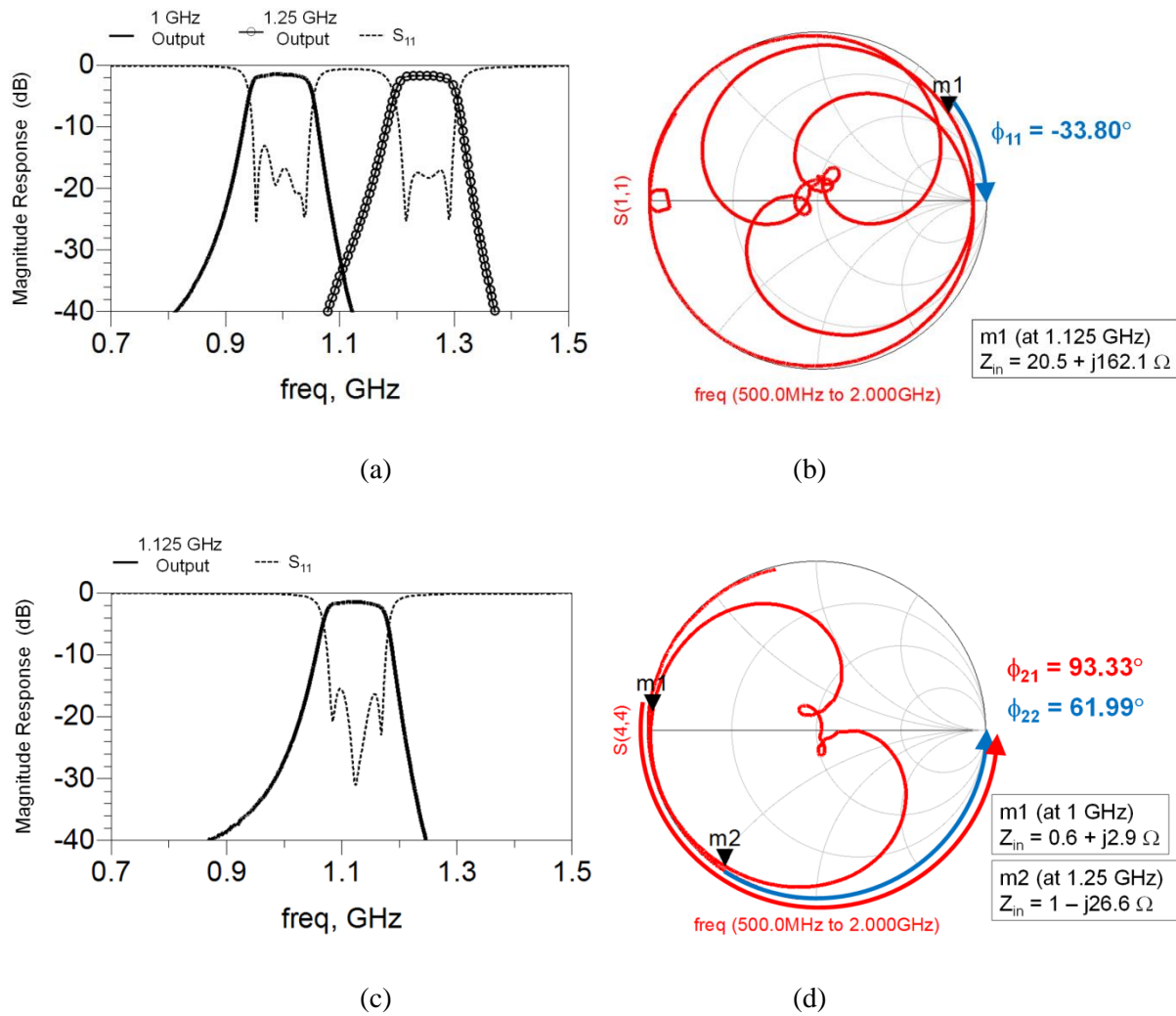


Figure 31. Performances of the diplexer and the filter used on proposed triplexer. (a) Magnitude response of the diplexer. (b) Input impedance of the diplexer shown on the Smith chart. (c) Magnitude response of the filter. (d) Input impedance of the filter shown on the Smith chart.

4. Combine a diplexer with a RH TL and connect a filter with a CRLH TL. In the proposed triplexer, the CRLH TL, designed in the procedure 3, and the 1.125 GHz filter make dual-band isolation circuit, and the combination of the diplexer and the conventional RH TL makes single-band isolation circuit.
5. Connect two isolation circuits with common input port.

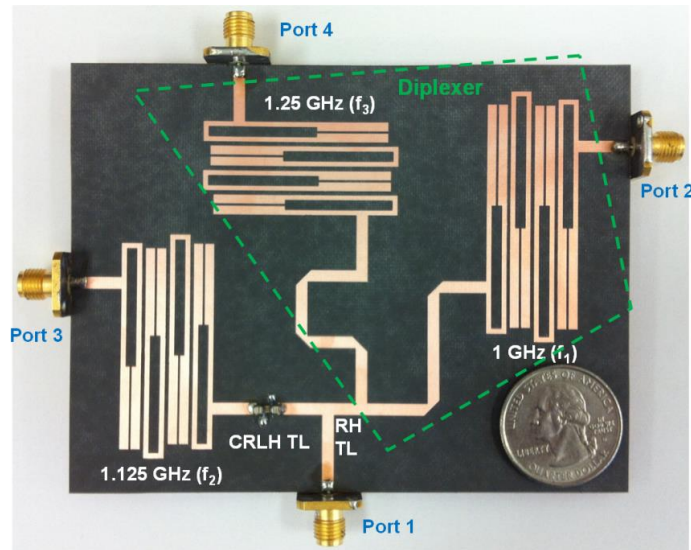


Figure 32. Fabricated contiguous channel triplexer based on CMTC.

3.4 Contiguous Triplexer

The proposed triplexer is composed of the single-band isolation circuit, a combination of the diplexer and the conventional TL, and the dual band isolation circuit, which consists of a filter and a CRLH TL. In order to verify the design concept, the proposed triplexer is designed and fabricated. In Section 3.3, the design process of the triplexer has been investigated, and the derived data are summarized in Table 8. In the fabricated triplexer picture shown in Fig. 32, the diplexer is located on the right side of the picture and the 1.125 GHz filter is on left side. A RT/Duroid 5870 substrate ($\epsilon_r = 2.33$, Height = 0.787 mm) is used for the triplexer and hairpin-line BPFs are printed on the substrate for filtering circuits [5]. The lumped elements and the microstrip lines are used to form the CRLH TL. The LH part of the CRLH TL is realized by the lumped elements, and the microstrip lines are used for the RH part. For a single band isolation circuit, the microstrip line which has 33.80° phase delay at 1.125 GHz is used.

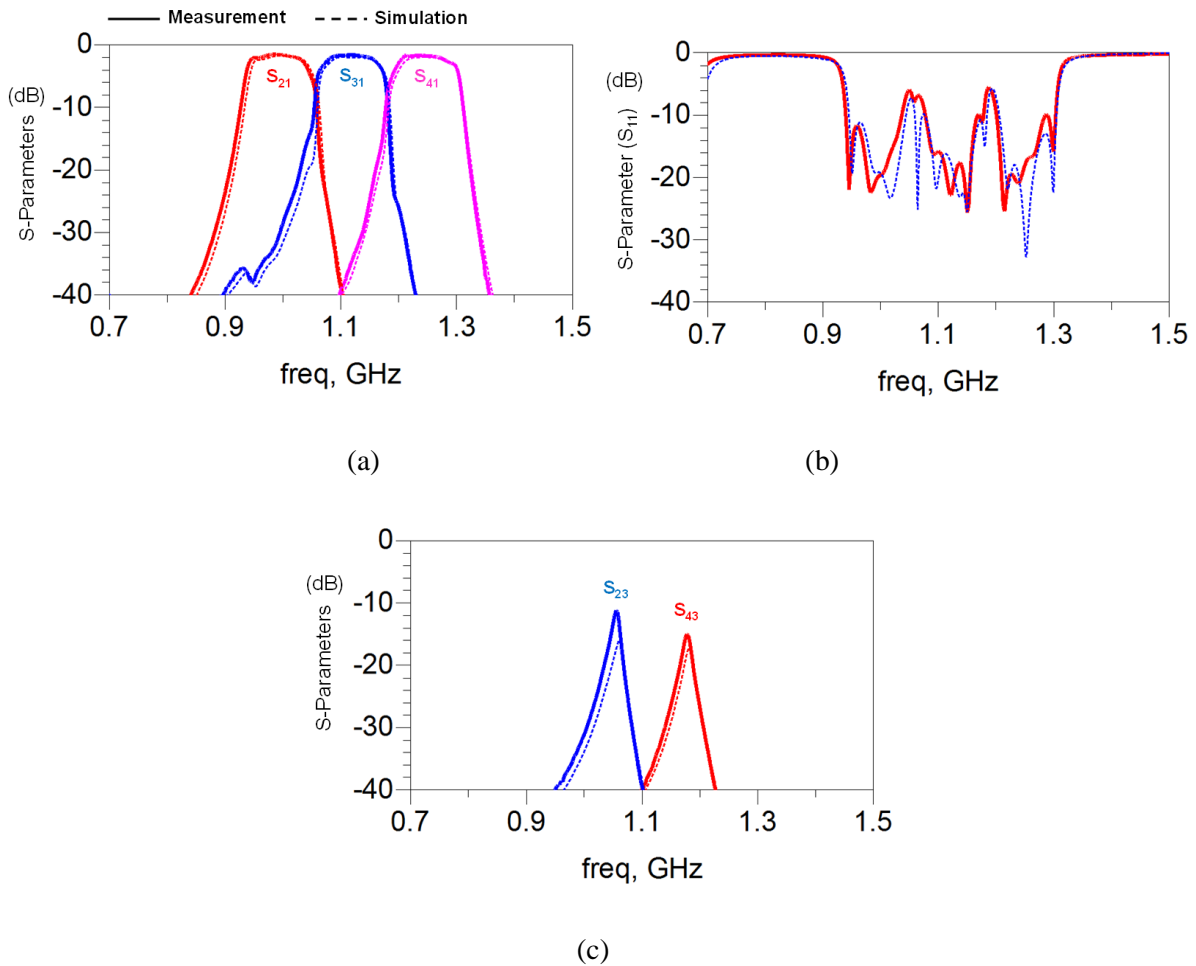


Figure 33. Simulated and measured results of proposed triplexer. (a) Insertion loss. (b) Matching at port 1. (c) Isolation.

Fig. 33 shows the simulated and measured results of the contiguous triplexer. Figure 33(a) shows the insertion losses, which are less than 1.8 dB. The measured guard bandwidth is around 25 MHz. The return losses, shown in Fig. 33(b), are larger than 10 dB, whereas Fig. 33(c) shows that the isolation is greater than 11.2 dB.

3.5 Conclusion

A contiguous channel triplexer based on CMTC has been presented. The measured results of the proposed triplexer show good agreement with the simulation results. The concept, theories, and design process have been explained to help the reader design and fabricate this type of triplexer. It is usually difficult to design a contiguous or small guard band triplexer because of the strong interaction between the channels, and a designer is required to optimize filters or use a specific filter type. However, the proposed triplexer provides straightforward and simple design method. In addition, a system designer can choose any filter or diplexer without modification. Although a star-junction or a manifold-junction triplexer based on isolation circuits also has same advantages, it is difficult or nearly impossible to design CRLH TLs for a contiguous channel triplexer. Hence, the proposed triplexer is very attractive to a system designer.

Table 8. Summary of Contiguous Channel Triplexer

		Circuit 1 (RH TL + Diplexer)		Circuit 2 (CRLH TL + Filter)	
		At 1.125 GHZ	20.5 + j162.1	At 1 GHZ	0.6 + j2.9
Impedance of Filtering Circuits (Ω)				At 1.25 GHZ	1 - j26.6
Required Phase Response (deg.)		ϕ_{11}	-33.80	ϕ_{21}	93.33
				ϕ_{22}	61.99
Circuit Parameters of CRLH TL (L : nH, C : pF)	L_R			1.96	
	C_R			0.78	
	L_L			7.50	
	C_L			3.00	

3.6 References

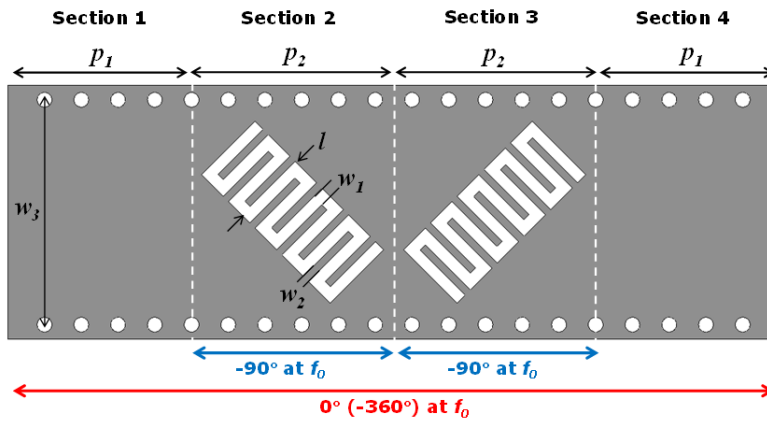
- [1] H. Lee and T. Itoh, "Isolation circuits based on metamaterial transmission lines for multiplexers", *Journal of Electromagnetic Engineering and Science*, vol. 13, no. 3, pp.141-150, Sep. 2013.
- [2] I. Lin, M. Vincentis, C. Caloz, and T. Itoh, "Arbitrary dual-band components using composite right/left-handed transmission lines," *IEEE Trans. Microwave Theory Tech.*, vol. 52, pp. 1142–1149, April 2004.
- [3] C. Caloz and T. Itoh, *Electromagnetic Metamaterials, Transmission Line Theory and Microwave Applications*, New York: Wiley, 2005.
- [4] H. Lee, J. S. Sun, and T. Itoh, "Contiguous triplexer based on combining method of two filtering circuits using CRLH and RH isolation circuits," *2013 European Microwave Conference*, Oct. 2013.
- [5] H. Lee, C. M. Wu, and T. Itoh, "Study and analysis of contiguous channel triplexer based on combining method of two filtering circuits using CRLH and RH isolation circuit", *International Journal of Microwave and Wireless Technologies*, vol. 6, pp.287-295, June 2014.
- [6] J.-S. Hong and M.J. Lancaster, *Microwave Filters For RF/Microwave Applications*, Wiley, New York, 2011.

Chapter 4 Circularly Polarized Single Radiator CRLH SIW Leaky-Wave Antenna

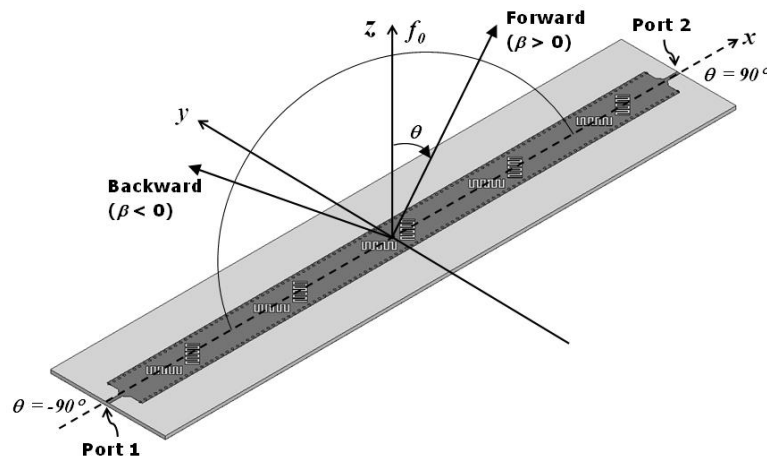
4.1 Introduction

In a real communication environment, maintaining precise alignment between the antennas may be improbable. Under these circumstances, circularly polarized antennas have been widely adapted over the linearly polarized antennas to minimize the polarization mismatch loss. A waveguide antenna with two inclined slots is popular way to make circular polarization [1]. However, it cannot be used in the applications demanding beam scanning ability. Recently, circular polarization capability has been integrated to CRLH based leaky wave antennas [2]-[4]. In doing so, circular polarization feature can be obtained in addition to the frequency scanning capability over broad operation bandwidth. However, [2] and [3] that are based on CRLH microstrip technology may suffer from the polarization purity of the radiated fields. Since the fields radiated not only from the series capacitors but also from the inductive stubs, overall radiated field pattern may be distorted. Also, inductive stubs generate undesired addition of loss and phase shift [2]-[3]. High-Q and high power handling advantages of substrate integrated waveguide (SIW) have been utilized in designing CRLH frequency scanning leaky-wave antennas. CRLH SIW antennas are advantageous over the CRLH microstrip based antennas because the fields radiate only from the interdigital slots, thereby producing much purer linearly polarized waves. With these advantages, CP CRLH SIW LWA has been developed by orthogonally feeding the two linearly polarized CRLH SIW LWAs that are placed side-by-side [4].

In this chapter, CP CRLH SIW LWA is further improved by eliminating the quadrature feeding network and the use of two linearly polarized CRLH SIW LWAs. Instead, the proposed



(a)



(b)

Figure 34. Proposed antenna configuration. (a) Unit-cell of the proposed CP LWA. (b) Whole structure of the proposed CP LWA. (Unit-cell parameters: $p_1 = 10$ mm, $p_2 = 11$ mm, $l = 4.1$ mm, $w_1 = 0.63$ mm, $w_2 = 0.4$ mm, $w_3 = 12.24$ mm.)

antenna is designed to produce circularly polarized field using a single radiator without the help of extra external circuits, while preserving all the advantages of the CRLH SIW LWAs.

4.2 Antenna Structure and Operation Concept

The proposed CP CRLH-inspired SIW LWA is shown in Fig. 34. The unit-cell shown in Fig. 34(a) consists of four parts, which are two conventional CRLH unit-cells with the interdigital

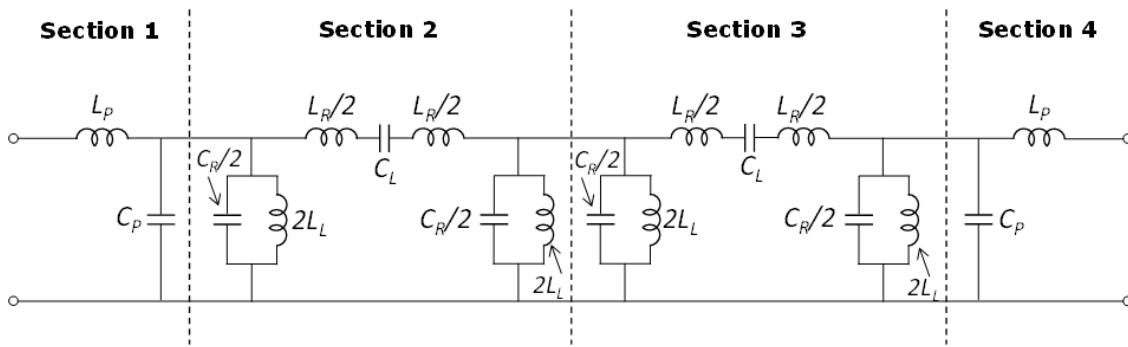


Figure 35. Equivalent circuit model of the unit-cell shown in Fig. 34(a).

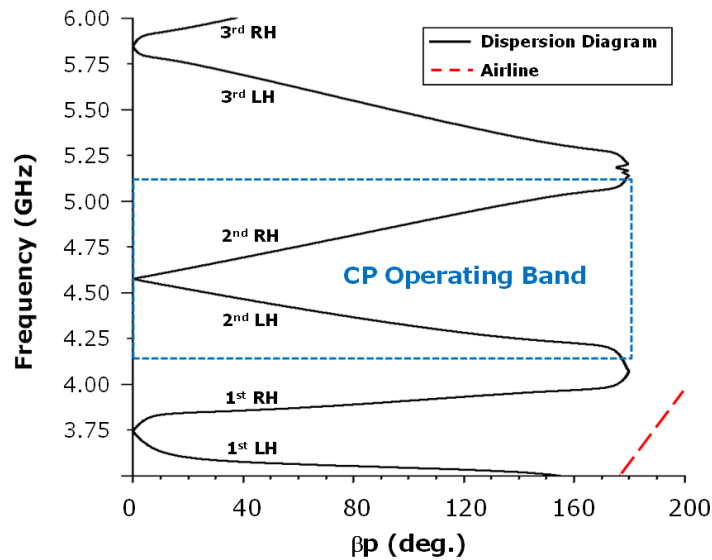


Figure 36. Dispersion diagram of the proposed circular polarized antenna unit-cell ($p = 2 \times p_1 + 2 \times p_2$).

slot oriented to $+45$ and -45 degrees (orthogonal to each other) [4] and two right handed (RH) TLs. The phase delay between the centers of two interdigital slots are designed to provide 90° phase shift at the center frequency f_o . Therefore, circularly polarized wave is created from these two slots composing two orthogonal linear polarized waves and fed with 90° phase difference. Each RH TLs also provide 90° phase delay, thereby providing additional 180° phase delay to the entire unit-cell. The total phase delay between the input and output ports of the unit cell is 0° (-

360°) at the center frequency. Strictly speaking, the proposed unit-cell cannot be considered as a unit-cell of CRLH TL because of the periodicity of the proposed unit-cell shown in Fig. 34(a) does not satisfy an effectively homogeneous condition ($p < \lambda_g/4$, λ_g : guided wavelength) [5]. However, the overall response shows CRLH like characteristic that supports both LH and RH propagations. The prototype of the proposed LWA shown in Fig. 34(b) has broadside beam direction at the center frequency f_0 .

The equivalent circuit of the proposed CP antenna unit-cell (shown in Fig. 34(a)) is presented in Fig. 35. The equivalent circuit is comprised of 4 sections. Sections 2 and 3 are same as the equivalent circuit of a conventional CRLH SIW unit-cell [6]. The series capacitance C_L is realized by the interdigital slot and vias provide the shunt inductance L_L . The conductor surface and the ground contribute to the series inductance L_R and the shunt capacitance C_R . Sections 1 and 4 (composed with L_p and C_p) are generated from the RH TLs, and are used for providing additional phase delays. The proposed unit-cell structure has multiband characteristic, and this is similar to that of a dual-band (DB) CRLH unit-cell [7]. However, the proposed CP antenna only uses one specific frequency band because the antenna does not support CP radiation in other frequency bands.

Fig. 36 shows the dispersion diagram of the proposed unit-cell obtained from the simulated scattering parameters. As mentioned above, the proposed unit-cell has a dispersion diagram that shows three LH regions and three RH regions, however only in second band the proposed antenna radiates circular polarized beam. The center frequency of the structure is 4.54 GHz and a balanced condition is achieved with respect to the unit-cell described here. The proposed structure can support CP radiation throughout the entire center band from 4.2 GHz to 5.07 GHz.

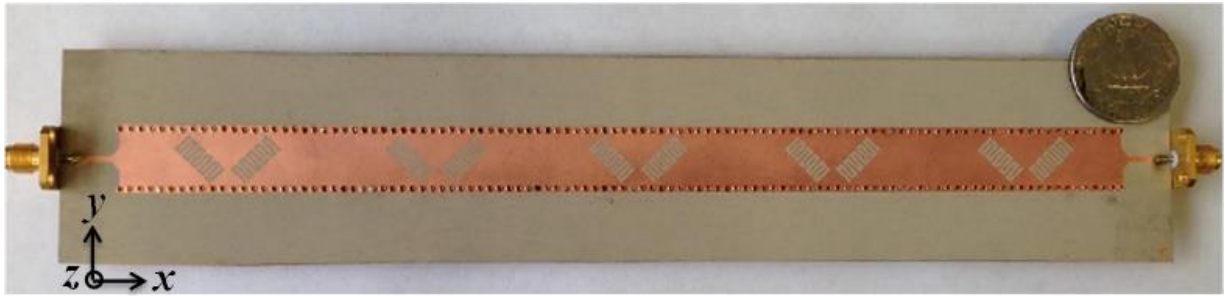


Figure 37. Fabricated novel CP CRLH SIW leaky-wave antenna.

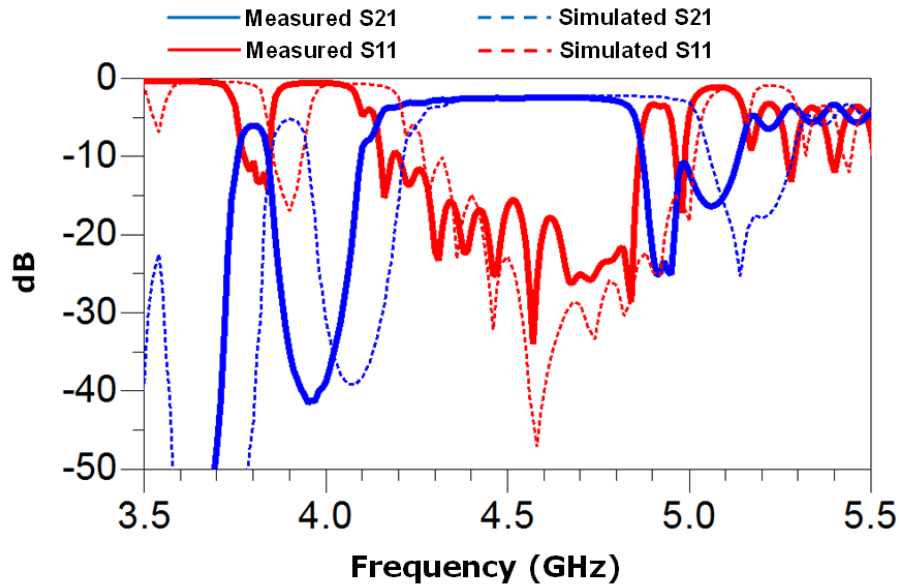


Figure 38. Measured and simulated S-parameters of the proposed CP LWA antenna.

4.3 Proposed CP Antenna

To demonstrate the proposed antenna, 5 cell circularly polarized antenna is designed and fabricated. The proposed antenna is realized using RT/Duroid 6010 substrate ($\epsilon_r = 10.2$, $h = 1.27$ mm) and via holes with the diameter of $d = 0.8$ mm. Conductive wall is created by placing the vias with the center-to-center spacing of $s = 2.0$ mm. Fig. 37 shows a photograph of the fabricated antenna.

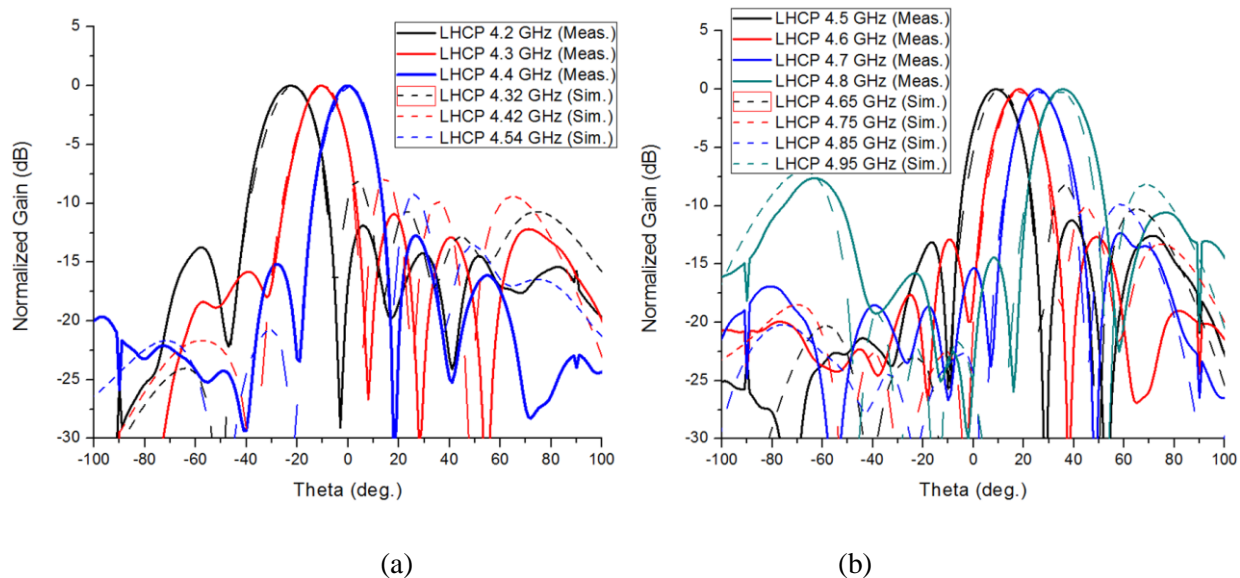


Figure 39. Measured and simulated far field patterns of the proposed circularly polarized antenna in x - z plane. (a) From LH to broadside region. (b) RH region.

The simulated and measured S-parameters of the proposed antenna are shown in Fig. 38. Slight frequency shift is observed due to fabrication errors. The measured S_{11} is below -10 dB in the whole operating band.

The far field pattern and axial ratio (AR) of the proposed CP antenna are measured in a near field antenna chamber. The proposed antenna can support both left-handed circular polarization (LHCP) and right-handed circular polarization (RHCP). LHCP and RHCP are generated when the antenna is fed from port 1 and port 2 respectively. The normalized radiation patterns from backward direction to broadside (*in x - z plane*) are shown in Fig. 39(a). Fig. 39(b) shows the radiation patterns for forward direction. Because of the frequency shift of the fabricated antenna, simulated radiation patterns at slight higher frequencies are used to compare the measured results. The measured center frequency is 4.4 GHz. The simulated and measured AR (*in x - z plane*) is plotted in Fig. 40. The proposed antenna shows good axial ratio of less than 3 dB within the beam scanning range.

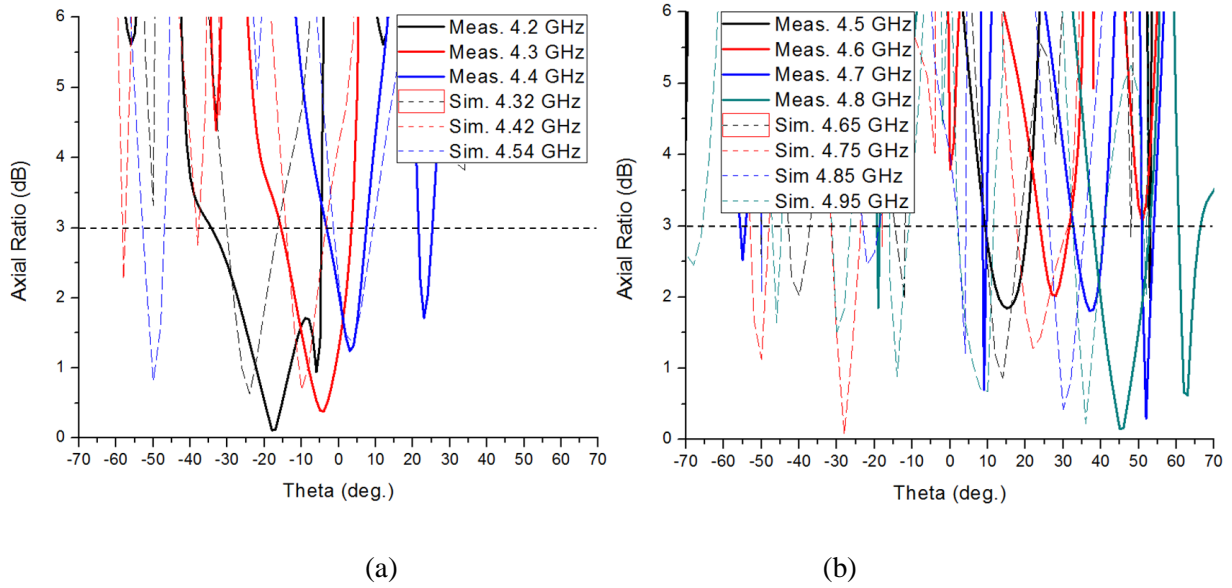


Figure 40. Measured and simulated axial ratio of the proposed circularly polarized antenna in x-z plane. (a) From LH to broadside region. (b) RH region.

4.4 Conclusion

A new method to realize novel circular polarized CRLH-inspired SIW leaky wave antenna (LWA) is explained. The proposed frequency scanning antenna provides CP fields using a single radiating transmission line, which can avoid the complexity of previous design [4]. LHCP and RHCP can be easily generated by feeding the antenna from either port 1 or 2. In addition, the proposed antenna has low profile and is fabricated with low cost PCB process. Hence the proposed antenna may serve as a good candidate for wireless applications requiring CP frequency scanning features.

4.5 References

- [1] G. Montisci, "Design of circularly polarized waveguide slot linear arrays," *IEEE Transactions on Antennas and Propagation*, vol. 54, no. 10, pp. 3025 - 3029, Oct. 2006.
- [2] K. Kitatani, Y. Mitsuhashi, Y. Okamura, "Circularly polarized leaky wave antenna without phase shifter using CRLH transmission line," *2012 European Conference on Antennas and Propagation (EUCAP)*, 2012.
- [3] D. Piazza and M. D'Amico, "Pattern and polarization reconfigurable CRLH leaky wave antenna," *2010 European Conference on Antennas and Propagation (EUCAP)*, 2010.
- [4] Y. Dong and T. Itoh, "Substrate Integrated Composite Right-/Left-Handed Leaky-Wave Structure for Polarization-Flexible Antenna Application", *IEEE Transactions on Antennas and Propagation*, vol. 60, no. 2, pp. 760 - 771, Feb. 2012.
- [5] C. Caloz and T. Itoh, *Electromagnetic Metamaterials, Transmission Line Theory and Microwave Applications*, New York: Wiley, 2005.
- [6] Y. Dong and T. Itoh, "Composite right/left-handed substrate integrated waveguide and half mode substrate integrated waveguide leaky-wave structures," *IEEE Transactions on Antennas and Propagation*, vol. 59, no. 3, pp. 767-775, Mar. 2011.
- [7] M. R. Hashemi and T. Itoh, "Dual-band composite right/left-handed metamaterial concept," *IEEE Microwave and Wireless Components Letters*, vol. 22, no. 5, pp.248-250, May 2012.

Chapter 5 Single Radiator Circularly Polarized CRLH SIW Leaky-Wave Antenna Equipped Compact Unit-Cell

5.1 Introduction

Leaky-wave antennas (LWAs) have attracted researchers for many years because of their unique frequency beam scanning capability and broad operational bandwidth [1]-[7]. Recent birth of metamaterial transmission line concept has even further accelerated the study of leaky-wave antennas [8]-[12]. Composite right/left handed (CRLH) transmission line (TL) is a type of metamaterial TL that can be systematically designed to have both positive and negative phase velocity that allows the antennas to steer the beam not only toward endfire but also toward backfired directions. Moreover, a CRLH TL even supports broadside radiation under the balanced condition. With above mentioned advantages, microstrip line based single radiator circularly polarized (CP) CRLH LWAs have been proposed [13]-[15]. The inherent quadrature phase relation of a series and a shunt radiation component for a CP radiation is analyzed in [15]. Such CP LWAs are particularly aimed for wireless application under dynamic motion, requiring high signal throughput. For example, satellites use CP antennas since it is difficult to align the antennas polarization in advance [16]. Likewise, devices receiving information from the satellites such as GPS are also equipped with CP antennas [17]. Nowadays, personal mobile devices such as WiFi modems and RFID systems have also started to use CP signal to enhance the wireless performance [18]. In general, for wireless devices that are under constant motion and operating in electromagnetically crude environments, CP antenna is the preferred choice.

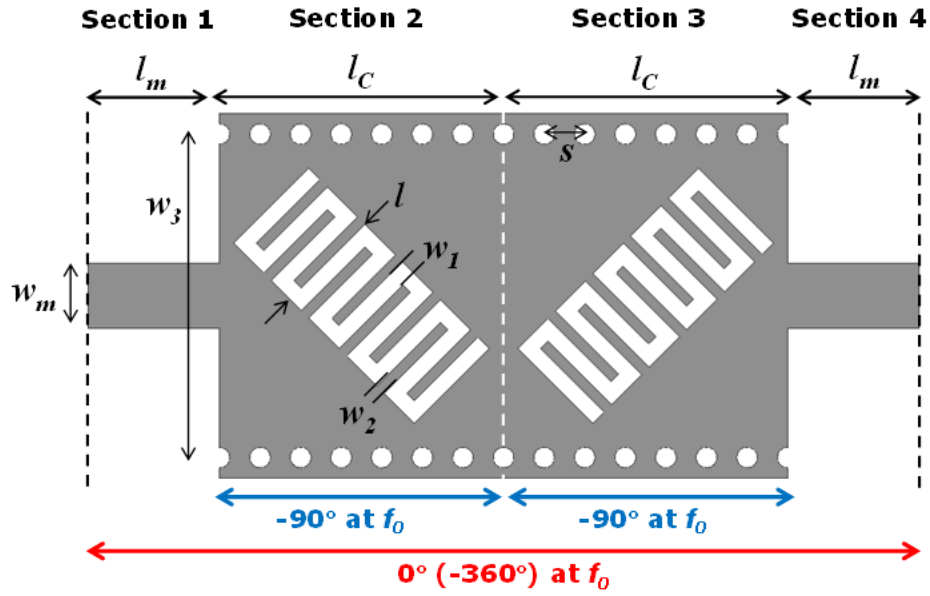
Recently, CP LWA has been developed using CRLH SIW technologies [19], [20]. Fields radiated by the interdigital slots produce relatively pure polarization, thus CRLH SIW LWAs have recently attracted much attention. In [19], two CRLH LWAs with interdigital slots rotated

in an orthogonal direction with respect to each other are placed side-by-side. CP polarization is then generated by feeding the antennas with quadrature hybrid coupler. In the previous chapter, an improved CP CRLH-inspired SIW LWA has been developed in which an external quadrature feeding network is eliminated and a single radiating element is used instead of using two radiators. The unit-cells consist of four components, two conventional CRLH SIW cells with 45° rotated interdigital slots and two 90° long conventional SIW structures.

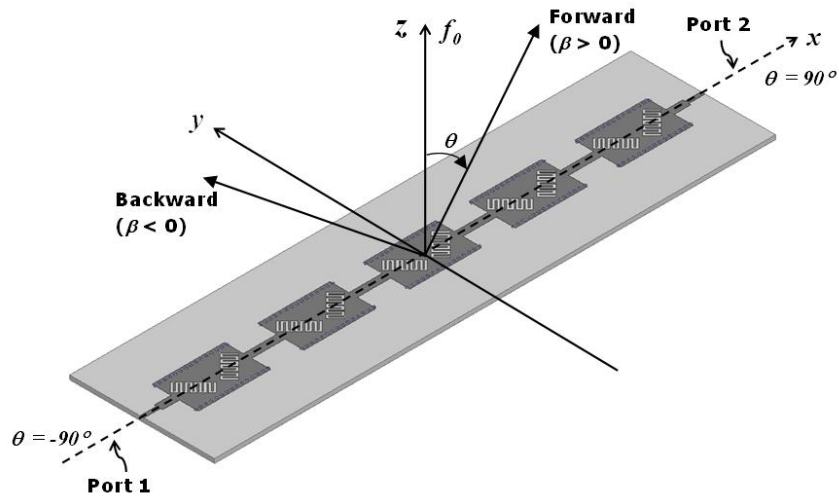
In this chapter, a single element CP CRLH-inspired SIW LWA [20] is further improved by replacing the conventional SIW delay sections with microstrip lines to reduce the unit-cell size. In a certain antenna size, a smaller unit-cell allows larger number of radiators thereby increasing an antenna efficiency. The modification not only enables miniaturization of the unit-cell but also adds intrinsic matching network within the antenna, thus eliminating the need of external matching circuits and improving CP purity. Furthermore, similar to [7], periodically integrated microstrip delay lines enable efficient broadside radiation. The chapter is organized as follows: The proposed antenna unit-cell structure and the operating concept are explained in section 5.2. Design procedures of a CRLH cell and a microstrip line are explained in detail in section 5.3. Lastly, the simulated and measured results of the proposed antenna are provided in section 5.4.

5.2 Unit-Cell Structure and Operating Concept

The unit-cell of the proposed CP CRLH-inspired SIW LWA consists of two conventional CRLH SIW cells with the interdigital slot rotated by $+45^\circ$ and -45° with respect to the wave propagation direction [19] and two microstrip lines shown in Fig. 41 (a). At the center frequency f_0 , two interdigital slots are separated by 90° phase delay. The two radiating slots etched on top of the SIW generate two orthogonal linearly polarized waves with quadrature phase difference,



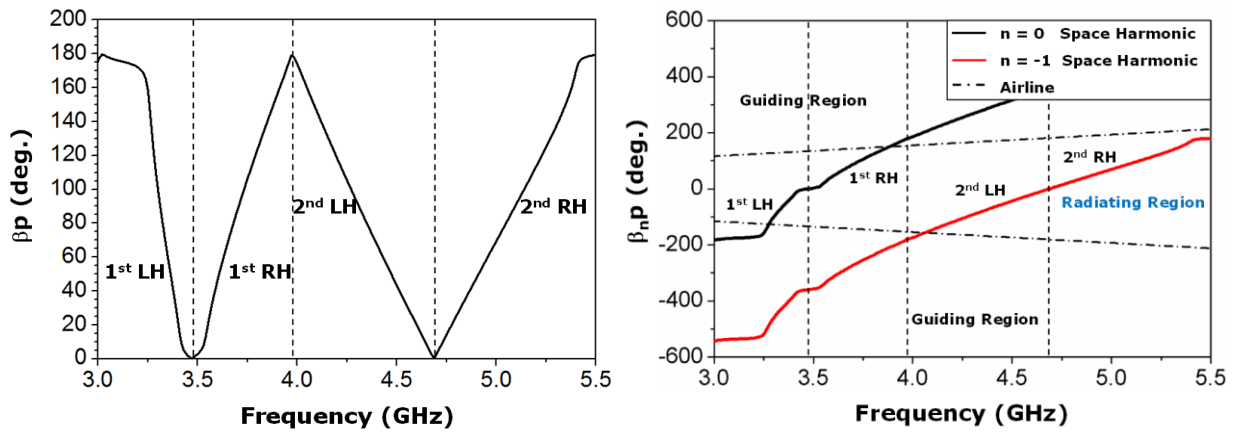
(a)



(b)

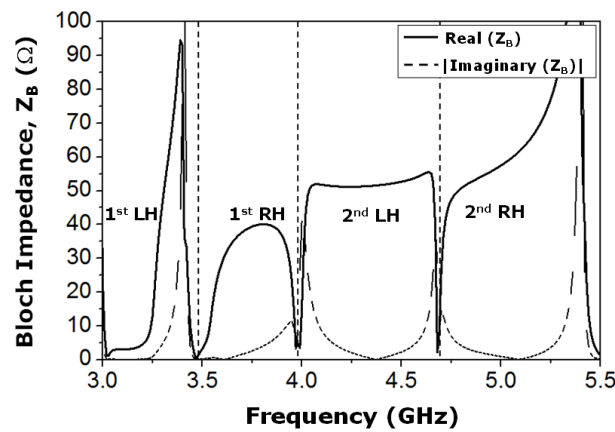
Figure 41. (a) Unit-cell of the proposed single radiator CP LWA. (b) Whole structure of the proposed CP LWA. (Unit-cells parameters: $l_m = 5.1$ mm, $l_C = 11$ mm, $l = 4.1$ mm, $w_1 = 0.63$ mm, $w_2 = 0.4$ mm, $w_3 = 12.54$ mm, $w_m = 2.5$ mm, $s = 1.57$ mm.)

thus radiating circularly polarized wave. The two microstrip lines sections attached on each side of the SIW structure also have 90° phase delay at f_0 , therefore adds additional 180° phase delay.



(a)

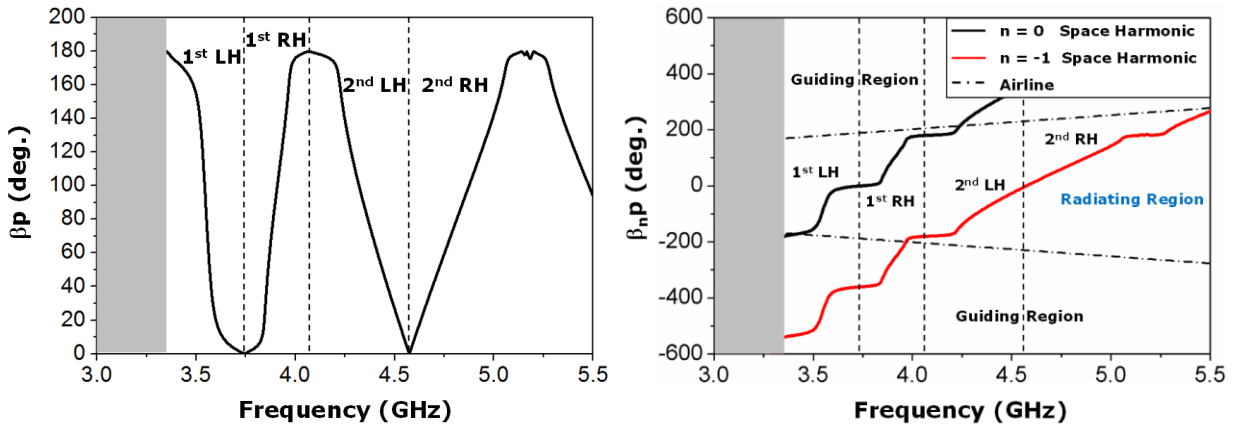
(b)



(c)

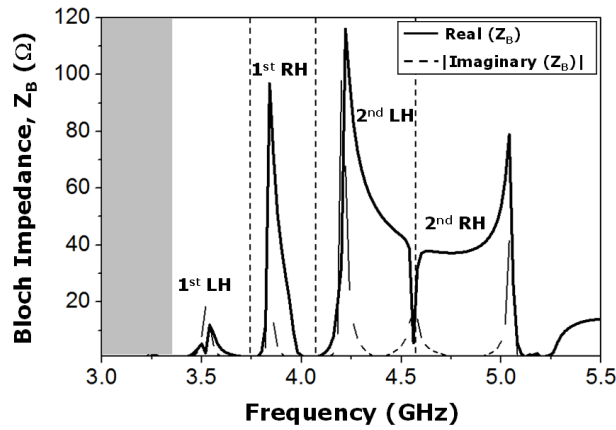
Figure 42. Characteristics of the proposed CP antenna unit-cell. (a) Dispersion diagram ($p = 2 \times l_m + 2 \times l_c$). (b) Space harmonics reconstructed from the dispersion diagram of the proposed unit-cell (n is mode number). (c) Bloch Impedance.

This ensures the radiated fields from each SIW unit-cells to add constructively in the far-field. The unit-cell of the proposed antenna shown in Fig. 41(a) thus has 0° (360°) phase delay response at the center frequency. Fig. 41(b) shows the prototype of the proposed five element LWA and the coordinate system. While maintaining the same operational concept, the unit-cell of the proposed structure can be realized with smaller overall dimension in comparison to the



(a)

(b)



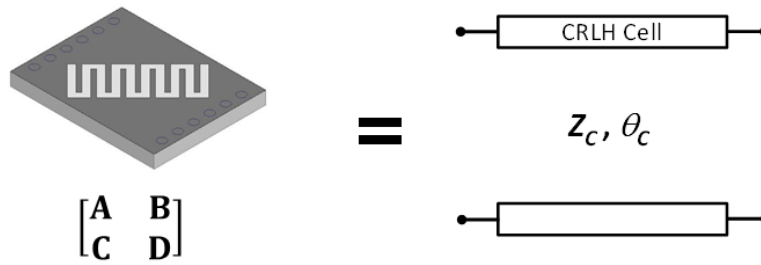
(c)

Figure 43. Characteristics of the previous CP antenna unit-cell [19]. (a) Dispersion diagram ($p = 2 \times l_s + 2 \times l_c$). (b) Space harmonics reconstructed from the dispersion diagram of the previous unit-cell (n is mode number). (c) Bloch Impedance.

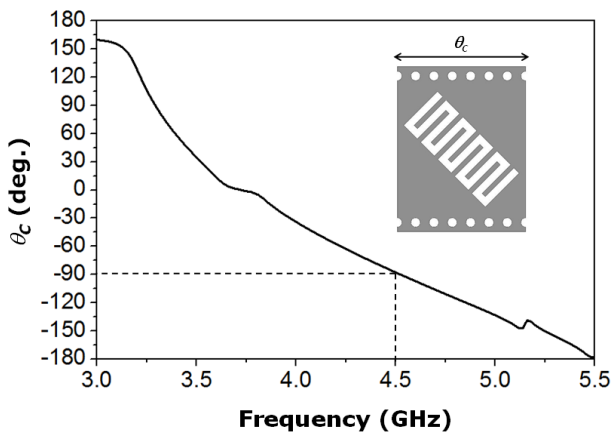
unit-cell of the previously proposed single radiator CP CRLH-inspired antenna entirely based on SIW structure [20]. The dimensions of the unit-cells are also provided in Fig.41.

Fig. 42(a) shows the dispersion diagram of the proposed unit-cell (from section 1 to 4). In this graph, we notice that the proposed unit-cell structure has multiband characteristic. This is similar to that of a dual-band (DB) CRLH unit-cell [21]. The center frequency of the proposed unit-cell

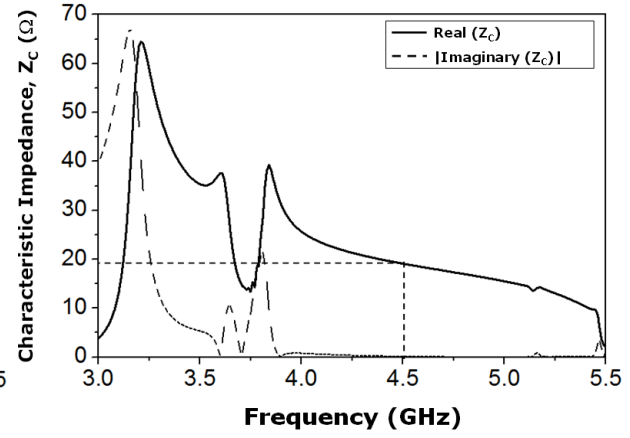
is 4.67 GHz and broadside radiation occurs at this frequency. In order to rigorously analyze the radiation mechanism of the proposed antenna, space harmonics of the proposed unit-cell are shown in Fig. 42(b) [22], [23]. Fundamental space harmonic is redrawn from the dispersion diagram of the unit-cell. Note that the proposed unit-cell supports first radiation band (3.28 GHz ~ 3.88GHz) in the fundamental space harmonic and the second radiation band (from 4.06 GHz) is supported by the $n = -1$ space harmonic. Conventional CRLH based leaky-wave antennas generally operate in the fundamental mode ($n = 0$). However, since the proposed CP antenna operates in $n = -1$ mode, it is periodic type rather than quasi-uniform type of LWA in the operating range [22]. The Bloch impedance of the proposed structure (shown in Fig. 42(c)) is maintained around 50Ω throughout the $n = -1$ radiation band. Therefore exterior matching circuit is not necessary. Fig. 42(c) is plotted assuming the periodic structure is infinitely long. The abrupt change in impedance around each transition frequency (frequency at which LH dispersion becomes RH) is due to the destructive cancelation of the incident wave and infinite sum of the reverse propagation waves generated at the imperfect discontinuities between the unit-cells. But for finite periodic condition, summation of reverse propagated waves could be negligible and minimally degrade the impedance mismatch loss at the transition frequency. Fig. 43(a) shows the dispersion diagram of the previous antenna unit-cell shown in Fig. 34(a). Compared with the dispersion diagram of the proposed antenna unit-cell shown in Fig. 42(a), the previous structure entirely based on SIW has band-gap between first band and second band. Fig. 43(a) also indicates that the previous unit-cell has faster phase change, reducing the operational bandwidth. Fig. 43(b) demonstrates space harmonics of the previous unit-cell. Similar to the proposed structure, circularly polarized wave is radiated in the second band which is supported by $n = -1$ space harmonic. The Bloch impedance of the unit-cell solely based on SIW shown in



(a)



(b)



(c)

Figure 44. (a) CRLH SIW cell and its transmission line model. (b) Phase response of the CRLH cell. (c) Characteristic impedance of the CRLH cell.

Fig. 43(c) however produces much broader impedance mismatch condition in comparison to the proposed case.

5.3 Antenna Design

The design procedure of the proposed antenna has two steps. First, a single CRLH cell is designed. Then, the dimensions of microstrip lines are determined.

5.3.1 Single CRLH Cell

The single CRLH SIW cell (section 2 or 3 of Fig. 41(a)) is expressed as a transmission line section in Fig. 44(a). The phase response θ_C and characteristic impedance Z_C of the TL can be calculated from the ABCD matrix as follows [24]:

$$\theta_C = \arccos(A) = \arccos(D) \quad . \quad (9)$$

$$Z_C = \frac{B}{j \sin(\theta)} = \frac{j \sin(\theta)}{C} \quad . \quad (10)$$

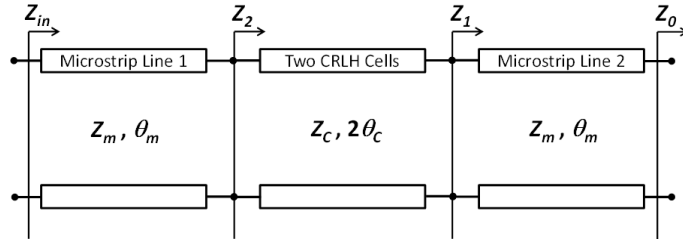
In addition, at the center frequency of the proposed antenna (f_0), the single CRLH cell provides 90° phase delay:

$$\theta_C(f_0) = -\frac{\pi}{2} \quad . \quad (11)$$

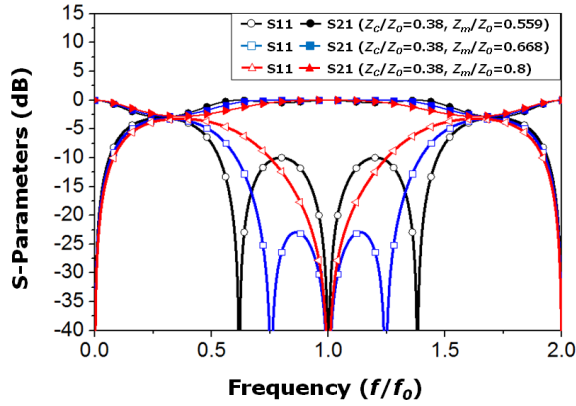
The corresponding phase response of a single CRLH SIW cell is shown in Fig. 44(b). The simulated center frequency is at $f_0 = 4.52$ GHz. This slight down shift of center frequency is due to parasitic effects at the microstrip line and SIW discontinuity in the total unit-cell shown in Fig. 41(a). If needed, additional tuning may be carried out to obtain the exact desired center frequency. The characteristic impedance of the single CRLH cell is shown in Fig. 44(c). This impedance value is used to determine the width of a microstrip line as will be shown in the following section. In the prototype antenna design, the ABCD matrix of the single CRLH cell is investigated based on the HFSS simulation.

5.3.2 Conventional Line

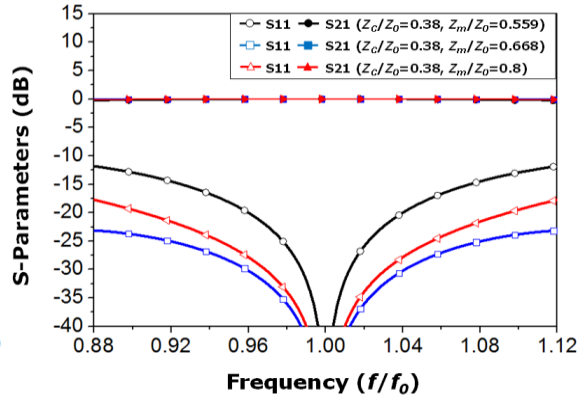
Conventional TL sections (section I and IV) not only provide additional phase delay, but also provide good matching at the center frequency. Thus the proposed antenna and the previous work [20] behave as efficient broadside radiators. The conventional SIW used in the previous



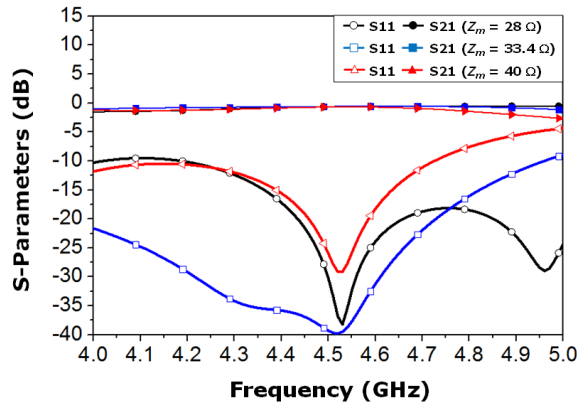
(a)



(b)



(c)



(d)

Figure 45. (a) Transmission line model of the proposed CP LWA unit-cell. (b) Scattering parameters of the TL model (with all ideal TLs) changing the characteristic impedance of the microstrip line, Z_m , with fixed Z_c . (c) Zoom view of Fig. 4(b) around the center frequency. (d) S-parameters of the TL model using the ABCD matrix of the CRLH cell (ideal TLs are used for microstrip lines).

antenna [20] operates in TE_{10} mode in which the wave impedance is frequency dependent [24].

This frequency dependent impedance degrades the CP purity as the operating frequency is shifted away from the optimal point. However, microstrip lines used in the proposed antenna has constant line impedance for broader frequency range thereby providing high quality CP radiation for much wider beam scanning angle. To design the width (w_m) and the length (l_m) of the microstrip line, the transmission line model of the proposed antenna unit-cell is investigated. Fig. 45(a) shows the transmission line model consisting of three TL sections. The characteristic impedance Z_C and the phase response θ_C of the CRLH SIW cell is calculated in (9). Since two CRLH SIW cells are used in the proposed antenna unit-cell, the phase delay of the CRLH SIW section in Fig. 45(a) is π radian or 180° at the center frequency from (10). The phase response of each microstrip line is $\theta_m = -90^\circ$ at the center frequency.

As shown in Fig. 45(a), the input impedance of a transmission line with an arbitrary load Z_o is expressed as follows [24]:

$$Z_1 = Z_m \frac{Z_o + jZ_m \tan \theta_m}{Z_m + jZ_o \tan \theta_m}. \quad (12)$$

where Z_m is the characteristic impedance of the microstrip line. For $\theta_m = -90^\circ$, above equation reduces to

$$Z_1(f_0) = \frac{Z_m^2}{Z_o}. \quad (13)$$

The input impedance value for each section is calculated in a similar manner. Then, we can express the input impedance looking to the right of the microstrip line 1 (Z_2) and the input impedance of the unit-cell (Z_{in}) as follows:

$$Z_2(f_0) = Z_1(f_0) = \frac{Z_m^2}{Z_o}. \quad (14)$$

$$Z_{in}(f_0) = Z_0. \quad (15)$$

When all microstrip sections are quarter wavelength long, regardless of the characteristic impedances Z_C and Z_m , the input impedance of the proposed antenna unit-cell will always be the same as the load impedance Z_0 at the center frequency. Therefore the proposed antenna can provide good broadside radiation without the need of an external matching circuit (this works with any arbitrary load impedance values). Fig. 45(b) shows the scattering parameters of the TL model (with all ideal TLs) shown in Fig. 45(a). With different microstrip line impedances (Z_m) values, we can observe various corresponding return loss responses [25]. Fig. 45(c) is the magnified view of Fig. 45(b). Fig. 45(d) shows the S -parameters of the TL model with the ABCD matrix of the CRLH cell simulated by HFSS and two ideal TLs. Considering both Fig. 45(c) and (d), Z_m is determined to be $0.668 \times Z_0$ or 33.4Ω in the proposed antenna thereby having high return loss in the operating range.

The design process is summarized in the following steps.

1. Design a single CRLH cell with 45° rotated interdigital slot. The center frequency of an antenna (f_0) is a design parameter of the CRLH cell as shown in (10). Using (9), the phase response and characteristic impedance of the cell can be calculated.
2. Adjust the characteristic impedance of a microstrip line (Z_m) based on the characteristic impedance at the center frequency and the ABCD matrix of the CRLH cell.
3. Determine the physical width w_m and the length l_m of the microstrip line. The microstrip line has the characteristic impedance Z_m as function of the width w_m . The length l_m is designed to provide: $\theta_m(f_0) = -90^\circ$.
4. Construct the unit-cell of the proposed antenna combining two CRLH cells (from step 1) and two microstrip lines (from step 3). Then, perform full-wave analysis and investigate

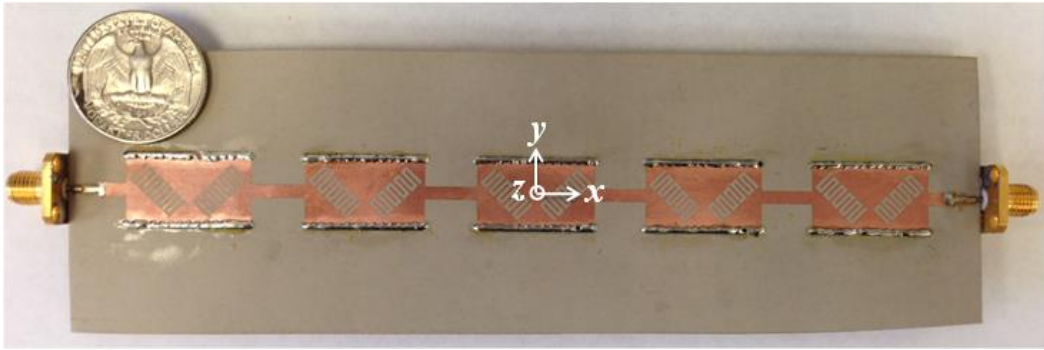


Figure 46. Fabricated novel CP CRLH-inspired SIW leaky-wave antenna.

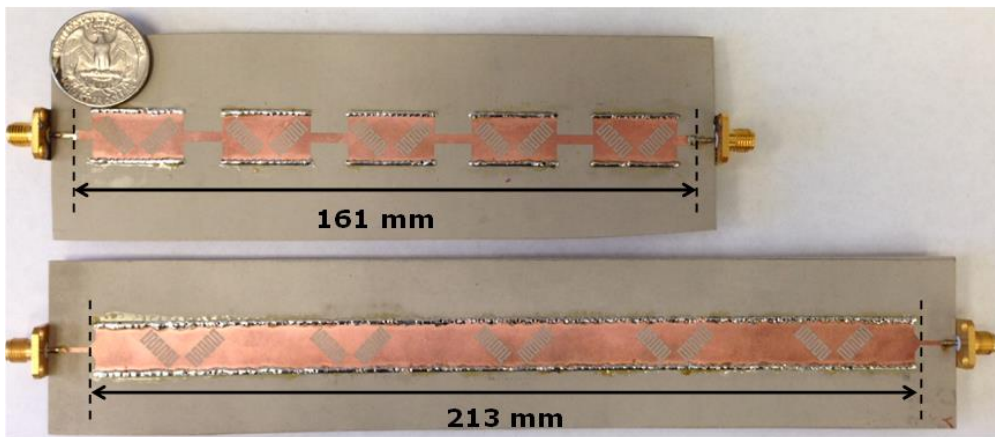


Figure 47. Comparison between the proposed CP antenna and the previous CP antenna having single radiator.

the characteristics of the proposed antenna unit-cell as shown in Fig. 42. In this stage, some tuning may be necessary to compensate parasitic effects at the discontinuity between the single CRLH SIW cell and the microstrip line.

5. Determine the number of unit-cells to meet the targeted radiated efficiency of the antenna. Longer antennas will produce higher efficiency and directivity.

5.4 Proposed Circular Polarized Antennas

Based on the procedure shown in section III, a compact five-cell circularly polarized antenna is designed and fabricated using RT/Duroid 6010 substrate ($\epsilon_r = 10.2$, $h = 1.27$ mm). Via holes

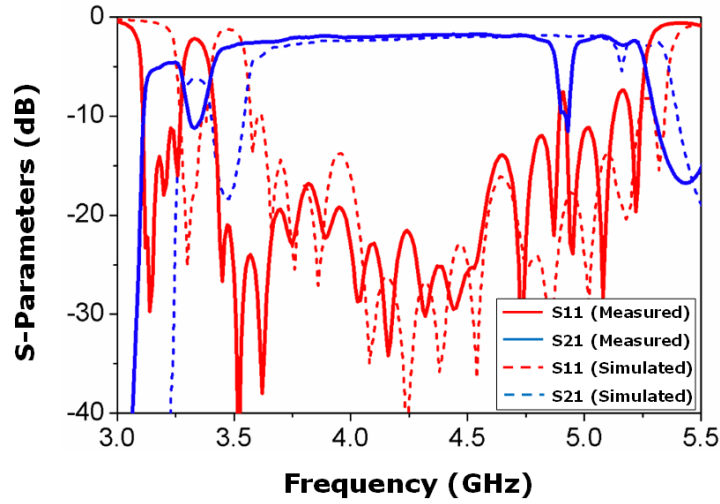


Figure 48. Measured and simulated S-parameters of the proposed CP LWA antenna.

with the diameter of $d = 0.8$ mm are placed on each sides of the SIW structure with the via center-to-center spacing of $s = 1.57$ mm to emulate side wall effects of the SIW. Fig. 46 shows a photograph of the fabricated antenna. A photograph of the proposed antenna and the previous CP antenna with five-cells is also shown in Fig. 47 [20]. Comparing to the previous five-cell CP antenna, the proposed antenna shows 24.4 % size reduction.

The simulated and measured S-parameters of the proposed antenna are shown in Fig. 48. Slight frequency discrepancy between the simulated and measured results are due to fabrication errors. The measured S_{11} is below -14 dB throughout the entire operating frequency band including at the center frequency.

The proposed antenna supports both left-handed circular polarization (LHCP) and right-handed circular polarization (RHCP) depending on the port of excitation. LHCP and RHCP are generated when the antenna is fed from port 1 and port 2, respectively. In this chapter, the antenna is fed at port 1 to produce LHCP. Fig. 49 shows the simulated gain patterns of the proposed antenna. The full-space beam-steering by frequency scanning is observed. For higher

efficiency and realized gain, the proposed antenna can simply be elongated by cascading more unite cells.

The far field pattern and AR of the proposed CP antenna are measured in the near-field chamber. The normalized measured radiation patterns for backward direction (*in x-z plane*) are shown in Fig. 50(a). Fig. 50(b) and (c) show the radiation patterns for broadside and forward

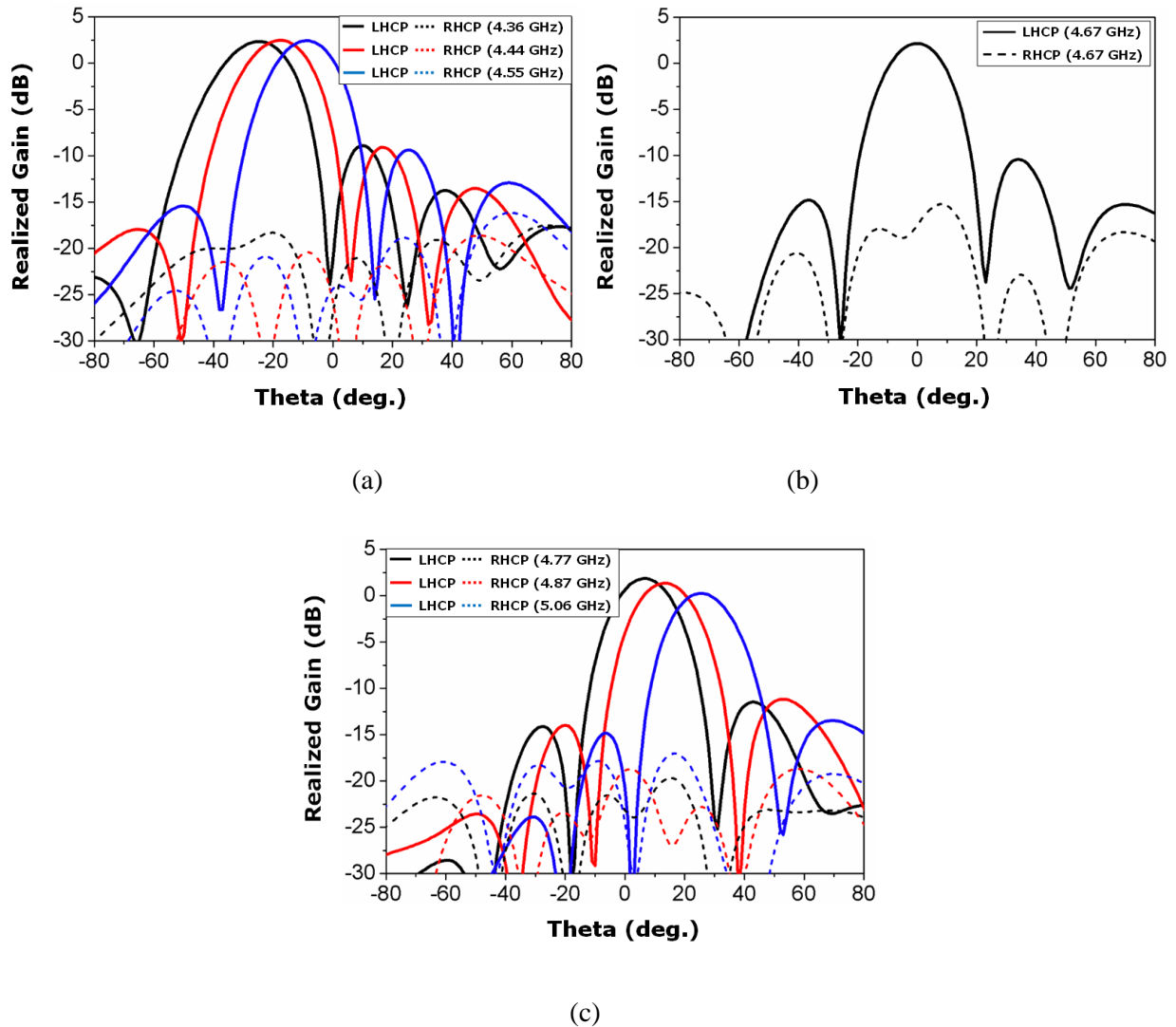
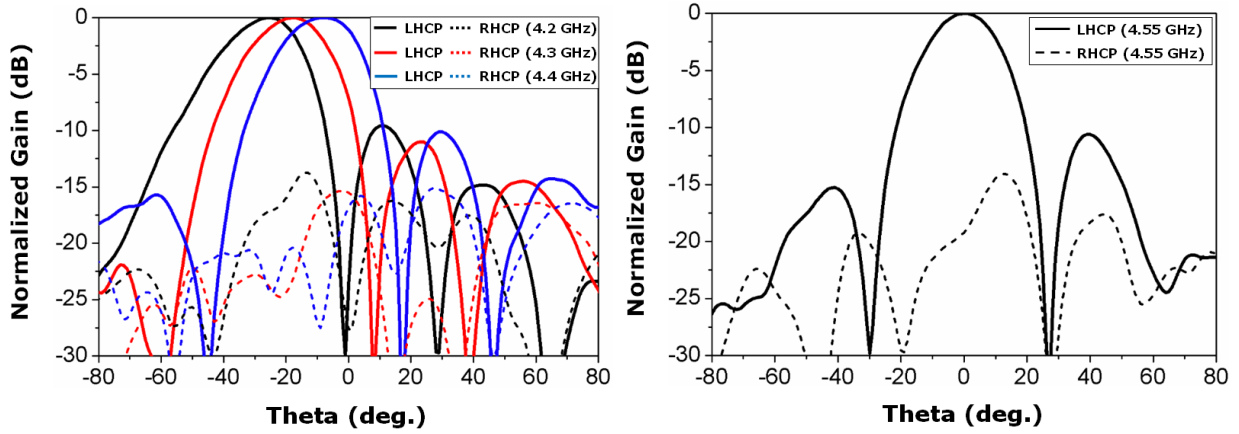


Figure 49. Simulated realized gain patterns of the proposed circularly polarized antenna in x-z plane. (a) LH region. (b) Broadside. (c) RH region.

direction, respectively. The cross-polarization (RHCP) patterns are also plotted. Simulated cross-pol level is 24 dB lower and measured cross-pol level is 15 dB lower than co-polarization patterns in the simulated measured results, respectively. The simulated and measured AR (*in x-z plane*) is plotted in Fig. 51. Because of the frequency shift of the fabricated antenna, simulated axial ratio at slight higher frequencies are used to compare the measured results. The proposed antenna shows good axial ratio of less than 3 dB within the beam scanning range. The discrepancy of simulate and measured AR at 4.85 GHz (measured frequency) is due to the self-resonance of interdigital slots. Table 8 compares the simulated axial ratio (AR) levels of the proposed antenna and the previous antenna with same scanning angles (θ). As we expected, the quality of CP radiation of the proposed antenna is better than the previous work. Overall, the experimental results are consistent with the simulation results.

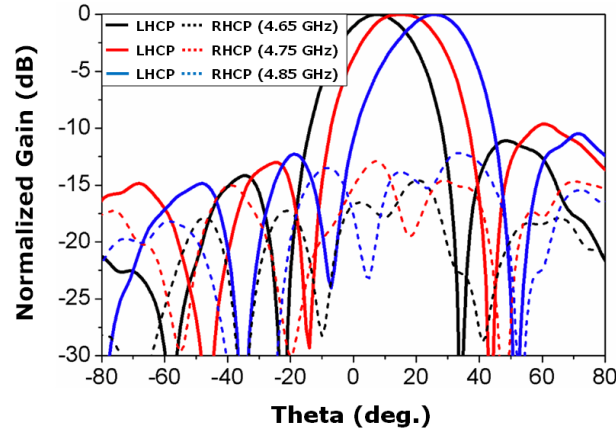
5.5 Conclusion

This chapter presents an improved single radiator circular polarized CRLH-inspired SIW leaky-wave antenna. The antenna provides CP frequency scanning with only a single radiator, thereby eliminating complex feeding network [18]. The size of the proposed unit-cell is much smaller than the previously designed structure [20]. The measured and simulated results show consistency and we have found that the proposed antenna provides high-quality CP beams with full-space scanning capability including broadside direction. Hence the proposed antenna may serve as a good candidate for wireless applications requiring CP frequency scanning features.



(a)

(b)



(c)

Figure 50. Measured radiation patterns of the proposed circularly polarized antenna in x-z plane. (a) LH region. (b) Broadside. (c) RH region

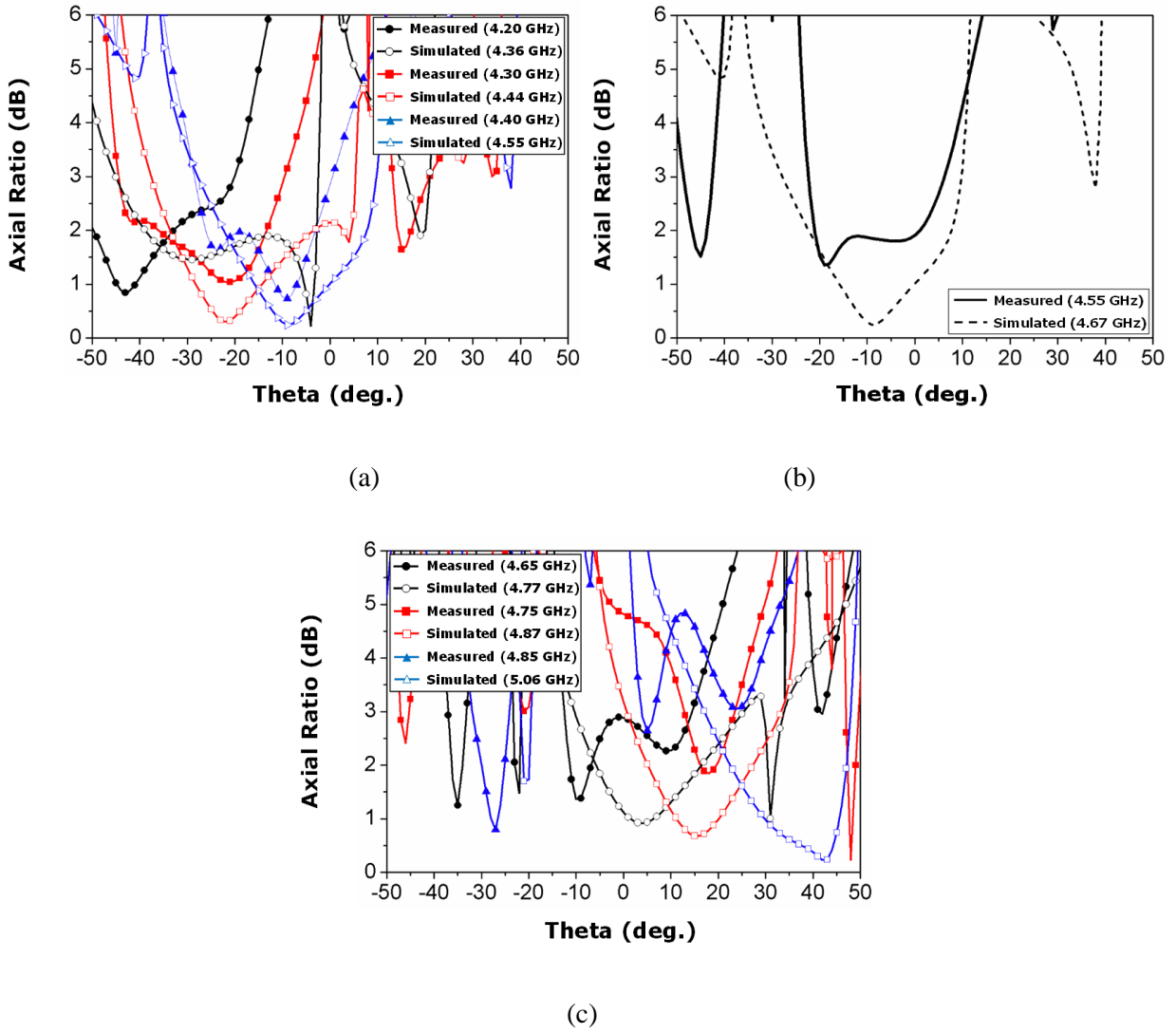


Figure 51. Measured and simulated axial ratio of the proposed circularly polarized antenna in x-z plane. (a) LH region. (b) Broadside. (b) RH region.

Table 9. Simulated Axial Ratio Comparison

Scan Angle θ (deg.)		-29	-18	-10	0	12	18	24
Axial Ratio (dB)	Proposed Antenna	2.8	0.6	0.1	1.8	0.8	0.9	1.4
	Previous Antenna [20]	3.2	0.2	0.6	2.7	1.5	2.5	3.3

5.6 References

- [1] A. Oliner and D. R. Jackson, "Leaky-wave antennas," in *Antenna Engineering Handbook*, C. J. L. Volakis, Ed. New York: McGraw-Hill, 2007.
- [2] D. R. Jackson and A. A. Oliner, "Leaky-wave antennas," in *Modern Antenna Handbook*, C. Balanis, Ed. New York: Wiley, 2008.
- [3] D. R. Jackson, C. Caloz, and T. Itoh, "Leaky-wave antennas," *IEEE Proceedings*, vol. 100, no.7, pp. 2194-2206, July 2012.
- [4] D. R. Jackson and A. A. Oliner, "A leaky-wave analysis of the high-gain printed antenna configuration," *IEEE Trans. Antenna Propag.*, vol. 36, no.7, pp. 905-910, Jul. 1988.
- [5] M. Guglielmi and D. R. Jackson, "Broadside radiation from periodic leaky-wave antennas," *IEEE Trans. Antenna Propag.*, vol. 41, no.1, pp. 31-37, Jan. 1993.
- [6] P. Burghignoli, G. Lovat, and D. R. Jackson, "Analysis and optimization of leaky-wave radiation at broadside from a class of 1D periodic structures," *IEEE Trans. Antenna Propag.*, vol. 54, no.9, pp. 2593-2604, Sep. 2006.
- [7] S. Paulotto, P. Baccarelli, F. Frezza, and D. R. Jackson, "A novel technique for open-stopband suppression in 1-D periodic printed leaky-wave antennas," *IEEE Trans. Antenna Propag.*, vol. 57, no.7, pp. 1894-1906, Jul. 2009.
- [8] L. Liu, C. Caloz, and T. Itoh, "Dominant mode (DM) leaky-wave antenna with backfire-to-endfire scanning capability", *Electron. Lett.*, vol. 38, no. 23, pp.1414 -1416, Nov. 2002.
- [9] S. Lim, C. Caloz, and T. Itoh, "Metamaterial-based electronically-controlled transmission line structure as a novel leaky-wave antenna with tunable radiation angle and beamwidth," *IEEE Trans. Microwave Theory Tech.*, vol. 53, no. 1, pp. 161-173, Nov. 2005.
- [10] T. Kokkinos, C. D. Sarris, and G. V. Eleftheriades, "Periodic FDTD analysis of leaky-wave structures and applications to the analysis of negative-refractive-index leaky-wave antennas," *IEEE Trans. Microwave Theory Tech.*, vol. 54, no. 4, pp. 1619-1630, Jun. 2006.
- [11] Y. Weitsch, T.F. Eibert, "A Left-Handed/Right-Handed Leaky-Wave Antenna Derived from Slotted Rectangular Hollow Waveguide", *2007 European Microwave Conference*, Oct. 2007.

- [12] Y. Dong and T. Itoh, "Composite right/left-handed substrate integrated waveguide and half mode substrate integrated waveguide leaky-wave structures," *IEEE Tran. Antenna Propag.*, vol. 59, no. 3, pp. 767-775, Mar. 2011.
- [13] K. Kitatani, Y. Mitsuhashi, Y. Okamura, "Circularly polarized leaky wave antenna without phase shifter using CRLH transmission line," *2012 European Conference on Antennas and Propagation (EUCAP)*, Mar. 2012.
- [14] M. Ishii, T. Fukusako, A. Alphones, "Design of leaky wave antenna with composite right-/left-handed transmission line structure for circular polarization radiation", *Progress In Electromagnetics Research C*, Vol. 33, 109-121, 2012.
- [15] S. Otto, Z. Chen, A. Al-Bassam, A. Rennings, K. Solbach, and C. Caloz, "Circular polarization of periodic leaky-wave antennas with axial asymmetry: Theoretical proof and experimental demonstration," *IEEE Trans. Antennas Propagat.*, vol. 62, no. 4, pp. 1817-1829, April 2014.
- [16] F. Ferrero, C. Luxey, G. Jacquemod, and R. Staraj, "Dual-band circularly polarized microstrip antenna for satellite applications," *IEEE Antennas Wireless Propag. Lett.*, vol. 4, pp. 13–15, 2005.
- [17] Y. Zhou, C. Chen, and J. L. Volakis, "Single-fed circularly polarized antenna element with reduced coupling for GPS arrays," *IEEE Tran. Antenna Propag.*, vol. 56, no. 5, pp. 1469-1472, May 2008.
- [18] T. Wu, H. Su, L. Gan, H. Chen, J. Huang, and H. Zhang, "A compact and broadband microstrip stacked patch antenna with circular polarization for 2.45-GHz mobile RFID reader," *IEEE Antennas Wireless Propag. Lett.*, vol. 12, pp. 623–626, May 2013.
- [19] Y. Dong and T. Itoh, "Substrate Integrated Composite Right-/Left-Handed Leaky-Wave Structure for Polarization-Flexible Antenna Application", *IEEE Transactions on Antennas and Propagation*, vol. 60, no. 2, pp. 760 - 771, Feb. 2012.
- [20] H. Lee, J. H. Choi, Y. Kasahara, and T. Itoh, "A circularly polarized single radiator leaky-wave antenna based on CRLH-inspired substrate integrated waveguide," *2014 IEEE MTT-S Int. Microwave Symp.*, June 2014.
- [21] M. R. Hashemi and T. Itoh, "Dual-band composite right/left-handed metamaterial concept," *IEEE Microwave and Wireless Components Letters*, vol. 22, no. 5, pp.248-250, May 2012.
- [22] A. Hessel, "General characteristics of traveling-wave antennas," in *Antenna Theory, Part 2*, R. E. Collin and F. J. Zucker, Eds. New York: McGraw-Hill, 1969.

- [23] O. Breinbjerg, "Properties of Floquet-Bloch space harmonics in 1D periodic magneto-dielectric structures," *2012 ICEAA*, pp. 1125-1128, Sep. 2012.
- [24] D. M. Pozar, *Microwave Engineering*, New York: Willey, 2005.
- [25] J.-S. Hong and M.J. Lancaster, *Microwave Filters For RF/Microwave Applications*, New York: Willey, 2011.

Appendix 1

An Circuit parameters of a CRLH TL with a dual-band characteristic can be determined by only two desired phase responses (ϕ_1 and ϕ_2), two target frequencies (ω_1 and ω_2), and termination impedance (Z_0) as follows:

$$L_R = \frac{Z_0[\phi_1(\omega_1 / \omega_2) - \phi_2]}{N_C \omega_2 [1 - (\omega_1 / \omega_2)^2]} \quad (16)$$

$$C_R = \frac{\phi_1(\omega_1 / \omega_2) - \phi_2}{N_C \omega_2 Z_0 [1 - (\omega_1 / \omega_2)^2]} \quad (17)$$

$$L_L = \frac{N_C Z_0 [1 - (\omega_1 / \omega_2)^2]}{\omega_1 [\phi_1(\omega_1 / \omega_2) - \phi_2]} \quad (18)$$

$$C_L = \frac{N_C [1 - (\omega_1 / \omega_2)^2]}{\omega_1 Z_0 [\phi_1(\omega_1 / \omega_2) - \phi_2]} \quad (19)$$

where N_C is the number of CRLH TL unit cells.

Appendix 2

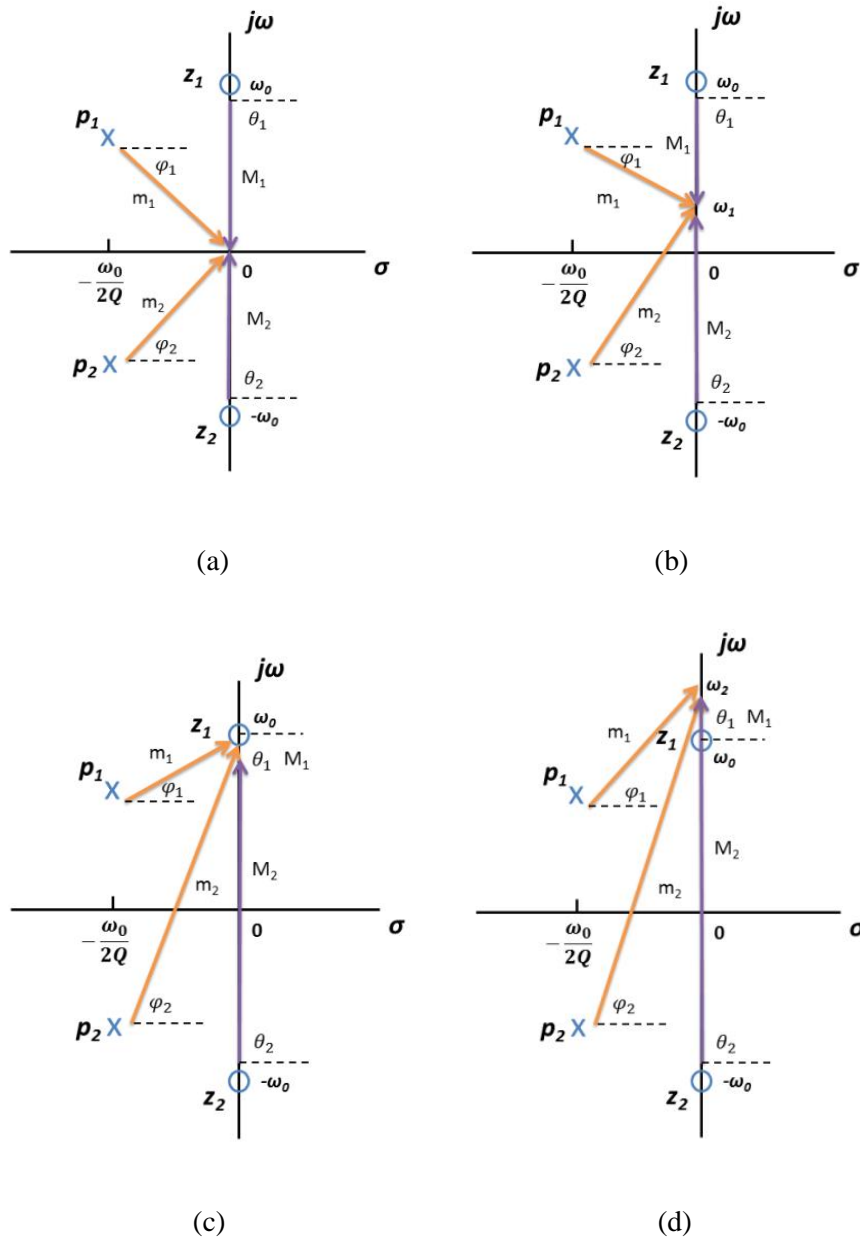


Figure 52. Pole-zero plots of the transfer function of reflection coefficient at (a) $\omega = 0$, (b) $\omega = \omega_1$, (c) $\omega = \omega_0$, and (d) $\omega = \omega_2$.

A second-order BPF has the transfer function of reflection coefficient of following mathematical form:

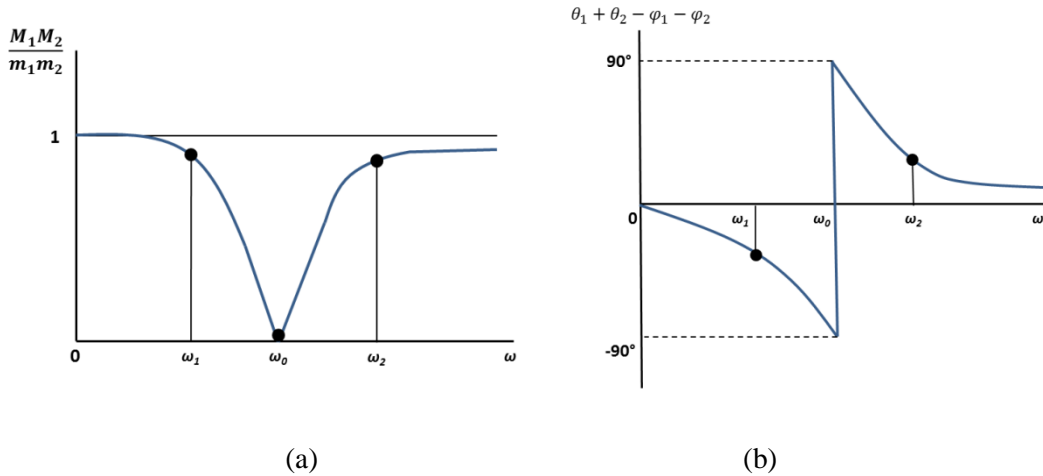


Figure 53. (a) Amplitude and (b) phase response of the reflection coefficient of a BPF.

$$H_{ref}(s) = \frac{A(s^2 + \omega_0^2)}{s^2 + (\omega_0 / Q)s + \omega_0^2} = A \frac{(s - z_1)(s - z_2)}{(s - p_1)(s - p_2)} \quad (20)$$

where $s = \sigma + j\omega$, which is the complex frequency, ω_0 is the center frequency of the BPF, and Q stands for the quality factor. In addition, the constant A accounts for the rejection type at DC and infinite frequency ($\omega \rightarrow \infty$). If the stop band input impedance is infinite (open), A is equal to 1, whereas if the input impedance is zero (short) then A becomes -1. The above equation can be further expressed with the factored form in terms of poles (p_i) and zeros (z_i).

It is found useful that the frequency response of reflection coefficient S_{11} can be visualized through the use of pole-zero plots. As an illustrative example shown in Fig. 52, four different frequencies from low to high ($\omega = 0$, $\omega = \omega_1$, $\omega = \omega_0$, and $\omega = \omega_2$) are picked in order to examine the frequency response of the transfer function.

We can then construct frequency responses of the amplitude and phase from Fig. 52. By denoting the magnitude and phase of the pole vectors to be m_i , φ_i , and those of the zero vectors to be M_i , ϑ_i , where $i= 1, 2$, we can plot the amplitude response of the transfer function (M_1M_2/m_1m_2)

and its phase response ($\vartheta_{1+} - \vartheta_2 - \varphi_1 - \varphi_2$) as depicted in Fig. 53. One can observe that the reflection zero occurs at ω_0 , and at this frequency the phase experiences an abrupt change from -90 degrees to +90 degrees. Overall, the phase is decreasing with respect to the frequency, which implies the transfer function of reflection coefficient has a positive group delay. As a result, the overall phase of the transfer function will be decreasing. Furthermore, if we plot the response on Smith charts, such characteristics will result in a clockwise rotation of S_{11} with frequency increasing. Fig. 24 plots the corresponding responses of S_{11} or input impedance of the filter when the rejection is open ($A = 1$) and short ($A = -1$), and they both rotate clockwise on the Smith charts.

Although the case discussed here is for a second order BPF, any high order BPFs' transfer functions can be decomposed to a multiplication of second order BPFs. Therefore, the same analysis can be used and will still result in the same conclusion for the sense of phase rotation.

Conclusion

The growth of wireless communication systems has brought challenges to a multiplexer and an antenna area such as multiple functionalities, size reduction, and analytical design process. Metamaterial transmission lines show potential for these challenges. The main objective of this dissertation is to demonstrate high performance multiplexers and antennas based on metamaterial transmission lines.

In the multiplexer design, an isolation circuit concept has realized to use filters without modification and to provide straightforward design process without an optimization. The isolation circuit consists of a transmission line connected with a filter. The presence of a metamaterial transmission line allows the isolation circuit operating at multiple frequencies. In addition to an isolation circuit, various junction types add more flexibility of designing multiplexers based on metamaterial transmission lines. A star-junction is simplest one and all isolation circuits use same type of a transmission line. In a manifold-junction concept, one isolation circuit uses multiple conventional transmission lines, but others have same configuration with an isolation circuit used in a star-junction type. Since one isolation circuit is composed with conventional lines, manifold-junction multiplexers based on metamaterial transmission lines have less complexity and more flexibility in a layout. With the approach connecting a metamaterial transmission line with a multiplexer instead of a filter, a channel number of a multiplexer is effectively increased. This novel junction method names the combining method of two filtering circuits (CMTC). Based on the CMTC, the triplexer, the quadruplexer, and the five-channel multiplexer are designed and fabricated. Comparing with the triplexer and the quadruplexer based on a star-junction or a manifold-junction, multiplexers based on CMTC show less complexity in terms of design process. Combining method of two

filtering circuits (CMTC) is also efficient method of designing a contiguous channel triplexer. A triplexer based on either a star-junction or a manifold-junction is not adequate for a contiguous channel configuration. In a conventional triplexer design, realizing a contiguous channel is also difficult because of strong coupling. However, the design of a triplexer based on CMTC is inherently easy to have contiguous channels configuration. The reason of this and the design procedure have been explained.

Many researchers have tried to design circular polarized SIW leaky-wave antennas based on metamaterial transmission lines. Most of approaches have used dual radiators and a broadband quadrature coupler. However, the novel approach proposed in this dissertation has provided the improved circular polarized SIW leaky-wave antenna with a single radiator thereby realizing a compact antenna system and reducing complexity. The unit-cell of the proposed leaky-wave antenna consists of two conventional CRLH SIW cells with the interdigital slot rotated by $+45^\circ$ and -45° with respect to the wave propagation direction and two conventional SIW lines. This approach is further improved by using a microstrip line instead of a SIW line for a phase delay. The modified unit-cell structure has more compact size than the original unit-cell. Therefore, in a same size, the antenna introduced in the last chapter has more radiating elements and it brings increased radiation efficiency.

To sum up, original contributions in two microwave areas have made: 1) the multiplexers based on metamaterial transmission lines with various junction types; 2) the single radiator circular polarized SIW leaky-wave antennas based on novel metamaterial line unit-cell.